

**INTERPRETATION OF AIRBORNE MAGNETIC DATA OVER
SELECTED AREAS OF WITBANK COALFIELD, SOUTH AFRICA:
AN AID TO MINE PLANNING.**

by

PHUTI JOSPHAT MAHANYELE

DISSERTATION

Submitted in fulfilment of the requirements
for the degree of

MAGISTER SCIENTIAE: EXPLORATION GEOPHYSICS

in the

FACULTY OF AGRICULTURAL AND NATURAL SCIENCES

at

UNIVERSITY of PRETORIA

SUPERVISOR: Dr. M. Combrinck

PRETORIA, 2010

DECLARATION

I declare that this thesis is my own work, conducted under supervision of Dr. M. Combrinck. No part of this research has been submitted in the past, or is being submitted, for a degree at any other university. It is being submitted for the Degree of Master of Science in the Faculty of Agricultural and Natural Science, Department of Geology, Pretoria University, Pretoria.

Phuti. J. Mahanyele



UNIVERSITEIT VAN PRETORIA
UNIVERSITY OF PRETORIA
YUNIBESITHI YA PRETORIA

“By trying often, the monkey learns to jump from the tree”

African Proverb

ABSTRACT

The main objective of this work is to aid coal mine planning by determining geological structures that affect mining such as faults, dykes and sills. Faults can displace the coal seams by breaking and throwing the coal seam on one side of the fault deeper; thereby constituting safety risks or even making exploitation uneconomical. Dykes are associated with devolatilisation of the coal around them. Both dykes and faults are also important in terms of groundwater management. The sills have the same devolatilisation effect as dykes but on a larger scale as they cover more area than the dykes. They also make mining difficult if one has to mine through them, especially if they are not weathered.

The study was based on high resolution airborne magnetic data which was flown on selected areas in the Witbank coalfield. The combined areas cover a total of ~171001 hectares. Total field magnetic data were collected. The data were processed and gridded. The resulting total field magnetic grids were enhanced for better delineation of structures by: reducing the data to the pole, calculation of the first vertical derivatives and computation of the analytic signal. Using the enhanced grids together with other datasets; topographic maps, borehole log information and infrastructure information from the surrounding mines, the geological structures were interpreted.

Intense geological activity is observed on the eastern areas of the coalfield (Belfast and Arnot). This is the region where numerous geological activities of different ages were recorded, e.g., the intrusion of Bushveld Complex, the Olifants River Dyke Swarm (ORDS) and the Karoo Basalts. Associated with the intense geological activity is the presence of dykes, faults and sills, which are observed throughout the areas.

In the central region, Vandyksdrif area 1 reveals the pre-Karoo basement rocks (felsites and diabases of the Bushveld Igneous Complex) and Vandyksdrif area 2 reveals the Karoo dolerite in the form of a sill. The sill corresponds to the high elevation area on the digital terrain model data suggesting that the sill might be unweathered. Unfortunately, the borehole logs do not mention the state of the dolerite.

The western areas reveal mainly the dolerite sill. Like in Vandryksdrif area 2, there is no mention of the state of the dolerite and the suspicion is that the dolerite is also unweathered there as well.

Table of contents	PAGE
0. ABSTRACT	i
1. CHAPTER 1. INTRODUCTION	
1.0. General.....	1
1.1. Regional Setting.....	1
1.2. Problem Statement.....	4
1.3. Objectives And Methodology.....	4
1.3.1. Objectives.....	5
1.3.2. Methodology.....	6
1.4. The General Geology Of The Witbank Coalfield.....	7
1.4.1. Local Geology Of Study Areas.....	8
1.4.1.1. Delmas Areas.....	8
1.4.1.2. Vandykdrif Area.....	12
1.4.1.3. Arnot Area.....	16
1.4.1.4. Belfast Area.....	19
2. CHAPTER 2. MAGNETIC CONCEPTS	
2.0. An Overview Of The Magnetic Method.....	22
2.1. The Earth's Magnetic Field.....	24
2.2. Magnetic Properties Of Materials.....	25
2.2.1. Magnetising Field.....	25
2.2.2. Magnetic Permeability (U).....	25
2.2.3. Induced And Remanent Magnetism.....	26
2.2.3.1. Induced Magnetism (J_i).....	26
2.2.3.2. Remanent Magnetism (J_r).....	27
2.2.4. Magnetic Susceptibility (K).....	28
2.2.5. Elements Of The Earth's Magnetic Field.....	28
2.3. Magnetic Lithologies.....	30
2.4. Instrumentation.....	31

2.5. Application Of Magnetic Methods In Mining	32
3. CHAPTER 3. DATA AQUISITION AND DATA PROCESSING	
3.0. Data Acquisition.	34
3.0.1. Aircraft And Acquisition Systems	34
3.0.2. Basic Survey Parameters Used	34
3.1. Data Processing.....	35
3.1.1. Phase 1 - Pre-Processing.....	35
3.1.2. Phase 2 - Processing.....	36
4. CHAPTER 4. ENHANCEMENT AND PRESENTATION OF DATA	
4.0. Introduction.....	38
4.1. Reduction To The Pole.	38
4.2. Computation Of Vertical Derivatives.....	39
4.3. Analytic Signal.....	39
5. CHAPTER 5. INTERPRETATION OF DIFFERENT DATASETS	
5.0. Introduction.....	41
5.1. Interpretation Of Delmas Data.....	44
5.2. Interpretation Of Vandyksdrif Area 1 Data.....	61
5.3. Interpretation Of Vandyksdrif Area 2 Data.....	71
5.5. Interpretation Of Belfast Data.....	100
5.6. Conclusions.....	109
6. ACKNOWLEDGEMENTS	111
7. REFERENCES.....	112

LIST OF FIGURES

PAGE

Figure 1. The location of the Witbank coalfield relative to other coalfields	2
Figure 2. Locality map of the study areas within the Witbank coalfield.....	3
Figure 3. Regional geology of Delmas study areas	10
Figure 4. The general stratigraphy of Delmas region.	11
Figure 5. Regional geology of Vandyksdrif study area 1	13
Figure 6. Regional geology of Vandyksdrif study area 2	14
Figure 7. The general stratigraphy of Vandyksdrif area.	15
Figure 8. Regional geology of Arnot study area.....	17
Figure 9. The general stratigraphy of Arnot study area.....	18
Figure 10. Regional geology of Belfast study area.....	20
Figure 11. The stratigraphy of Belfast study area.....	21
Figure 12. Cartoon illustration of the magnetic method.....	23
Figure 13. Components of the Earth's magnetic field.	29
Figure 14. Examples of how the faults were recognised on the dataset	43
Figure 15. Total field magnetic maps of Delmas study areas.....	46
Figure 16. First vertical derivative maps of Delmas study areas.....	47
Figure 17. Digital terrain model maps of Delmas study areas.....	48
Figure 18a. The geological log for borehole WTN4.....	49
Figure 18b. The geological log for borehole WTN4 continued.....	50
Figure 18c. The geological log for borehole WTN4 continued.....	51
Figure 18d. The end of geological log for borehole WTN4.	52
Figure 18a. The geological log for borehole R22.....	53
Figure 18b. The geological log for borehole R22 continued.....	54
Figure 18c. End of the geological log for borehole R22.....	55
Figure 20. The geological log for borehole R21. 5.22m thick dolerite is observed.	56
Figure 21. Positions of the boreholes used for interpretation superimposed on the first vertical derivative data.....	57
Figure 22. Interpreted structures for Delmas study areas superimposed on the first vertical derivative data.....	58

Figure 23. Interpreted sills for Delmas study areas superimposed on the DTM data.....	59
Figure 24. Positions of the proposed boreholes superimposed on the first vertical derivative data.....	60
Figure 25. Total field magnetic map of Vandyksdrif study area 1 data.....	63
Figure 26. Analytic signal map of Vandyksdrif study area 1 data.....	64
Figure 27. First vertical derivative map of Vandyksdrif study area 1 data.....	65
Figure 28. An area of both the ground and airborne data.....	66
Figure 29. Interpreted structures for Vandyksdrif area 1 data superimposed on the first vertical derivative map.....	67
Figure 30. Comparison of ground and airborne datasets in the same area.....	68
Figure 31. Coal seam 2 floor contours overlain on the first vertical derivative data of the airborne magnetic data.....	69
Figure 32. Comparison of ground and airborne datasets in the same area.....	70
Figure 33. Total field magnetic map of Vandyksdrif study area 2 data.....	73
Figure 34. Analytic signal map of Vandyksdrif study area 2 data.....	74
Figure 35. First vertical derivative map of Vandyksdrif study area 2 data.....	75
Figure 36. Digital terrain model map of Vandyksdrif area 2 data.....	76
Figure 37. The geological log for borehole.....	77
Figure 38. The geological log for borehole.....	78
Figure 39. The geological log for borehole.....	79
Figure 40. Positions of the boreholes used for interpretation.....	80
Figure 41. Interpreted structures for Vandyksdrif area 2 data superimposed on the first vertical derivative map.....	81
Figure 42. Interpreted sills superimposed on the digital terrain model data.....	82
Figure 43. Positions of the proposed boreholes superimposed on the first vertical derivative data.....	83
Figure 44. Total field magnetic intensity map of Arnot data.....	90
Figure 45. Analytic signal map of the Arnot data.....	91
Figure 46. First vertical derivative map of Arnot data.....	92
Figure 47. The geological log of borehole GP4506048.....	93

Figure 48. Interpreted structures for Arnot data superimposed on the analytic signal data.	94
Figure 49. Cultural features observed on the Arnot data superimposed on the analytic signal data.	95
Figure 50. Positions of the proposed boreholes and the profiles superimposed on the first vertical derivative data.	96
Figure 51. Profile AC.	97
Figure 52. Profile AE.	98
Figure 53. Profile AF	99
Figure 54. Total field magnetic intensity map of Belfast data.	102
Figure 55. Analytic signal map of Belfast data.	103
Figure 56. First vertical derivative map of Belfast data.	104
Figure 57. Interpreted structures for Belfast data superimposed on the analytic signal data.	105
Figure 58. Regional magnetic map of South of Africa.	106
Figure 59. Low magnetic bodies (labelled A, B and C) and suspected ring dykes (labelled 1 and 2) observed on Belfast data superimposed on the analytic signal data.	107
Figure 60. Cultural features observed on Belfast data superimposed on the analytic signal data.	108

LIST OF TABLES

PAGE

Table 1. Positions of the recommended boreholes (Delmas area data).	45
Table 2. Positions of the recommended boreholes (Vandyksdrif area 2 data).	72
Table 3. Positions of the recommended boreholes (Arnot data).	86

CHAPTER 1

INTRODUCTION

1.0. GENERAL

Operations in any mining activities are often disrupted by the surprise encounter of the geological features such as faults, dykes and sills. Advance knowledge of the geological and structural conditions ahead of the coal working phases and also at the planned development sites (such as shaft and boxcut positions) is of utmost importance in order to have an effective system of mine planning and operation, thus minimising the risks.

Faults and dykes are not always easily identifiable from drilling methods making efficient planning systems hard to achieve. Dykes can alter the quality of coal to such an extent that the coal is no longer economically viable for exploitation (Lurie, 1994). The common characteristic of dykes is burning of the coal seams in its vicinity. On the other hand the faults can disrupt the continuity of coal seams by breaking and displacing the seams to greater depths. One of the of the extreme examples is the Daarby fault with a displacement of $\pm 250\text{m}$ in the Waterberg coalfield, dividing the coalfield into a shallow open-castable western part and a deep north-eastern part, where coal occurs at depths of $\pm 300\text{m}$ below the surface and can only be extracted by underground mining (Dreyer, 1991).

Sills, like dykes, also influence the quality of coal but on a larger scale. At Delmas, according to the geologist at Exxaro resources (Schutte, F.J.P., personal comm., 2008), some sills are occurring over the coal seams resulting in wider devolatilised areas, making it hard to reach client specified product.

1.1. REGIONAL SETTING

The study areas (Delmas, Vandyksdrif, Arnot and Belfast) are situated within the Witbank coalfield, South Africa. Figure 1 shows the location of Witbank coalfield in relation to other coalfields. The geographic locations of the study areas and their positions in relation to Witbank coalfield are shown in Figure 2.

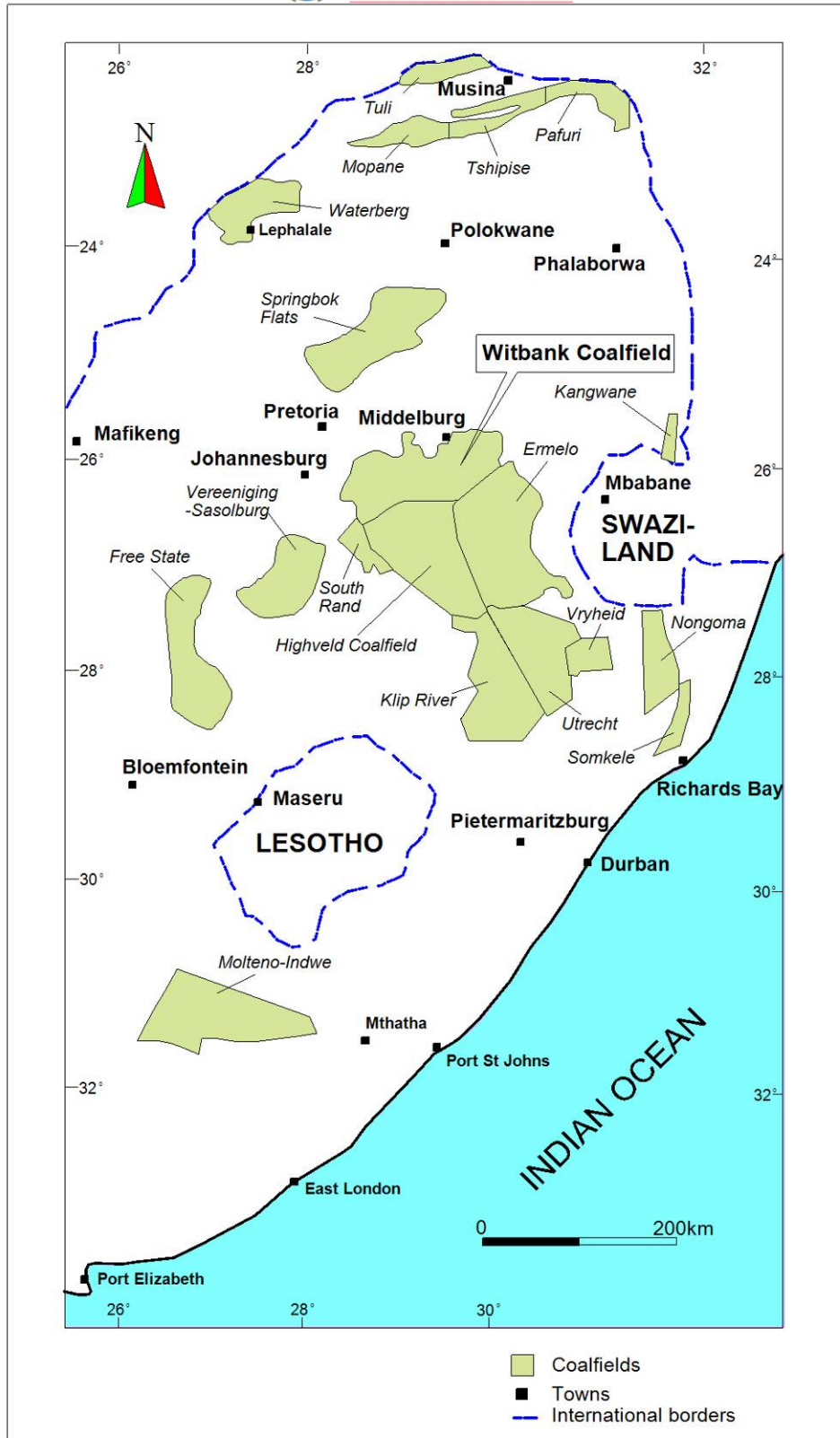


Figure 1. The location of the Witbank coalfield relative to other coalfields (after Snyman, 1998)

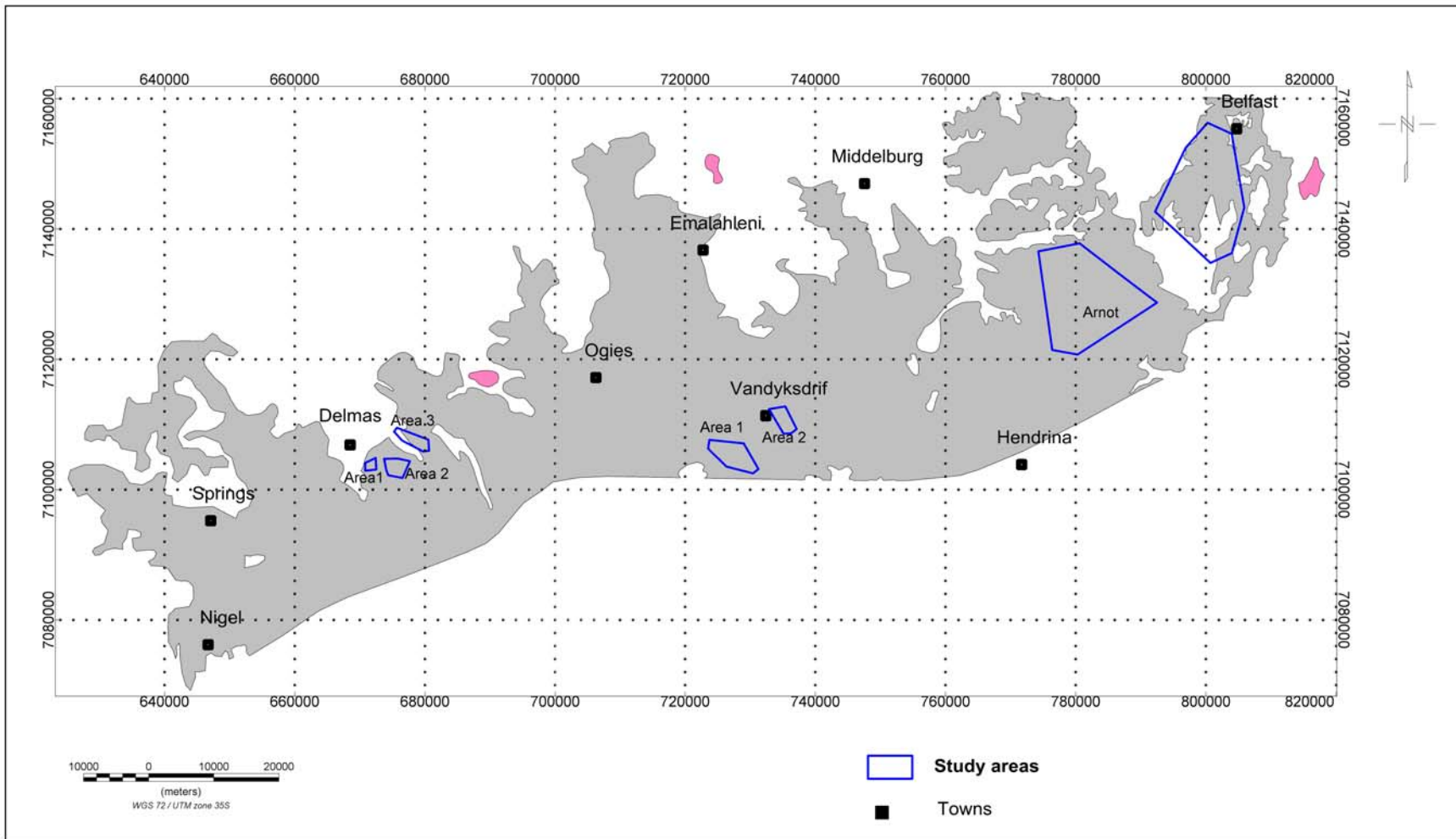


Figure 2. Locality map of the study areas within the Witbank coalfield.

The coalfield extends over a distance of approximately 180km from the Brakpan/Springs area in the west to Belfast in the east and about 40km in the north-south direction (Uludağ *et al.*, 2001). It is separated geologically from the Highveld and Ermelo coalfields to the south by the Smithfield Ridge, a broadly east-west trending crescent-shaped pre-Karoo ridge of felsites, granites and diabase of the Bushveld Complex (Le Blanc Smith, 1980).

The Delmas study areas are located approximately 10km southeast of the town of Delmas, approximately 80km east of Johannesburg and 70km southeast of Pretoria in the Mpumalanga province on the western edge of the Witbank coalfield. They are numbered 1, 2 and 3 (Figure 2).

The Vandyksdrif study areas are located approximately 34km south of Witbank. They are numbered 1 and 2 as seen on Figure 2.

The Arnot study area is approximately 43km by road from Middelburg, 65km by road from Carolina and 25 km by road from Hendrina.

The northeastern boundary of the Belfast study area is approximately 2km southwest of the town of Belfast. The N4 highway cuts the area almost in half in the northeast-southwest direction and the northern border is Exxaro Resources' North Block Complex colliery.

1.2. PROBLEM STATEMENT

From the opening remarks in the introduction three major problems related to mining are identified in which an airborne magnetic survey can play a key role in locating and delineating them. These problems are:

- Faults
- Dykes

- Sills

Mapping of these geological structures will help in:

- Planning of mine layouts.
- Placing of the boxcuts for underground mines.
- Assessments of possible groundwater problems into the mines due to the structures which could be connected to water sources in the vicinity of the mining area.
- Geotechnical studies for slope designs.
- Determination of whether further investigations are necessary to ensure mine safety.
- Ensuring that production is not lost due to the sudden encounter of dykes or loss of coal seams due to faulting.

1.3. OBJECTIVES AND METHODOLOGY

1.3.1. OBJECTIVES

The objectives of the airborne magnetic surveys were to locate and delineate:

- Lineaments interpreted as faults
- Lineaments interpreted as dykes
- Sills.

The interpreted lineaments and sills are then given to the geologist and mine engineer as ArcView shapefiles, which are overlain on top of other geological information and mine layouts to see their positions and possible influence on the planned mining activities.

It must be emphasised that the interpretation done for this work was concerned more with structural delineation than geological interpretation, and that geophysics is by no means a

substitute for drilling but contributes to the better delineation of structural features and aids in optimising borehole positions.

1.3.2. METHODOLOGY

High resolution airborne magnetic data provided by Exxaro Resources Limited were used in the studies. Airborne magnetic surveys were flown on four regions of the Witbank coalfield: a) three blocks to the east of Delmas town, b) two blocks; one east and another southwest of Vandyksdrif area, c) a block northeast of Hendrina town surrounding Arnot region, and d) a block southwest of Belfast town, Figure Figure2. The airborne magnetic data covers a total area of approximately 171001 hectares and the total coverage includes approximately 18817 line-kilometres of flight lines with $\pm 35\text{m}$ terrain clearance on 100m line spacing. The data were flown between December 2007 and March 2008 by Xcalibur airborne geophysics.

Magnetic methods measure the magnetic field, which is related to the percentage of magnetic minerals in a material. Magnetic minerals can be the primary component of the rock formation or can be introduced by the processes such as metamorphism and sedimentation (Hanna, 1969; Criss and Champion, 1984). From airborne data, ground follow-up surveys can be done to verify the results. Modelling can also be done to determine the dimensions of the features of interest.

Topographic maps were used to outline the cultural features such as the power lines and railway lines. The problem with the topographic maps is that they are old and are not updated regularly. Field trips were therefore taken to verify the features which had cultural noise characteristics but not appearing on topographic maps or databases from mines nearby.

Drilling was carried out at some areas in the past and the borehole logs, where available, were used for verification of the interpretations. The available borehole information does not cover the entire study areas and as such boreholes were suggested to verify some

features in each area. The past drilling in most boreholes stopped as soon as the tillite was intercepted and an average borehole depth is approximately 60m. Thus in some cases, even with borehole data, the magnetic features below 60m could not be verified from the borehole data.

1.4. THE GENERAL GEOLOGY OF THE WITBANK COALFIELD

Witbank coalfield is situated on the irregular-eroded northern margin of the Karoo Basin, south of eMalahleni (Witbank), (Pone *et al.*, 2007). The Coalfield is a basin like feature that extends from Brakpan in the West through to Belfast in the East. The northern boundary is the sub-crop against the pre-Karoo basement rocks of predominantly the Waterberg sandstones and the south is a prominent pre-Karoo basement ridge called the Smithfield ridge consisting of diabbases and felsites (Tudor, 2006).

The major controls on the development of the coal are proximity to undulations of the “basement” topography, through erosion channelling and sediment influx into swamp beds and finally erosion of the current erosion surface (Tudor, 2006). The coal measures of the Witbank occur in the Vryheid Formation of the Ecca Group (Winter *et al.*, 1987). Ninety-six per cent of the coal reserves are less than 200m below the surface and over half the reserves are contained in seams thicker than 4 m (Cadle *et al.*, 1993).

Within the Witbank area only the Vryheid Formation is well preserved, whilst southwards and eastwards of the Witbank Coalfield, the underlying and overlying Pietermaritzburg and Volksrust Formations are present (Grodner, 2002). The overlying Volksrust Formation is absent from the Witbank area, due to present-day erosion, whilst the underlying Pietermaritzburg Formation is absent due to non-deposition. The most distinctive post-depositional feature is the intrusion of dolerites related to the Lesotho Basalts that have resulted in a variety of sills and dykes of various ages (Tudor, 2006).

In the central towards the eastern parts of the Witbank coalfield (around Vandyksdrif and Arnot study areas) the Vryheid Formation either lies directly on the tillites, reworked

glaciofluvial tillite or shales of the Dwyka Group, sometimes forming complex interbedded sequences. Alternatively, it rests unconformably on pre-Karoo Proterozoic rocks; predominantly felsites of the Bushveld Igneous Complex (Hatten and Schweitzer, 1995).

The Dwyka Group consists of tillite, diamictite and reworked tillite and shale, overlain by sandstone (Stanimirovic, 2002).

Faults are rare, other than those associated with the emplacement of post-depositional dolerite sills and dykes (Holland *et al.*, 1989).

1.4.1. LOCAL GEOLOGY OF STUDY AREAS

The regional geological maps were digitised from 1:250 000 geological maps: 2628 East Rand (Delmas and Vandyksdrif areas), 2528 Pretoria (Arnot and half of Belfast) and 2530 Barberton (the other half of Belfast).

1.4.1.1. DELMAS AREAS.

In the area of Delmas the coal measures overly tillite of the Dwyka Formation, where the latter forms the lower-most stratigraphic unit of the Karoo Supergroup. The Karoo Supergroup in the area is represented by Dwyka Formation and Middle Ecca with little or no Lower Ecca. In this part of the Witbank coalfield, the pre-Karoo basement is comprised mainly of dolomite, chert and quartzite of the Malmani Group (Transvaal Supergroup), (Tudor, 2006).

The Dwyka tillite discordantly overlies the cherts and dolomites of the Malmani Formation of the Transvaal Supergroup (SACS, 1980). The Vryheid Formation is unconformably overlain by sandstones of the Volksrust Formation of the Ecca Group (SACS, 1980). The period of Dwyka glaciation, coupled with the fact that the glaciated surface is largely a dolomite sequence, resulted in a highly irregular and undulating basement onto which the Karoo sediments were deposited. Intrusion of the dolerite sill



very close to the pre-Karoo contact has resulted in large areas of bottom coal being devolatilised. Associated with the sill are a number of thin dolerite dyke-like structures that crosscut the stratigraphy.

Five geological units (Figure 3) are observed: Hospital Subgroup of Witwatersrand Supergroup (comprising partly ferruginous shale, quartzite and the contorted bed of banded ironstone), Malmani Subgroup (comprising dolomite and chert), Vryheid Formation of the Karoo Supergroup (comprising sandstone, shale and coal beds), dolerite and alluvium. Figure 4 shows the general stratigraphy of Delmas area.

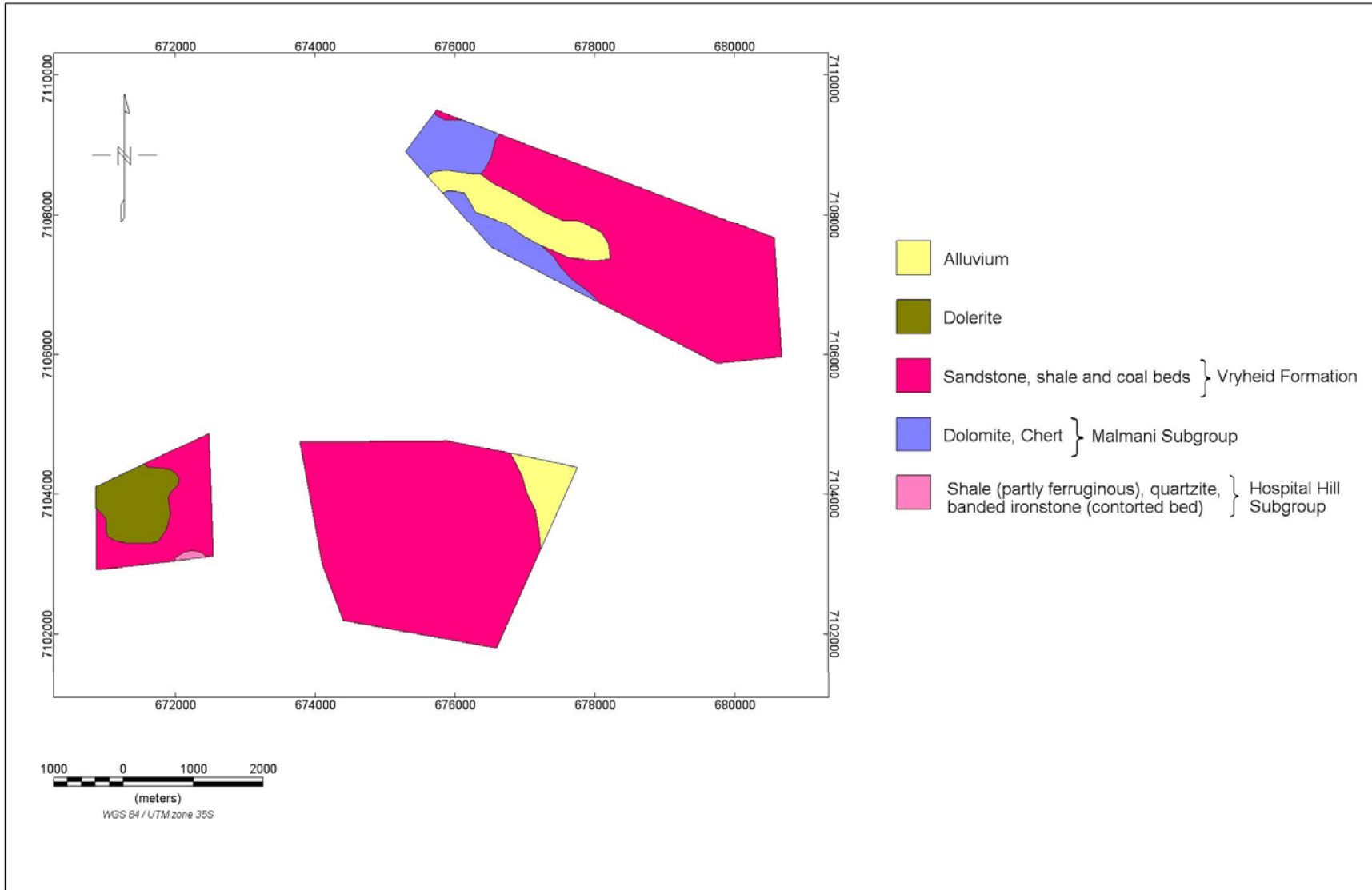


Figure 3. Regional geology of Delmas study areas (modified from 1:250 000, 2628 geological map of East Rand)

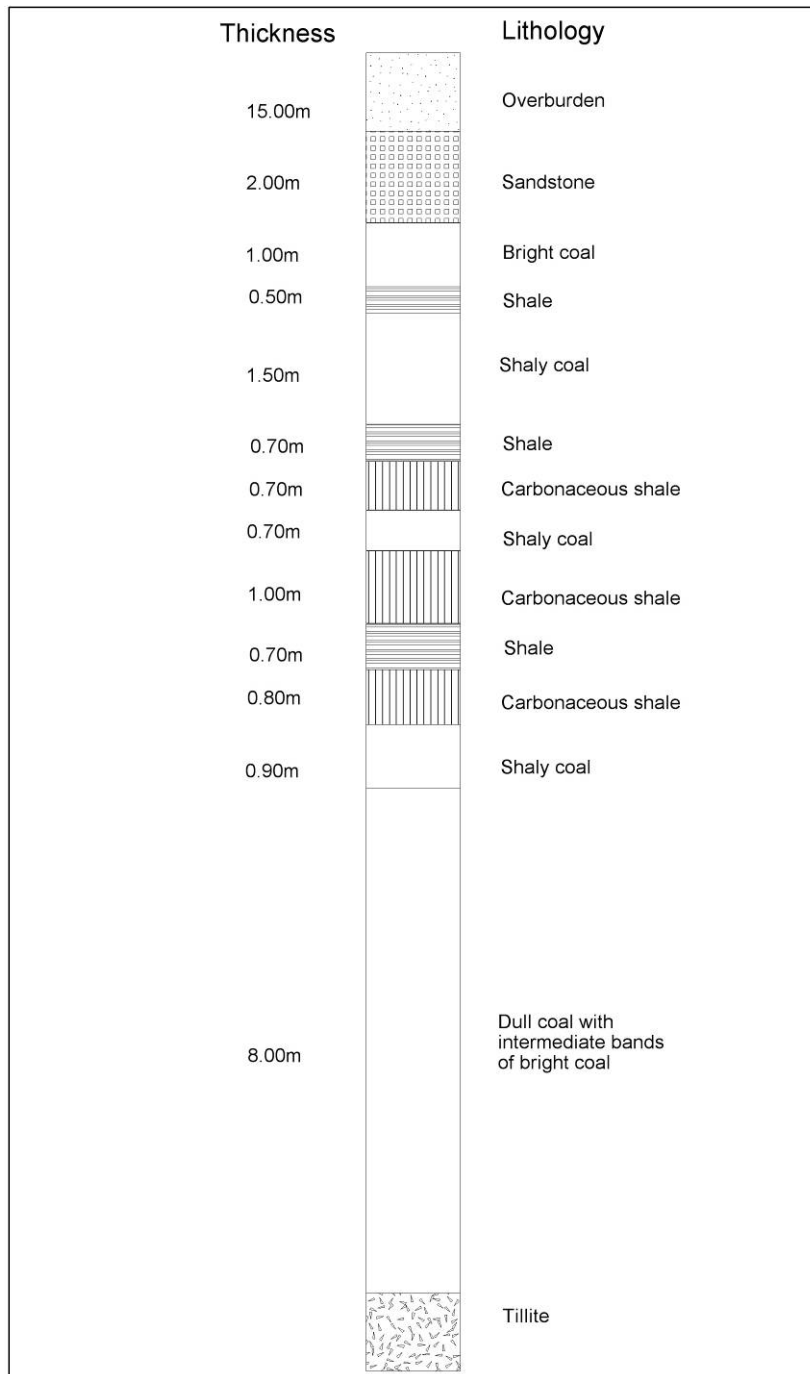


Figure 4. The general stratigraphy of Delmas region (from Tudor, 2006).

1.4.1.2. VANDYKDRIF AREA

The geology of both areas 1 and 2, and the stratigraphy is the same as discussed in the paragraphs that will follow but the geophysical interpretation was done separately.

Each area as seen on the regional geology maps (Figures 5 and 6) is over ninety percent covered by sandstones, shales and coal beds with a minor occurrence of alluvium and dolerite. Figure 7 shows the general stratigraphy.

The coal succession occurs within the Permian-age Vryheid Formation of the Ecca Group, which overlies the Dwyka Group. The sediments of the Karoo Supergroup were deposited on an irregular Pre-Karoo basement, which to some extent influenced the distribution of the overlying lithologies (Tudor, 2006). The pre-Karoo basement rocks generally comprise gabbros, diabases and felsites associated with the Bushveld Igneous Complex.

The generally flat-lying Vryheid formation sedimentary rocks consist of sandstones, thinly laminated siltstones and mudstones and coal Seams. The episodic intrusion of the dolerite dykes and sills have further complicated the geology, causing minor faults, where the displacement is less than the Seam thickness.

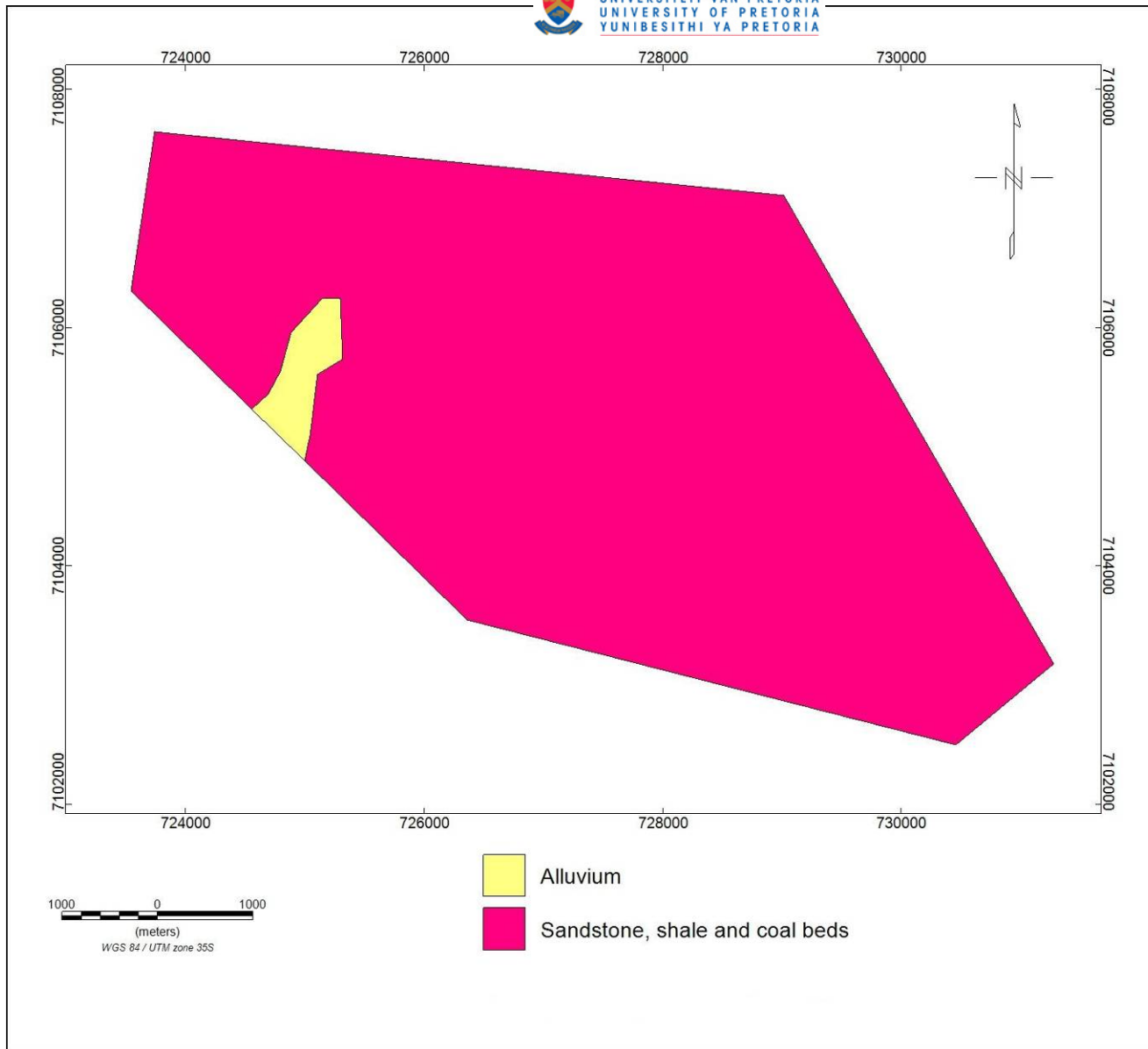


Figure 5. Regional geology of Vandyksdrif study area 1 (modified from 1:250 000, 2628 geological map of East Rand).

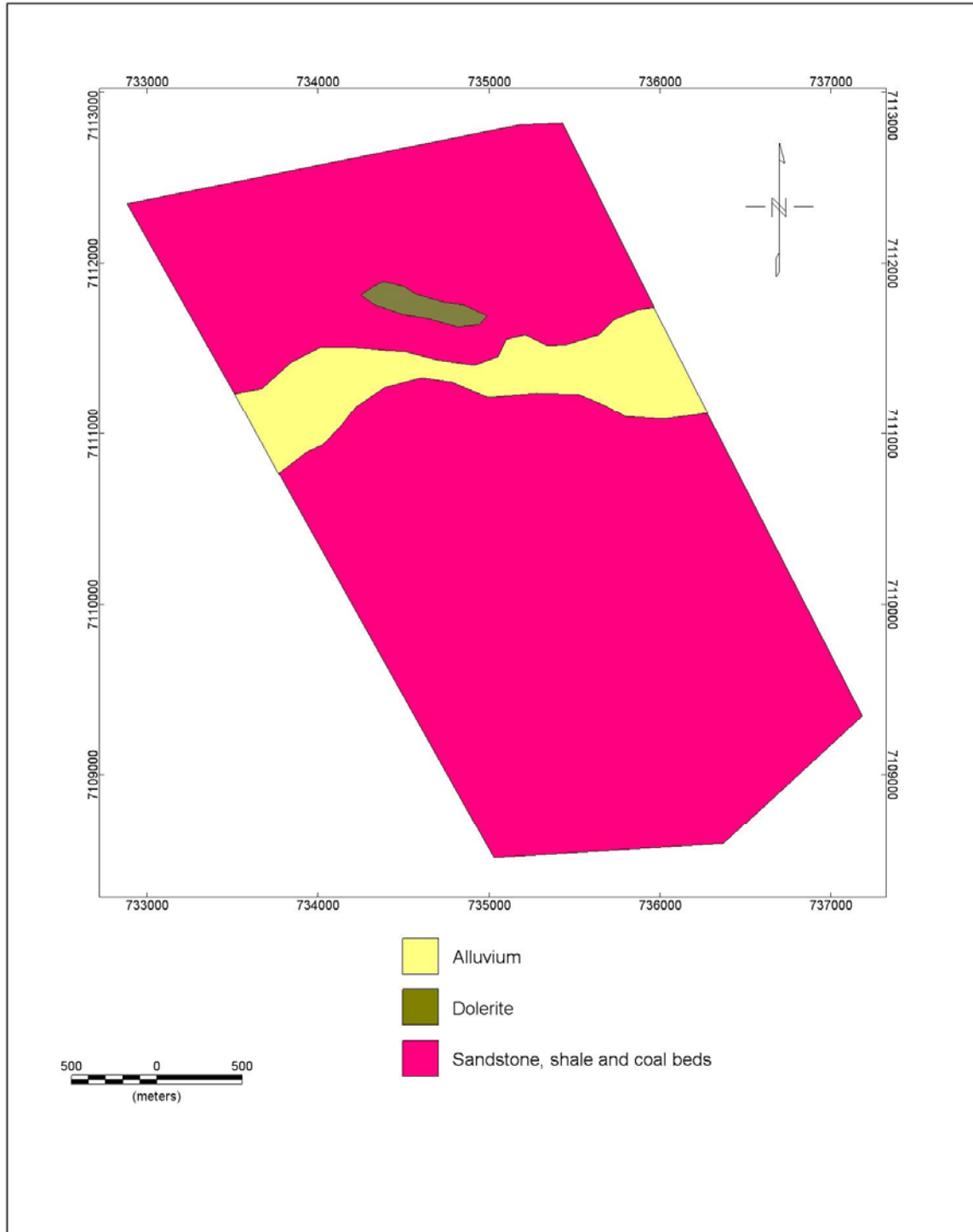


Figure 6. Regional geology of Vandyksdrif study area 2 (modified from 1:250 000, 2628 geological map of East Rand).

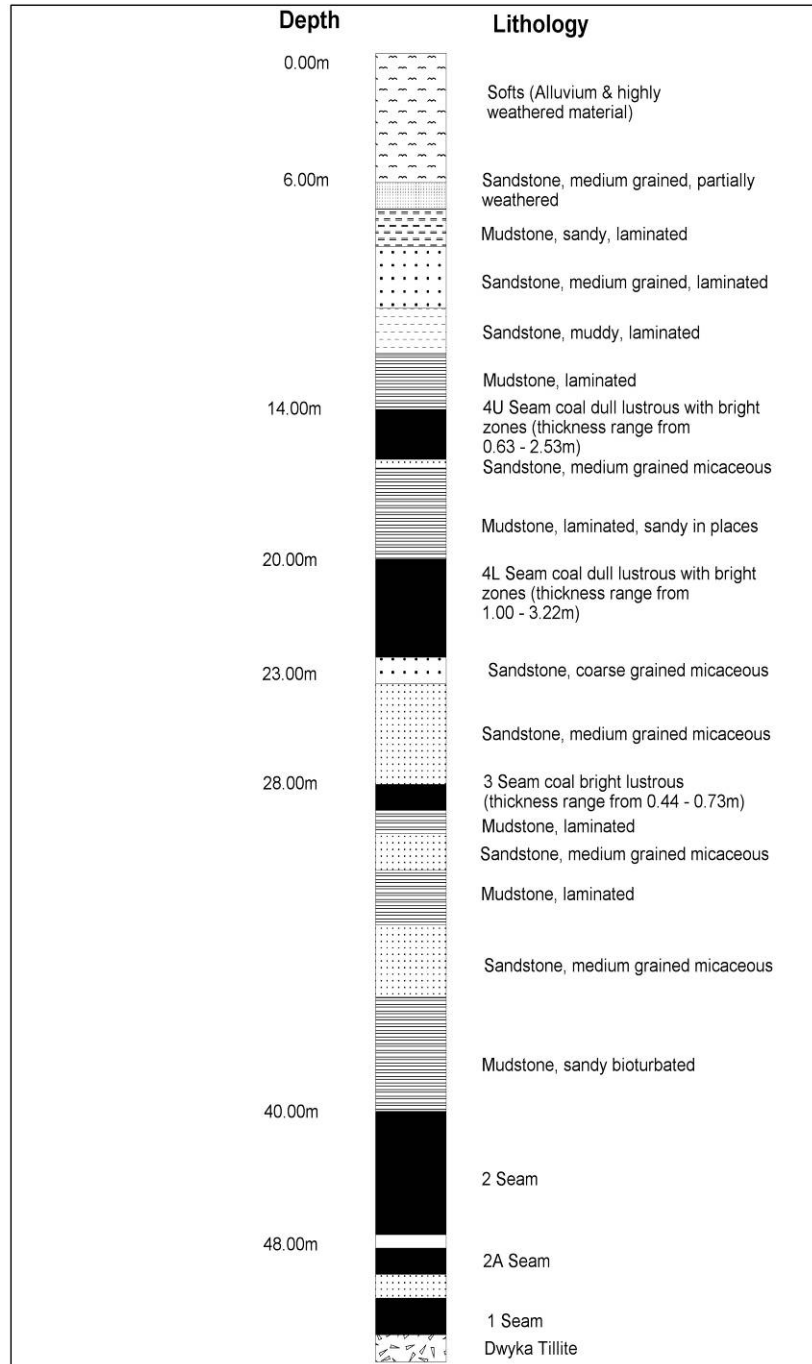


Figure 7. The general stratigraphy of Vandyksdrif area (from Tudor, 2006).

1.4.1.3. ARNOT AREA

The coal seams occur stratigraphically within the basal Dwyka Group, conformably overlain by the Vryheid Formation of the Eccca Group. Pre-Karoo basement rocks consist of both Felsite and Diabase intrusives associated with the Transvaal Supergroup and the Bushveld Igneous Complex respectively. The diabase occurs over most of the area as dyke and plug like bodies (Tudor, 2006). The top of the pre-Karoo is a generally highly weathered horizon unconformably overlain by Karoo sediments. The top of the pre-Karoo is undulating forming palaeo “valleys” and palaeo “highs” and a gentle regional dip from the northeast to southwest is noted.

The Dwyka Group is a conglomerate with the matrix ranging from sandstone to shale. The clasts are generally of pre-Karoo origin with sizes ranging from angular fragments to boulders. The Dwyka Group attains a maximum thickness of 2m and is generally absent over palaeo-highs.

The Vryheid Formation consists of a number of depositional sequences (culminating in a peat formation) and is overlain by a number of transgressive events. The Vryheid Formation conformably overlies the Dwyka Group, with the conglomerates grading into a gritty sandstone and minor shale lenses.

A limited number of dolerite dykes are known to have intruded the Karoo sediments in the area. The dykes are believed to be generally non magnetic (Campbell, 1994) and that they are not responsive to magnetic methods. A well-developed dolerite sill is present in the topographically elevated areas in the south-eastern portion of the Coalfield. The feeder dykes are expected to occur in the vicinity of the sill. Faults with displacement in excess of 2.5m are rare.

Figure 8 shows the regional geology of Arnot area and Figure shows the general stratigraphy.

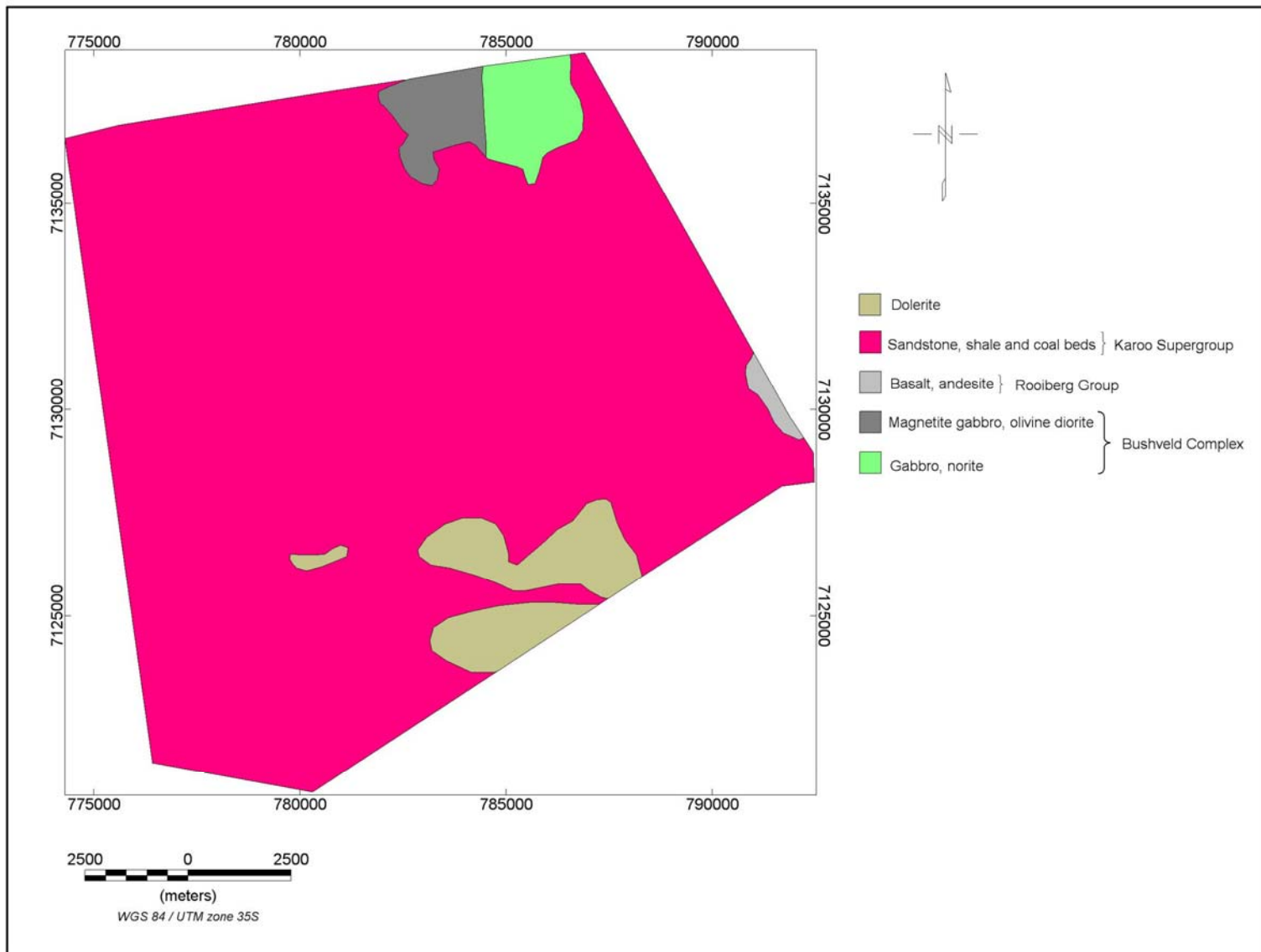


Figure 8. Regional geology of Arnot study area (modified from 1:250 000, 2528 geological map of Pretoria).

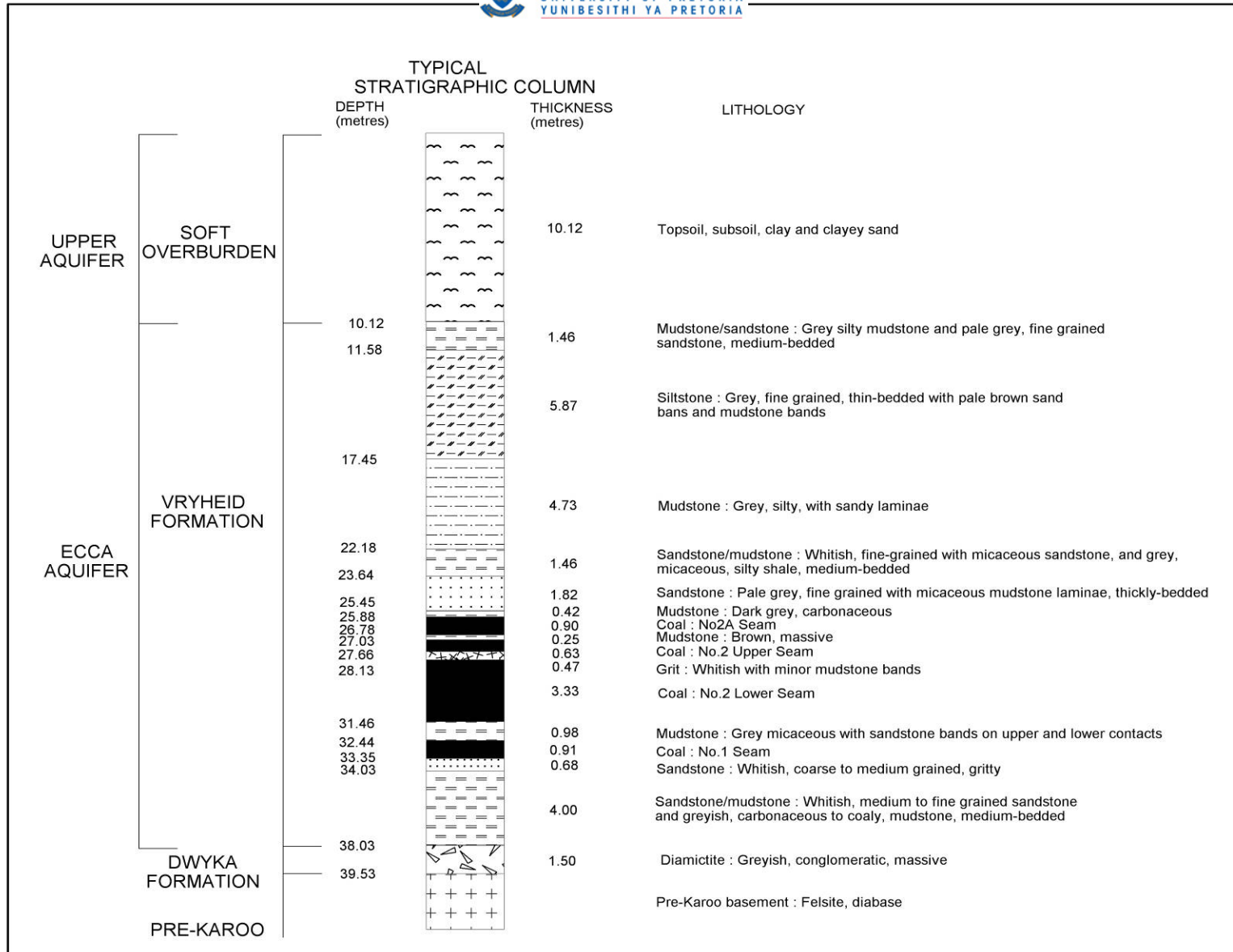


Figure 9. The general stratigraphy of Arnot study area (from Gemmel, 2001).

1.4.1.4. BELFAST AREA

The Karoo Sequence in the area is represented by the Dwyka Formation and the Middle Ecca with little or no lower Ecca Development. The Middle Ecca sequence of coal horizons interbedded with the sediments is highly truncated due to erosion with only very minor areas where the full sequence is developed. The generally flat-lying Vryheid formation sedimentary rocks consist of sandstone, thinly laminated siltstone and mudstone and coal Seams. The pre-Karoo basement rocks generally comprise gabbros, diabases and felsites associated with the Bushveld Igneous Complex.

The primary control on the development of the peat in this area is the pre-Karoo basement palaeotopography of the Bushveld Igneous Complex lithologies and the current weathering induced by the current erosion surface (Tudor, 2006). Subsequent intrusion of a dolerite sill very close to the pre-Karoo contact has resulted in some areas being heat affected and faulted.

Figure 10 shows the regional geology map and Figure 11 shows the general stratigraphy.

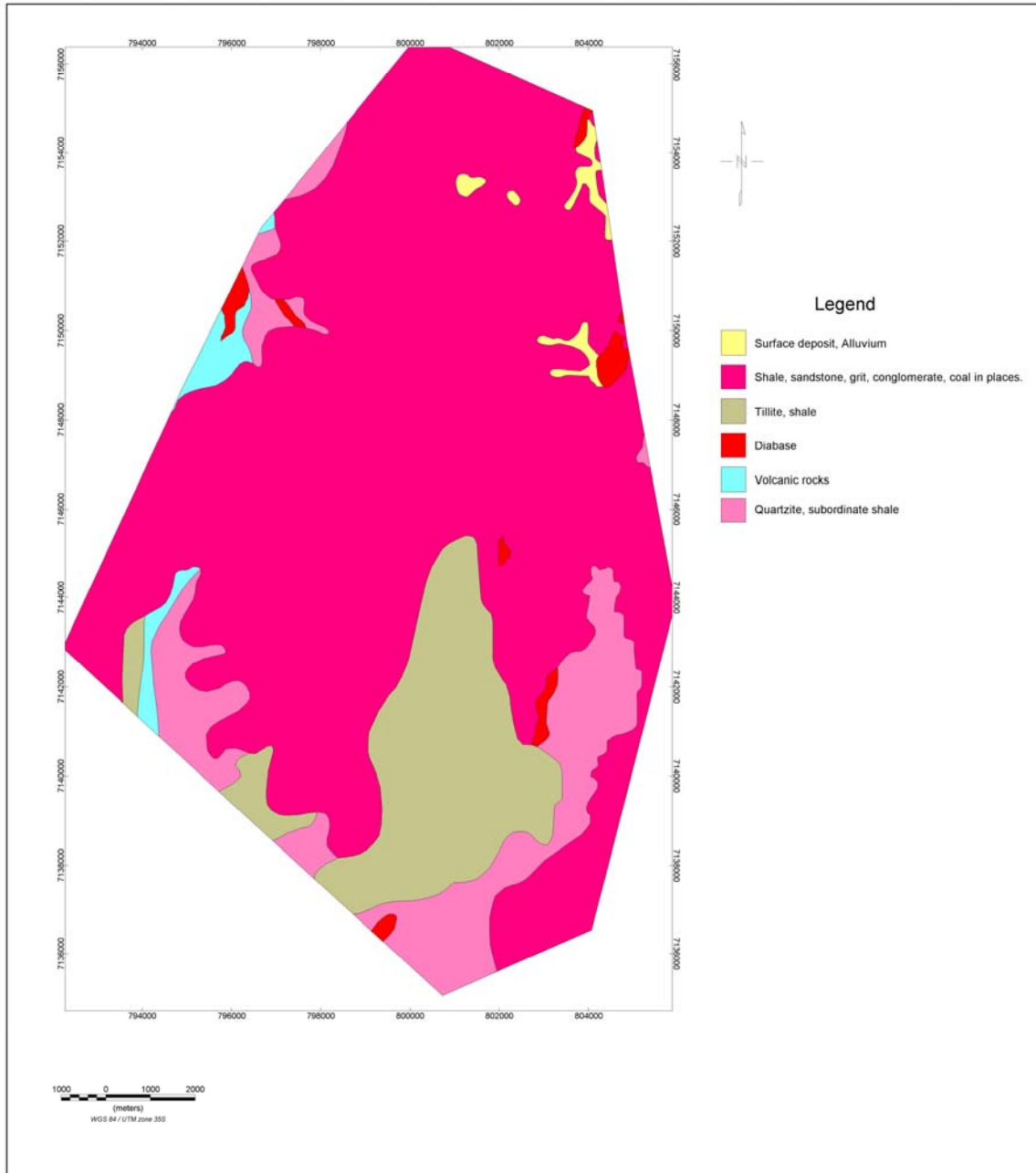


Figure 10. Regional geology of Belfast study area (modified from 1:250 000, 2528 geological map of Pretoria and 1:250 000, 2530 geological map of Barberton).

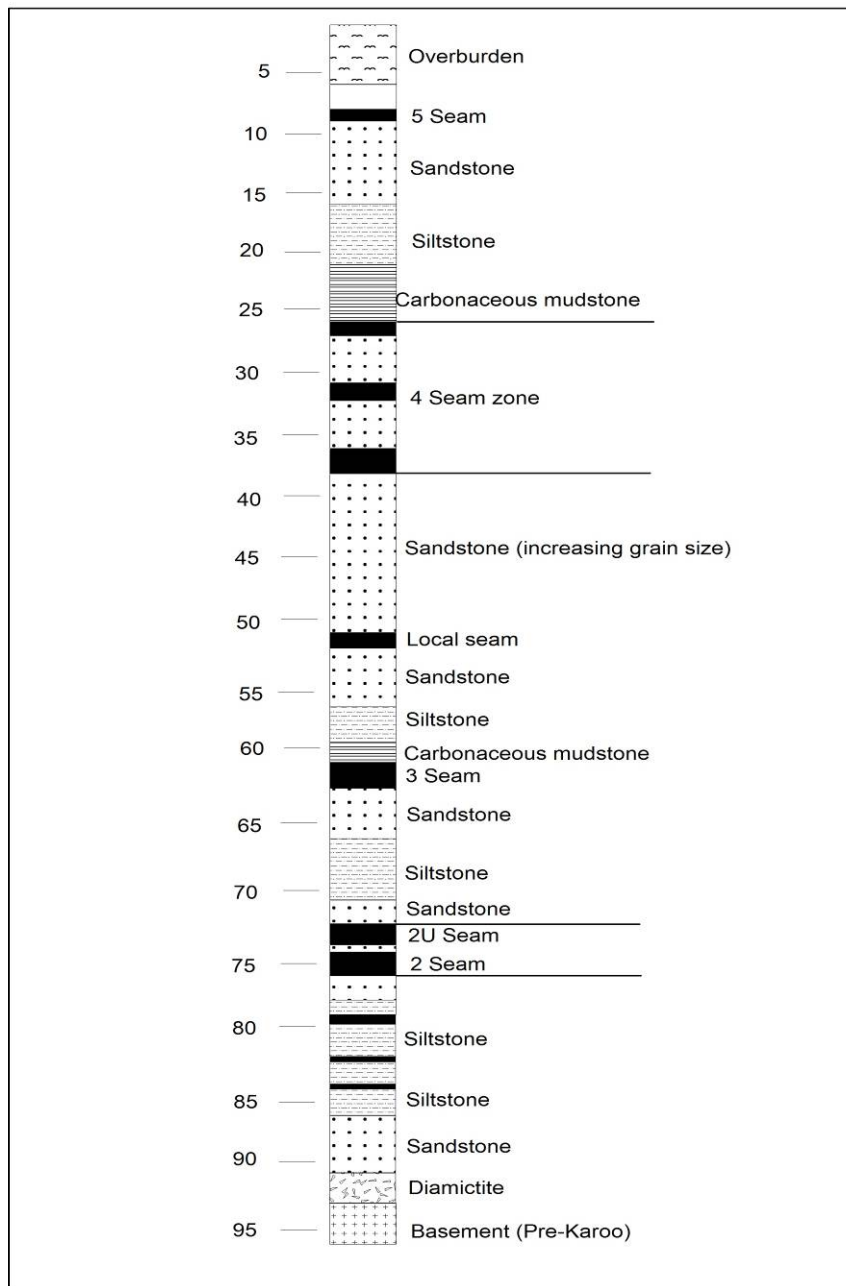


Figure 11. The stratigraphy of Belfast study area (from Tudor, 2006)

CHAPTER 2

MAGNETIC CONCEPTS

2.0. AN OVERVIEW OF THE MAGNETIC METHOD

Magnetic surveys measure the magnitude and orientation of the Earth's magnetic field.

Geological structures (like faults, dykes and folds) may produce small magnetic fields that distort the main magnetic field of the earth. Such a disturbance is called a magnetic anomaly.

The anomalies can be detected by measuring the Earth's magnetic field on or near the surface of the ground. Above the ground, magnetic measurements are made from an aircraft flown along closely spaced, parallel flight lines. Additional flight lines are flown in a perpendicular direction to assist in data processing. These measurements are then processed and presented as digital aeromagnetic maps. Assisted by computer programs, structural interpretations are developed from these data; incorporating already mapped geologic structures and other geophysical information, where available. By analysing magnetic measurements, geophysicists are able to learn about geologic structures, even when the structures may be concealed entirely below the earth's surface (Dobrin and Savit, 1988; Blakely, 1995). The illustration of magnetic method is shown on Figure 12.

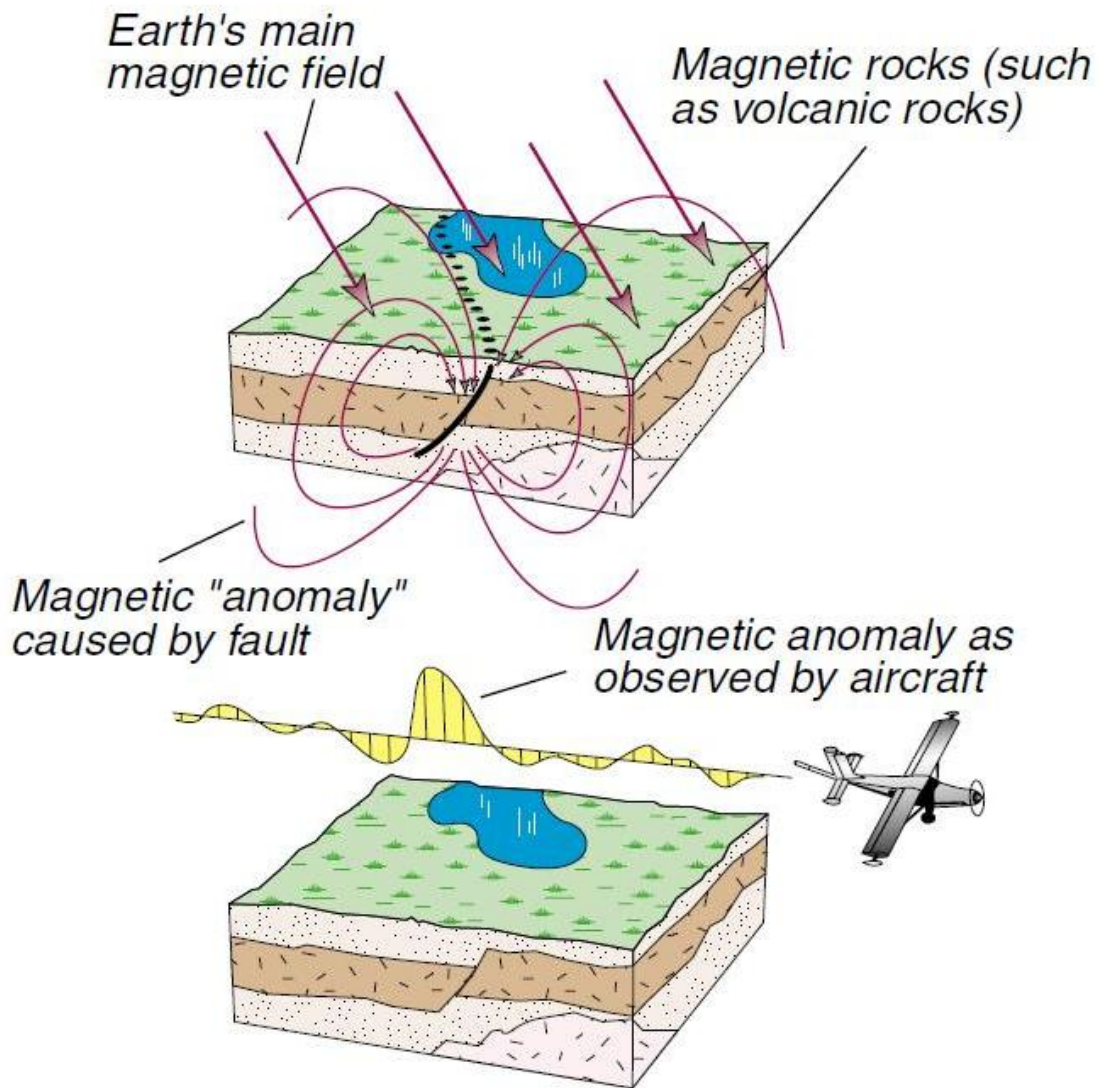


Figure 12. Cartoon illustration of the magnetic method (from Blakely et al., 2000). Magnetic rocks (such as the faulted volcanic unit shown here) produce small magnetic fields that perturb the much larger field originating from the earth's core. Much can be learned about magnetic rocks by measuring the magnetic field near the topographic surface, even though those rocks may be completely concealed.

2.1. THE EARTH'S MAGNETIC FIELD.

The Earth possesses a magnetic field caused primarily by sources in the core. (www.usace.army.mil/usace-docs/eng-manuals/em1110-1-1802/toc.htm). The form of the field resembles that of a large bar magnet with two poles (North and South) located near the earth centre and aligned sub-parallel to the geographic axis. Magnetic poles always exist as *dipoles*; pairs of poles of opposite polarity. If one pole is sufficiently distant so that it does not affect the other, it is said to be a *monopole*.

Magnetic dipoles can also interact with one another at distance, by means of their magnetic fields. Coulomb has shown that the force \mathbf{F} between two magnetic poles of strengths m_1 and m_2 separated by a distance r obey an inverse distance squared law, i.e.

$$\mathbf{F} = \frac{\mu_0 m_1 m_2}{4\pi\mu_R r^2} \quad (1)$$

where, μ_0 and μ_R are constants corresponding to the magnetic permeability of vacuum and the magnetic permeability of the medium separating the poles, respectively. The force is attractive if the poles are of opposite sign and repulsive if they are of like sign.

A **magnetic field** is the space in which a magnetic pole experiences a force or it is the space around a magnet in which the influence of the magnet is felt. The magnetic field strength vector \mathbf{B} (magnetic induction), is defined as the magnetic force experienced by a unit pole placed at that point. If a magnetic pole of strength m placed at a point in a magnetic field experiences a force \mathbf{F} , the magnetic induction at that point is:

$$\mathbf{B} = \frac{\mathbf{F}}{m} \quad (2)$$

where, m is essentially the instrument used in measurement (Telford *et al.*, 1976).

The magnetic field strength can also be defined in terms of current flowing through a loop of wire by Biot-Savart's Law. The magnetic field produced is equivalent to a magnetic dipole at the centre of loop.

Magnetic fields can also be defined in terms of a potential. Magnetic potential is defined as the work required to bring a unit pole from infinity to some point in space in the presence of a magnetic field and is given by:

$$V = \frac{\mu_0 m_1}{4\pi\mu_R r} \quad (3)$$

The magnetic field in any direction is then given by the partial derivative of the potential in that direction.

2.2. MAGNETIC PROPERTIES OF MATERIALS

2.2.1. Magnetising field

The magnetic field used to magnetise a material is called the magnetising field. It is denoted by **H**.

2.2.2. Magnetic permeability (μ)

Magnetic permeability is the ability of the material to allow the passage of magnetic lines of force through it. Magnetic permeability μ of a medium is also defined as the ratio of magnetic induction **B** inside the medium to the magnetising field **H** inside the same medium.

$$\therefore \mu = \frac{\mathbf{B}}{\mathbf{H}} \quad (4)$$

2.2.3. Induced and remanent magnetism

Magnetic anomalies in the Earth's magnetic field are caused by two types of magnetism: induced and remanent magnetism. The induced magnetism of the body is in the same direction as the day's Earth field whereas the remanent magnetism need not be in the same direction and could even oppose the earth's field. If the Earth's field could be removed the induced magnetism would disappear but remanent magnetism would remain.

2.2.3.1. Induced magnetism (J_i)

When a magnetisable material is placed in a magnetic field it will become magnetised in the direction of the applied field. This phenomenon is called *induced magnetisation*. The intensity of the induced magnetisation of a magnetic material is defined as the magnetic moment per unit volume of the material, i.e.,

$$J_i = \frac{M}{V} \quad (5)$$

The magnetic moment of a magnet (M) is defined as the product of the pole strength and the distance between the two poles.

The intensity of the induced magnetisation, J_i , is proportional to the strength of the magnetic field (and is in the direction of the field) and to the ability of the material to enhance the local field, a property called magnetic susceptibility.

$$J_i = kH \quad (6)$$

where,

J_i = Intensity of Magnetisation

k = magnetic susceptibility (unitless)

\mathbf{H} = Field intensity in Tesla (T)

If \mathbf{J}_i is constant and is in the same direction throughout the body, the body is said to be uniformly magnetised by induction. For most rock materials k is much less than 1 and usually of the order of 10^{-3} in SI units.

2.2.3.2. Remanent magnetism (\mathbf{J}_r)

This is due to the previous history of the rock. Remanent magnetisation is the permanent magnetisation of a material in the absence of an external magnetic field, and thus occurs only in the materials which exhibit hysteresis, i.e. irreversibility of magnetic behaviour with applied field (Hunt *et al.*, 1994). The direction of this magnetisation, \mathbf{J}_r , may not necessarily be in the direction of the inducing vector (Earth's magnetic field) and could even oppose the field.

The ratio between \mathbf{J}_r and \mathbf{J}_i is called the Königsberger ratio, Q . Königsberger ratios attest the comparative importance of remanent and induced magnetisation, with remanence dominant for $Q > 1$ and induced for $Q < 1$ (Alva-Valdivia *et al.*, 2003).

The direction and strength of the present Earth's field is known. However, we may know nothing about the remnant magnetisation of a rock. For this reason, and because in strongly magnetised rocks the induced field dominates, it is often assumed that all the magnetisation is induced. The true magnetisation is the vector sum of the induced and remnant components, i.e.:

$$\mathbf{J} = \mathbf{J}_i + \mathbf{J}_r \quad (7)$$

2.2.4. Magnetic susceptibility (k)

Magnetic susceptibility is a property which determines how easily and how strongly a material can be magnetised. Susceptibility of a magnetic material is defined as the ratio of intensity of magnetisation \mathbf{J}_i induced in the material to the magnetising field \mathbf{H} in which the material is placed (or the amount of magnetic minerals, mainly magnetite and pyrrhotite, contained within a rock). Rock forming minerals (quartz, feldspar, etc) are virtually non-magnetic so the magnetic susceptibility is related to the amount of minor accessory minerals in a rock which contains iron such as magnetite and pyrrhotite (Fourie, 1998). Campbell (1994) indicates that most basic intrusions such as dolerite dykes or dunite pipes carry accessory magnetite and thus can be mapped from magnetic surveys.

From equation 6, magnetic susceptibility k becomes:

$$k = \frac{\mathbf{J}_i}{\mathbf{H}} \quad (8)$$

2.2.5. Elements of the Earth's magnetic field

The magnetic field at any point on the Earth's surface is a vector field and can be described by 3 vectors and 2 angles. Figure shows the components of Earth's magnetic field.

The 3 vectors are:

- Horizontal field (\mathbf{H})
- Vertical field (\mathbf{Z})
- Total field (\mathbf{T})

The 2 angles are:

- Declination (D)
- Inclination (I)

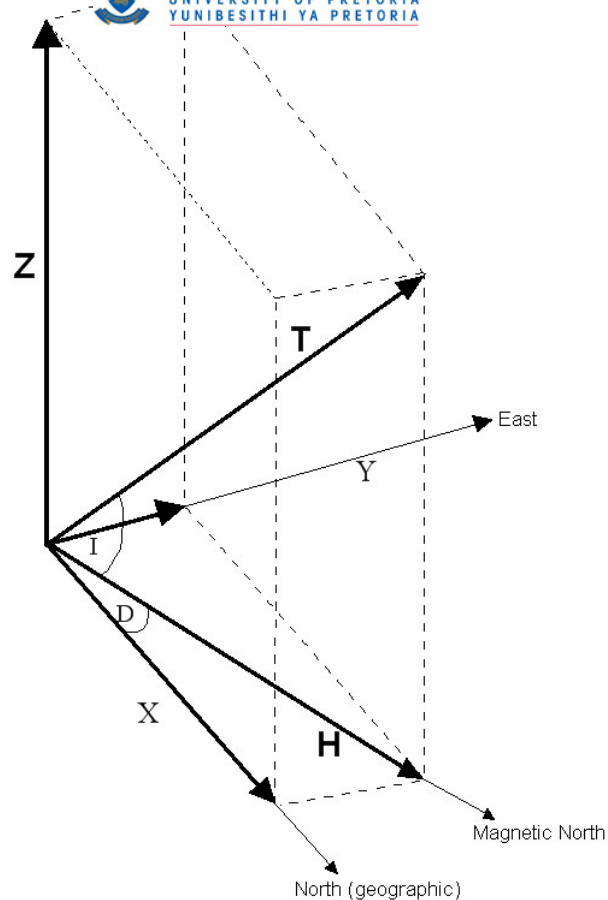


Figure 13. Components of the Earth's magnetic field.

Equations relating the 3 vectors and 2 angles include:

$$\mathbf{H} = \mathbf{T} \cos (I)$$

$$\mathbf{Z} = \mathbf{T} \sin (I) = \mathbf{H} \tan (I)$$

$$\mathbf{X} = \mathbf{H} \cos (D)$$

$$\mathbf{Y} = \mathbf{H} \sin (D)$$

$$\mathbf{X}^2 + \mathbf{Y}^2 = \mathbf{H}^2$$

$$\mathbf{X}^2 + \mathbf{Y}^2 + \mathbf{Z}^2 = \mathbf{T}^2 = \mathbf{H}^2 + \mathbf{Z}^2$$

In the southern hemisphere the Total field vector, \mathbf{T} , is directed upwards and away from the south magnetic pole. It makes an angle I° (the inclination) to the horizontal component \mathbf{H} and is negative. The horizontal component \mathbf{H} has an angle D° (declination) from the geographic north. At the magnetic equator the magnetic field is horizontal ($I =$

0) and at the magnetic poles the field is vertical ($I = 90$). The average values of I , D and T in the survey areas are approximately -62° , -18° and 28800 nT (nanoteslas) respectively.

The magnetic field intensity varies considerably by location over the surface of the earth. It is greatest at the magnetic poles and least at the magnetic equator. Time variations can have a large effect on the field surveys and a means for removing them must be an integral part of survey design.

Two temporal variations of the Earth's magnetic field are of interest to geophysicists:

- *Diurnal Variations* - These are variations in the magnetic field that occur over the course of a day and are related to the variations in the Earth's external magnetic field. This variation can be on the order of 20 to 30 nT per day (Telford *et al.*, 1990) and should be accounted for when conducting exploration magnetic surveys.
- *Magnetic Storms* - Occasionally, magnetic activity in the ionosphere will abruptly increase. The occurrence of such storms correlates with the enhanced sunspot activity. The magnetic field observed during such times is highly irregular and unpredictable, having amplitude changes as large as 1000 nT (Telford *et al.*, 1990). Exploration magnetic surveys should not be conducted during magnetic storms.

2.3. MAGNETIC LITHOLOGIES

Since the Karoo Basin rocks are weakly magnetic (Tudor, 2006), the most ubiquitous magnetic lithologies would be the basement rocks: felsites, dolerites and diabases in the form of intrusions. Long-wavelength, low amplitude anomalies associated with Bushveld complex basement rocks and short-wavelength, high amplitude anomalies associated with intrusions are expected. Faults that offset these units often produce magnetic anomalies that appear as linear trends on aeromagnetic maps (Mahanyele and Botha, 2008). Parts of

some of the study areas are covered with relatively non-magnetic alluvial deposits, and the alluvium-filled basins are expected to produce only subdued aeromagnetic patterns (Campbell, 1994). Basic flows (dolerite and diabase dykes and sills) contain higher concentrations of magnetic minerals, thus they can be outlined with magnetic measurements when they occur within a sedimentary sequence that normally contains little or no magnetic minerals.

2.4. INSTRUMENTATION

The instrument used to measure magnetic fields is called a magnetometer. Below is a description of the magnetometers used:

- Fluxgate
- Alkali vapor.

The *fluxgate magnetometer* was developed during World War II for airborne antisubmarine warfare applications (Nabighian *et al.*, 2005). After the war, it was immediately adopted for exploration geophysics and remained the primary airborne instrument until the proton precession magnetometer was introduced in the 1960s.

The fluxgate magnetometer is based on the properties of the magnetisation curves of a highly magnetically permeable material (Urquhart, 2003). The two bars of this material are oriented such that, in the absence of a magnetic field, the magnetisation curves of the two bars are equal but opposite. In the presence of a magnetic field, the magnetisation of the two bars is different and the difference is measured as a voltage in an output coil.

It records either the total magnetic intensity or one of its three vector components and has a wide dynamic range.

A three axis fluxgate magnetometer is typically included in all airborne survey systems to support data correction for magnetic interference from the aircraft or other sources. A

three axis fluxgate magnetometer records the orientation of the aircraft in the Earth's main magnetic field and this information is used to correct the main magnetic measurements for the orientation effects of the aircraft in a process called "magnetic compensation" correction. The effectiveness of compensation is called the Figure of Merit (FOM). A detailed discussion of the fluxgate magnetometer can be found in Telford *et al.*, (1990).

The *Alkali vapor magnetometers*, with sensitivities around 0.01 nT and sample rates of 10 Hz, appeared in laboratories about the same time that proton precession magnetometers became popular field instruments (Nabighian *et al.*, 2005). But because they were more fragile than proton precession magnetometers, and because the increased sensitivity was of marginal value, their use as field instruments was mostly restricted to gradiometers until the late 1970s. Today, alkali vapor magnetometers are the dominant instrument used for magnetic surveys, although some proton precession instruments are still in use for ground surveys, and fluxgates are used for borehole surveys.

Alkali vapor magnetometers are based on the excitation of electrons to the different energy levels by irradiating an alkali gas (e.g. sodium or caesium vapour) with light of a specific energy. The electrons of the gas are optically raised (pumped) to a higher energy level which is a function of the magnetic spin moment and the ambient magnetic field. The amount of the light which is absorbed by the gas in exciting the electrons to a higher energy level is proportional to the total magnetic field. A detail discussion of the alkali vapor magnetometers can be found in Telford *et al.*, (1990).

2.5. APPLICATION OF MAGNETIC METHODS IN MINING

The following information is based on Fourie, (1998). As early as 1928 iron-ore deposits; rich in magnetite, ilmenite, pyrrhotite or some other strong magnetic minerals, have been located by magnetic methods (Brough *et al.*, 1928). In 1935, the course of Acklington Dyke Northumberland was plotted by means of Watts Magnetic Variometer (Poole *et al.*, 1935) and during 1959 D.A. Robson resurveyed this dyke using a Proton magnetometer.

This instrument was claimed to be of “high sensitivity” (Robson, 1964). In addition to confirming the position of this dyke, more accurate information on various geological aspects of the dyke were obtained due to the more sophisticated equipment being used.

Campbell (1994) reported that the earlier ground magnetic work in the Ermelo district of the previously eastern Transvaal had shown the dolerite intrusions to be only weakly magnetic and of variable strike orientation. To map this large target area ($\pm 200\text{km}^2$) cost effectively the first aeromagnetic survey to do ‘detailed dyke mapping’ was done during 1983. Since this early start the sophistication of aeromagnetic surveys has increased significantly and this technique is now routinely used by the South African coal mining industry.

Aeromagnetic surveys are routinely flown as part of the information gathering process for mine planning purposes to identify the geological structures such as dykes, sills and faults. They are also used in exploration for outlining the geological targets for drilling, e.g. mapping magnetite in iron ore exploration. The information is also used for investigations on areas earmarked for the boxcut positions in order to avoid placing the boxcuts in positions of unsuitable geological conditions such as shear zones.

CHAPTER 3

DATA ACQUISITION AND PROCESSING

3.0. DATA ACQUISITION.

The following is a list of acquisition systems and the parameters used for data collection on all the study areas (Steenkamp, 2008).

3.0.1. AIRCRAFT AND ACQUISITION SYSTEMS

- Aircraft type: Air Tractor
- Survey navigator: AgNav
- Data acquisition: XAGDAS
- Data positioning: Real time differential GPS
- GPS type: 2100LR, 12 channel, Omnistar
- Resolution: $\pm 3\text{m}$
- Magnetometers: 1 x Geometrics G822A Cesium Vapor
- Base station magnetometer: GEM Systems (GSM-19TW)
- Compensation: RMS AARC5000
- Resolution: 0.001nT
- Radar altimeter: King

3.0.2. BASIC SURVEY PARAMETERS USED

- Line direction: North - South with respect to UTM Zone 35S, WGS84 coordinate system.
- Line spacing: 100 meters
- Tie line direction: East - West with respect to UTM Zone 35S, WGS84 coordinate system.

- Tie line spacing: 1000 meters
- Ground clearance: 35 meters
- Sample spacing: 6.6 meters
- Data collected:
 - Total Field Magnetism with wing mounted Cesium Vapor sensor
 - Digital Terrain Model (DTM) with real time differential GPS and Radar altimeter.

DTM is calculated by subtracting the radar altimeter readings from the differential GPS height.

3.1. DATA PROCESSING

Processing of the aeromagnetic data was done by Xcalibur Airborne Geophysics using Geosoft software and the resultant total field magnetic grids, vertical derivative grids and analytic signal grids were given for interpretation. Processing involved a number of steps and Xcalibur Airborne Geophysics followed the processing steps given below (Steenkamp, 2008). Phase 1 processing was done in the field while the second phase was done in the office.

3.1.1. Phase1 – Pre-processing

- Download and backup of binary data
- Verification of the raw data:
 - flight path
 - altimeter and digital GPS data
 - sample density
 - DTM
 - compensated magnetic data
 - diurnal magnetic field
 - raw magnetic data

Verification involved inspection of the data for spikes, gaps, instrument noise or any other irregularities in the data. This was carried out in the field so that errors attributable to data acquisition could be corrected in the survey aircraft as quickly as possible and re-flights carried out if necessary before demobilisation.

- Locating the data in x and y

After checking and editing the navigation data, it was merged with the magnetic data for location of the magnetic data.

The second part of processing followed some of the processing procedures given by Luyendyk (1997):

3.1.2. Phase 2 - Processing

- *Parallax corrections*

This is done to synchronise magnetic and navigational data since the distance between the navigation reference point along the axis of the aircraft and magnetometer recording instrument is not zero.

- *Diurnal variation correction*

Base station magnetometer recordings were used.

- *GRF - Removing the Earth's regional magnetic field*

This processing step involves subtracting a well-defined model of the Earth's regional field, the so called **Geomagnetic Reference Field (GRF)**, from the data.

- *Levelling*

Levelling was done using the tie lines, which were flown perpendicular to the survey lines. The points where survey lines intersect the tie lines are called *crossover points*. The magnetic reference to which the magnetic data are levelled is time invariant and, therefore, any discrepancy at a crossover point represents an error. Levelling reduces the discrepancies between the magnetic readings at crossover points by systematically proportioning them between survey and tie lines.

- *Micro-levelling*

Micro-levelling is a general term that refers to the removal of the remaining residual errors in the aeromagnetic data after standard processing and the application of levelling process (Saul and Pearson, 1998). A de-corrugation filtering technique was applied for micro-levelling.

- *Gridding*

When dealing with two-dimensional data, it is useful to represent the data by determining its value at points located equally far apart at the nodes of a grid. Data in grid format is suitable for a number of two-dimensional processes, such as image processing and two-dimensional filtering (Geosoft Inc., 1998).

The datasets for all the study areas were gridded using minimum curvature gridding algorithm. The resultant total field magnetic intensity (TMI) grids were then displayed as maps. The gridded magnetic maps for all the study areas will be shown together with other forms of datasets for individual areas for ease of reference.

CHAPTER 4

ENHANCEMENT AND PRESENTATION OF DATA

4.0. INTRODUCTION

Airborne geophysical data presentation can be enhanced by a range of linear and non-linear filtering algorithms, which selectively enhance certain features of the data such as: the edges of magnetic bodies, shallow magnetic features, magnetic features at depth, subtle magnetic anomalies, etc., (Milligan and Gunn, 1997). After applying corrections to the magnetic data, the values are normally displayed as profiles, contours and images. In many cases it is possible to apply filtering and transformation processes prior to the display of these datasets to produce secondary products with obviously improved information content.

The transformations explained below were used. Some of them are a selection from those given by Gunn (1975):

4.1. REDUCTION TO THE POLE.

The shape of any magnetic anomaly depends on the inclination and the declination of the main magnetic field of the Earth, i.e., the same magnetic body will produce a different anomaly depending on where it is located and its orientation. Reduction to the pole takes the magnetic anomalies, as measured at any latitude, and transforms them into that which would have been measured if the magnetic body had lain at the magnetic pole, i.e., the region where the inclination is vertical and the declination is zero. In this way the interpretation of the data is made intuitive because vertical bodies will produce induced magnetic anomalies that are centred at the body and symmetrical (Spector, 1968).

It is important to understand that the reduction to the pole/equator is in fact an interpretation and that the results are not the real representation of the field at the pole or

equator, but only an approximation. Also reduction to the pole or equator only works if the magnetisation is induced. When there's any remanent magnetisation present it will result in erroneous results (Spector, 1968). It therefore has to be used with extreme caution.

4.2. COMPUTATION OF VERTICAL DERIVATIVES.

Vertical derivatives of magnetic field data can be computed by multiplying the amplitude spectra of the field by a factor of the form (Gunn 1975): $A'(f) = A(f) \cdot (if)^n$, where $A(f)$ is the amplitude at a frequency before filtering, $A'(f)$ the corresponding amplitude after filtering, $i = \sqrt{-1}$ and n the order of the vertical derivative. The first vertical derivative (vertical gradient) is physically equivalent to measuring magnetic field simultaneously at two points vertically above each other, subtracting the data and dividing the result by vertical spatial separation of the measurement points. The second vertical derivative is the vertical derivative of the first vertical derivative and so on. The process enhances high frequencies relative to low frequencies, enhancing shallow geological features.

The vertical derivative enhancements of TMI data for the study areas, where applicable, are shown together with other datasets for individual areas for easy reference.

4.3. ANALYTIC SIGNAL.

The analytic signal can enhance and sharpen regional structure and the edges of the anomalies in a grid (Fitzgerald & Associates, 1996). Roest *et al.*, (1992) show that the amplitude of the analytic signal can be easily derived from the three orthogonal gradients of the total magnetic field using the expression:

$$|A(x, y)| = \sqrt{\left(\frac{\partial m}{\partial x}\right)^2 + \left(\frac{\partial m}{\partial y}\right)^2 + \left(\frac{\partial m}{\partial z}\right)^2}$$

where \mathbf{m} = magnetic anomaly.

The resulting shape of the absolute value of the analytic signal is independent of the orientation of the magnetisation of the source and is centred on the causative body. This means that all bodies with the same geometry have the same analytic signal (Milligan and Gunn, 1997). It, however, varies with the strike of the body (Schouten, 1971) as does the amplitude of a magnetic anomaly. Maxima of the analytic signal indicate the positions of magnetic contrasts.

The analytic signal enhancements of TMI data for the study areas are shown together with other datasets for individual areas for easy reference.

CHAPTER 5

INTERPRETATION OF DIFFERENT DATASETS

5.0. INTRODUCTION

A combination of the following datasets was used for interpretation:

- Total field magnetic maps
- Vertical derivative maps
- Analytic signal maps
- Digital terrain model maps
- Topographic maps
- Geological borehole logs
- Geological maps
- 1: 1000 000 regional magnetic map of the country
- Available infrastructure information from mines in the vicinity of study areas

Magnetic data interpretation methodology consisted of the inspection of the digital magnetic data, maps of magnetic data, infrastructure information from the mines surrounding the survey areas, topographic maps and borehole logs to define the following:

a) Structures dislocating or affecting the anomaly amplitude of magnetic units.

The points below (from Gunn *et al.*, 1997) describe how the faults were recognised and Figure shows the examples:

- Offsets of similar magnetic units
- Sudden discontinuities of magnetic units

- An abrupt change in the depth to magnetic sources (manifested by change in amplitude of the magnetic signal)
- A linear narrow magnetic low caused by weathering along a fault plane oxidising magnetic minerals to non-magnetic minerals (joints can have the similar expression)
- A linear magnetic high, which maybe discontinuous in nature due to the magnetic minerals precipitated in fault plane

b) Lithological units.

Lithological identification was based on the following (Gunn *et al.*, 1997):

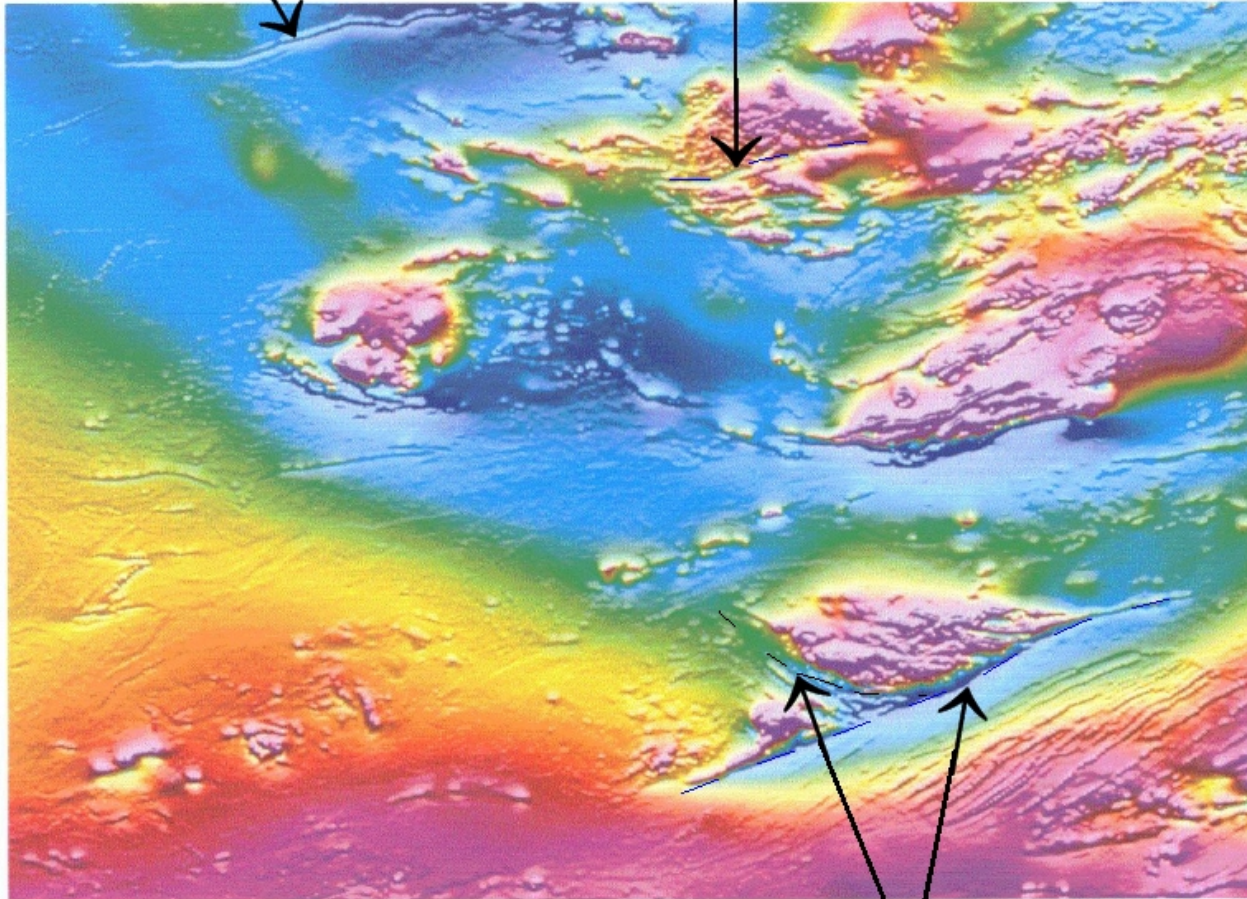
- Correlations of magnetic data with the outcrop geology and drill hole data
- Amplitude of the response, which can indicate the possible lithology - for example amplitude of several thousand nanoteslas may indicate magnetite-rich ironstone. A basic knowledge of different relative responses likely to arise from different rock units is required to be able to make plausible identifications. Clark (1997) provides a basis for the knowledge.
- The texture or character of the magnetic units, which can also give clues to their origin. For example, lava flows generally exhibit a semi-random internal anomaly character, owing to inhomogeneity of the magnetic properties of the flow.

c) Cultural features.

Cultural features can be identified by their high amplitudes and shapes. They are almost always too “straight” to be geological features. Topographic maps and infrastructure information (if available) are used to identify these features as the first step of interpretation.



A linear magnetic low



Sudden discontinuity of a magnetic unit

Figure 14. Examples of how the faults were recognised on the dataset (modified from Gunn *et al.*, 1997).

5.1. INTERPRETATION OF DELMAS DATA.

The three areas around Delmas were interpreted together for continuity in interpretation. Figure, 16, 17, 18, 19 and 20 show the datasets used for interpretation: *total field magnetic data*, *first vertical derivative data*, *digital terrain model data* and *the three geological logs* respectively. It was decided not to fly already mined areas and as such no information is available for the areas in between the flown areas. Figure 21 shows the positions of the boreholes used to aid interpretation and Figure 22 shows the interpreted features superimposed on the vertical derivative map. The analytic signal did not prove useful and thus its use in interpretation was omitted.

The prominent features are the high magnetic zones believed to be the unweathered parts of the dolerite sills observed (Figures 15 and 16). Sills were identified in all the areas as seen on the interpretation map (Figure 22). A number of faults were also interpreted in the regions of the outlined sills. This could mean that faulting was due to the intrusion of the sills. The faults are concentrated mainly on area 2 with less intensity on areas 1 and 3.

A sill observed on the eastern corner of area 3 covers the eastern part of that area, becoming less prominent towards the centre. An intriguing feature is also observed north of the area on the first vertical derivative data. This feature was at first thought to be an extension of the dolerite sill just to the eastern side but the borehole information (Figures 18a to 18d, representing borehole WTN4 on block 3) shows no presence of the dolerite. It could still be the dolerite at depth, where a reverse fault could be expected to have thrown that part down. A possible fault that could be attributed to that is observed near the edge of the feature and the sill. Unfortunately there is no data coverage further north to better explain the feature.

The sills observed on areas 1 and 2 are believed to be portions of one continuous sill that covers over half of these areas. The magnetic data suggest that the sill may be continuing further northwards and maybe southwards as well. It was initially believed that the extend of the sill is only limited to the high magnetic areas but the borehole logs show the

presence of weathered dolerite in the areas of intermediate magnetic signature as well. Figures 19a to 19c, representing borehole R22 on block 2, show the geological log with an eleven metre thick dolerite and borehole R21 shows a 5.5m dolerite (Figure 20). Unfortunately the borehole logs do not mention the state of the dolerite.

On area 2 the sill is broken by two north-south trending faults and cut through in the middle by an east-west trending fault. The north-south faults seems to be normal faults as the magnetic signature on both the total field and the vertical derivative suggests that the western part of the faults was thrown up and exposed to weathering, hence the varying character of the texture of the magnetic signature observed on the vertical derivative data. This weathered part of the sill corresponds to the high elevation areas on the digital terrain model data (Figure 23), again supporting the upward movement.

Only one possible dyke was identified at the north-eastern edge of area 2. The possible dyke is associated with the magnetic feature seen on the north-eastern edge of this area. The feature could be the unweathered dolerite at depth as the pre-Karoo rocks in the area are composed of non-magnetic Transvaal Supergroup rocks. Looking at areas 2 and 3 together, there's an indication that the feature could be extending into area 3.

Two boreholes are recommended to verify the features on blocks 2 and 3 and the coordinates are given in the Table 1. The positions of the proposed boreholes are indicated on Figure 24. The boreholes are normally drilled down to the Karoo basement (tillite), which is between 40m and 200m in the Witbank coalfield (Cadle *et al*, 1993). Below the Karoo tillites there's no interest for coal mining in South Africa. Since the commodity is relatively shallow, the boreholes are mainly drilled vertically. All the other recommended boreholes in the coming sections will be vertical holes as well.

Table 1. Positions of the recommended boreholes.

ID	UTM X	UTM Y
A	676685.584	7104527.224
B	677621.885	7108868.255

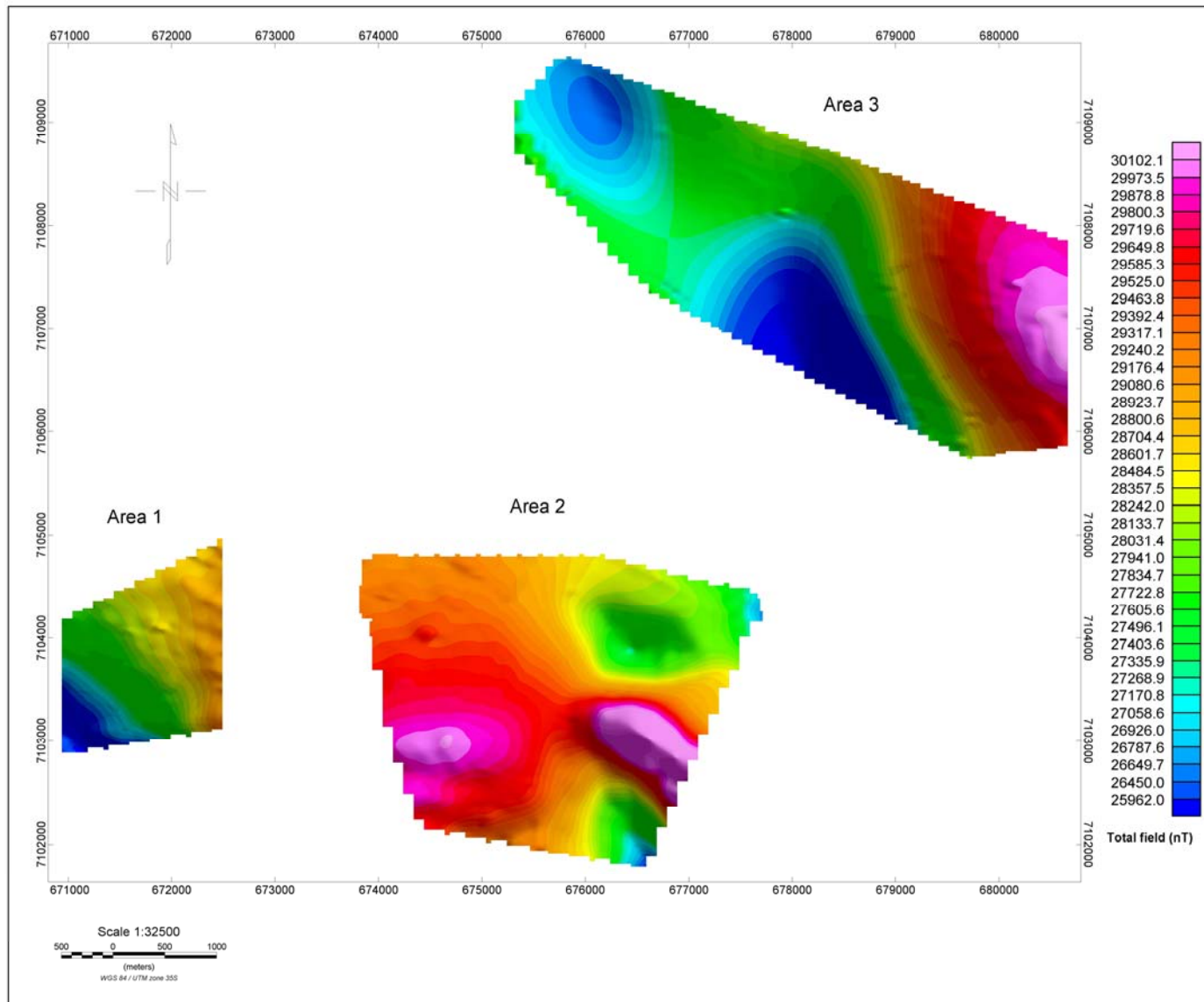


Figure 15. Total field magnetic maps of Delmas study areas.

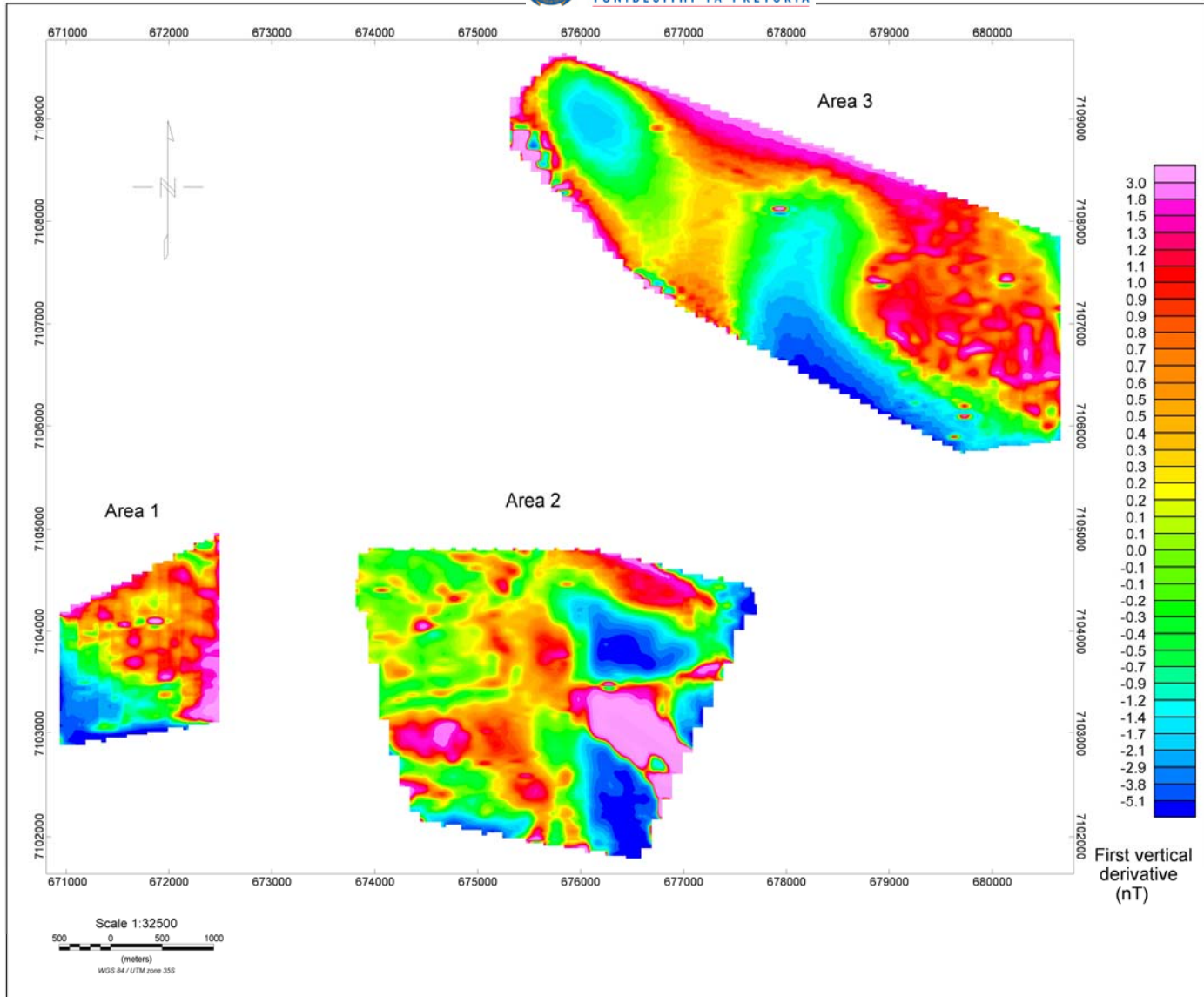


Figure 16. First vertical derivative maps of Delmas study areas.

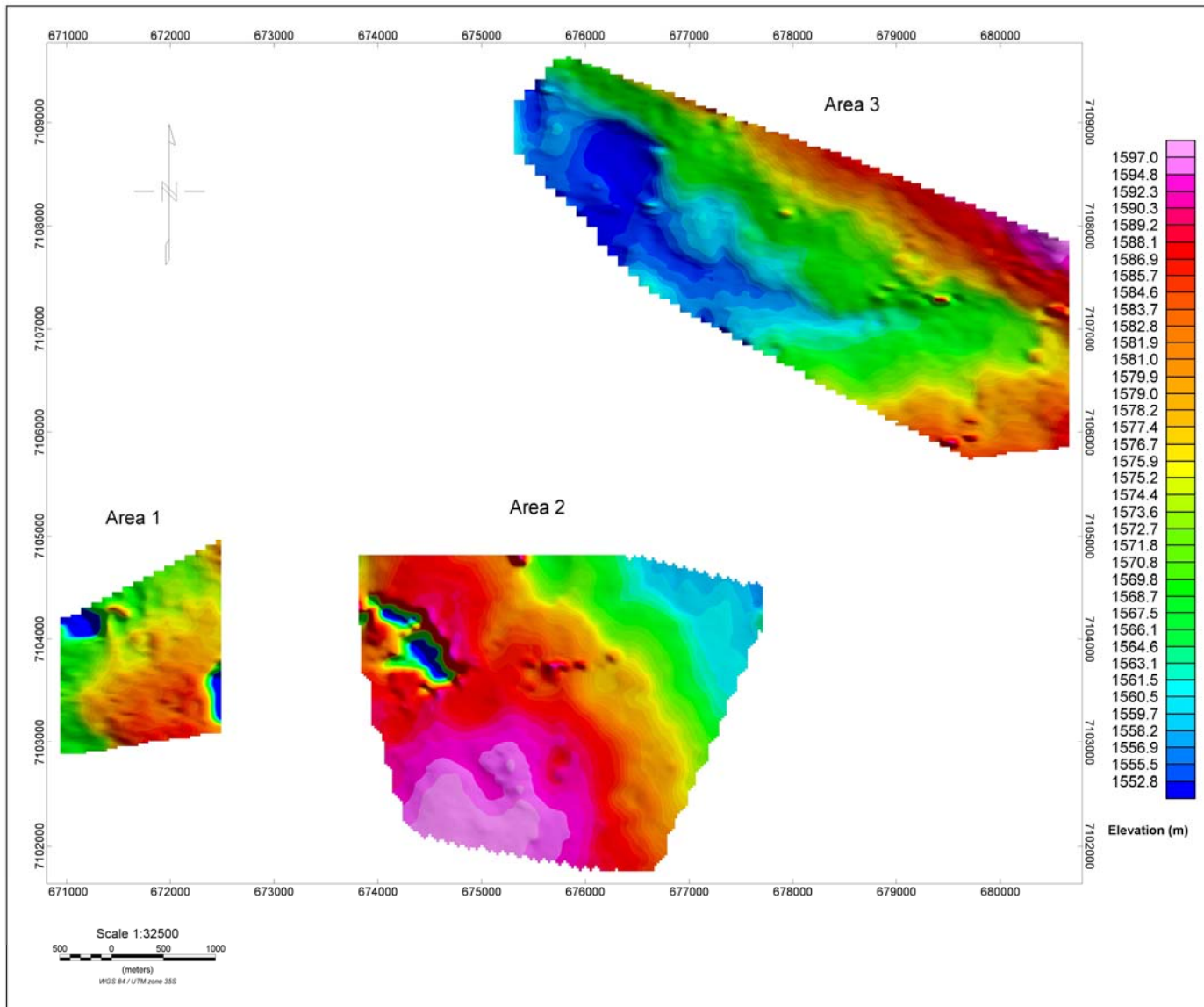


Figure 17. Digital terrain model maps of Delmas study areas.

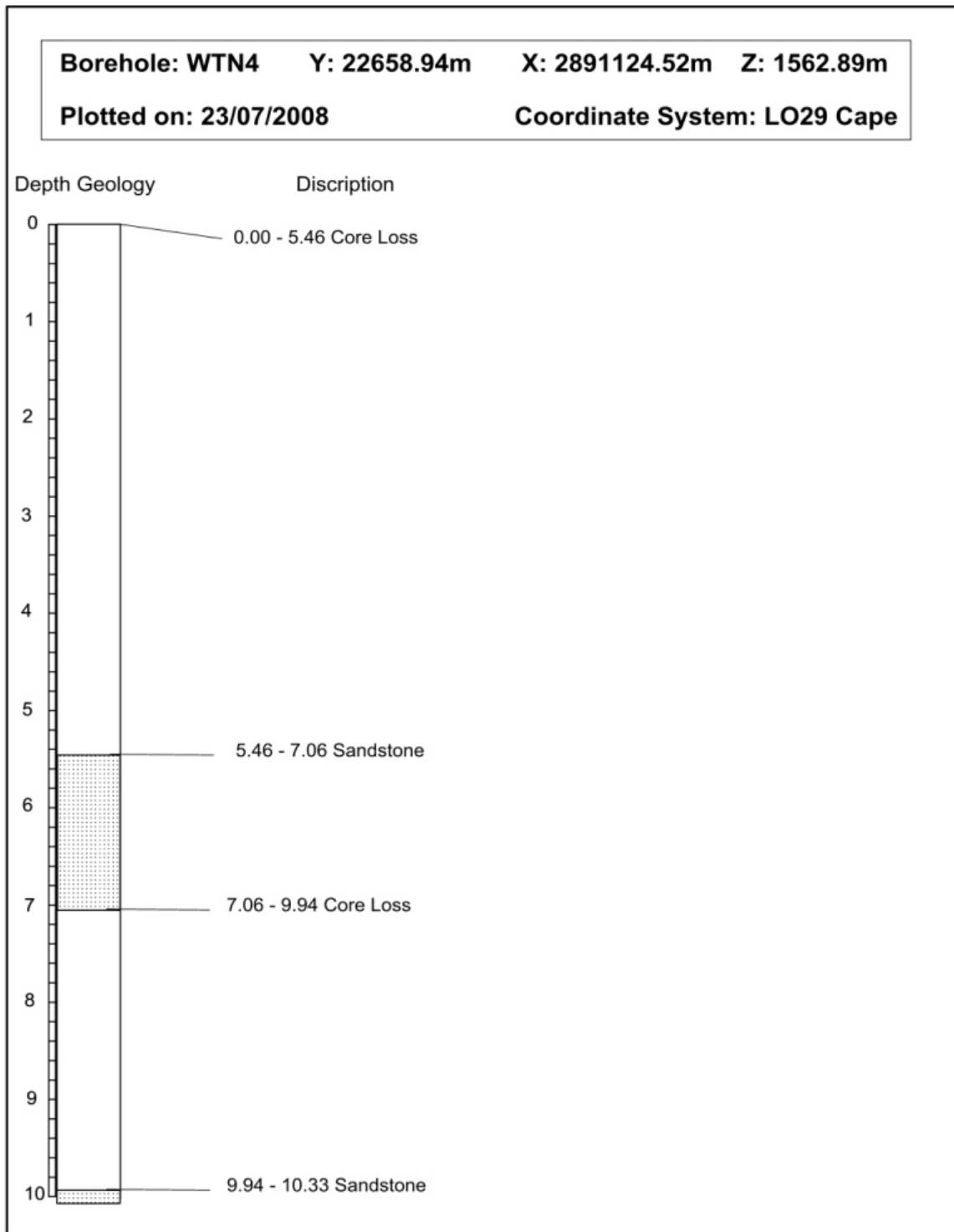


Figure 18a. The geological log for borehole WTN4 (from Van Ryneveld, 2008).

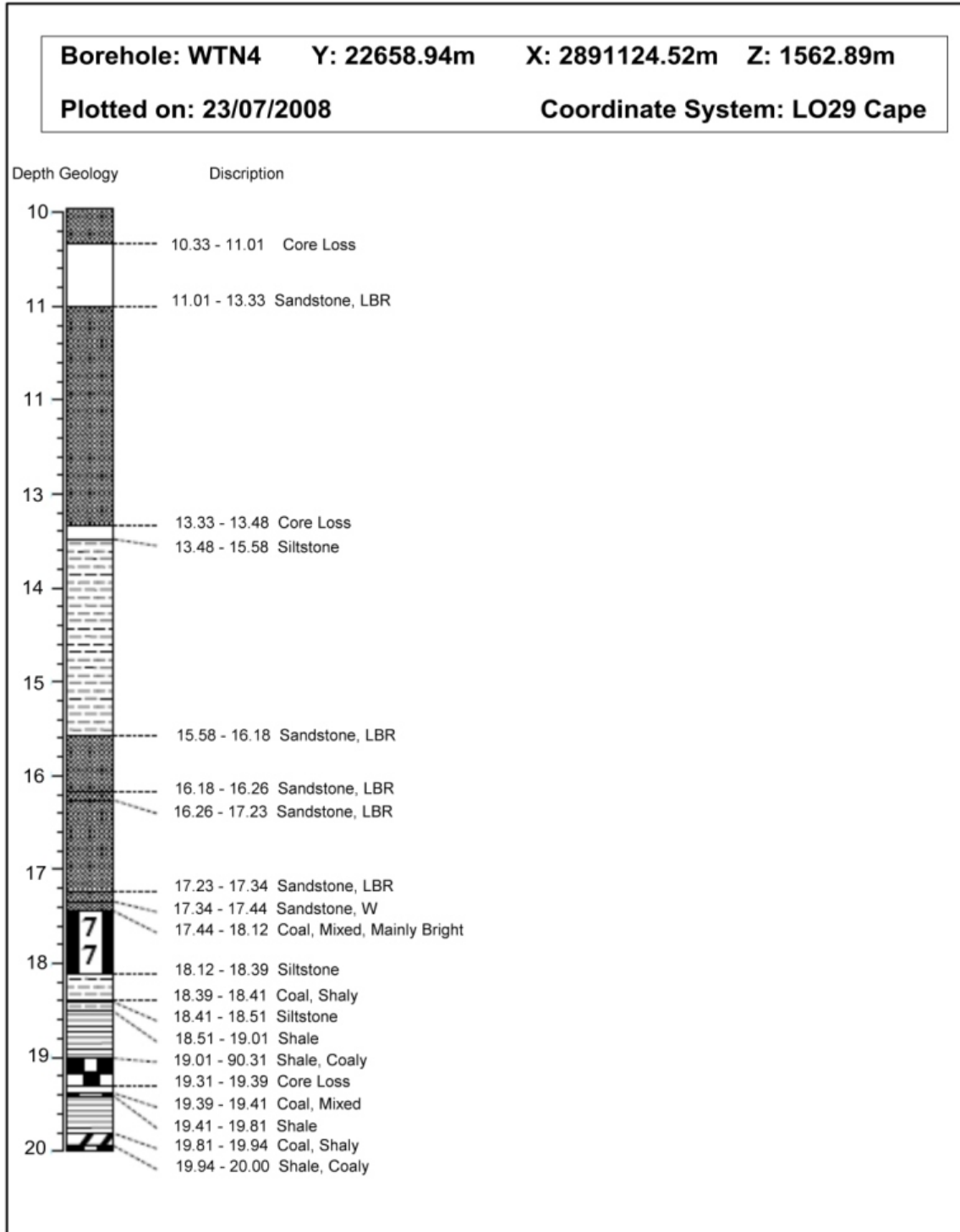


Figure 18b. The geological log for borehole WTN4 continued.

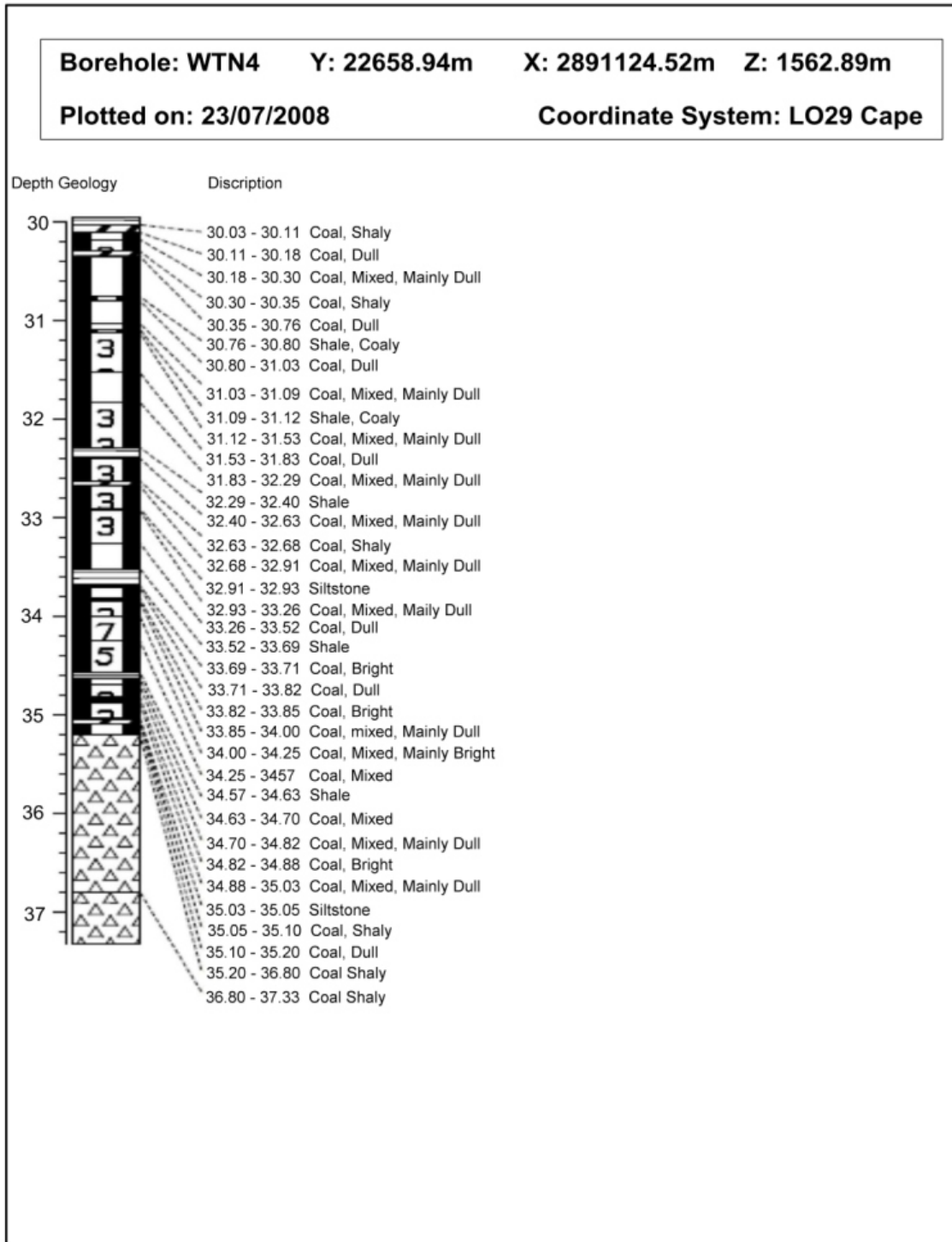


Figure 18d. The end of geological log for borehole WTN4.

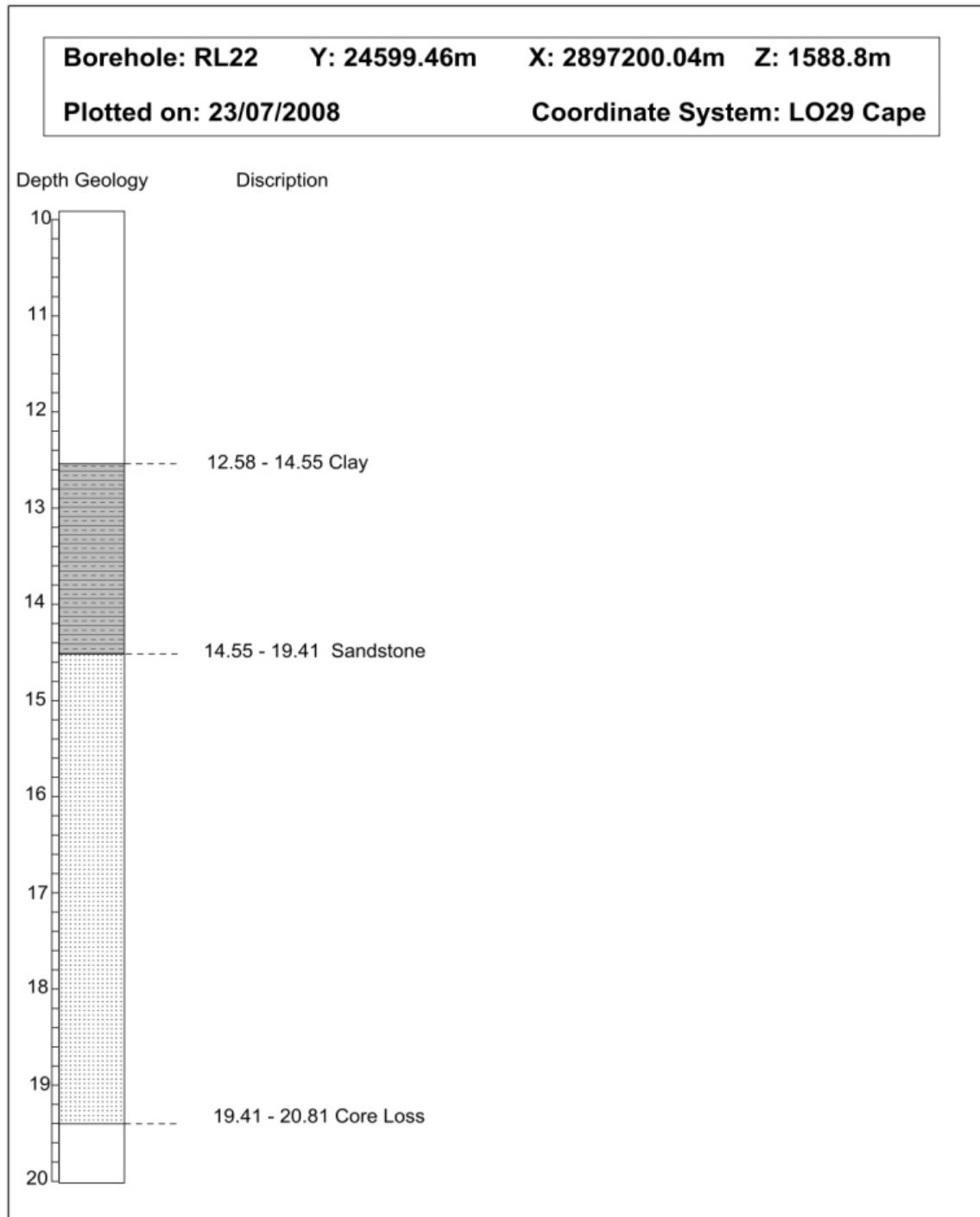


Figure 1a. The geological log for borehole R22 (from Van Ryneveld, 2008). The log starts at 10m due to core loss.

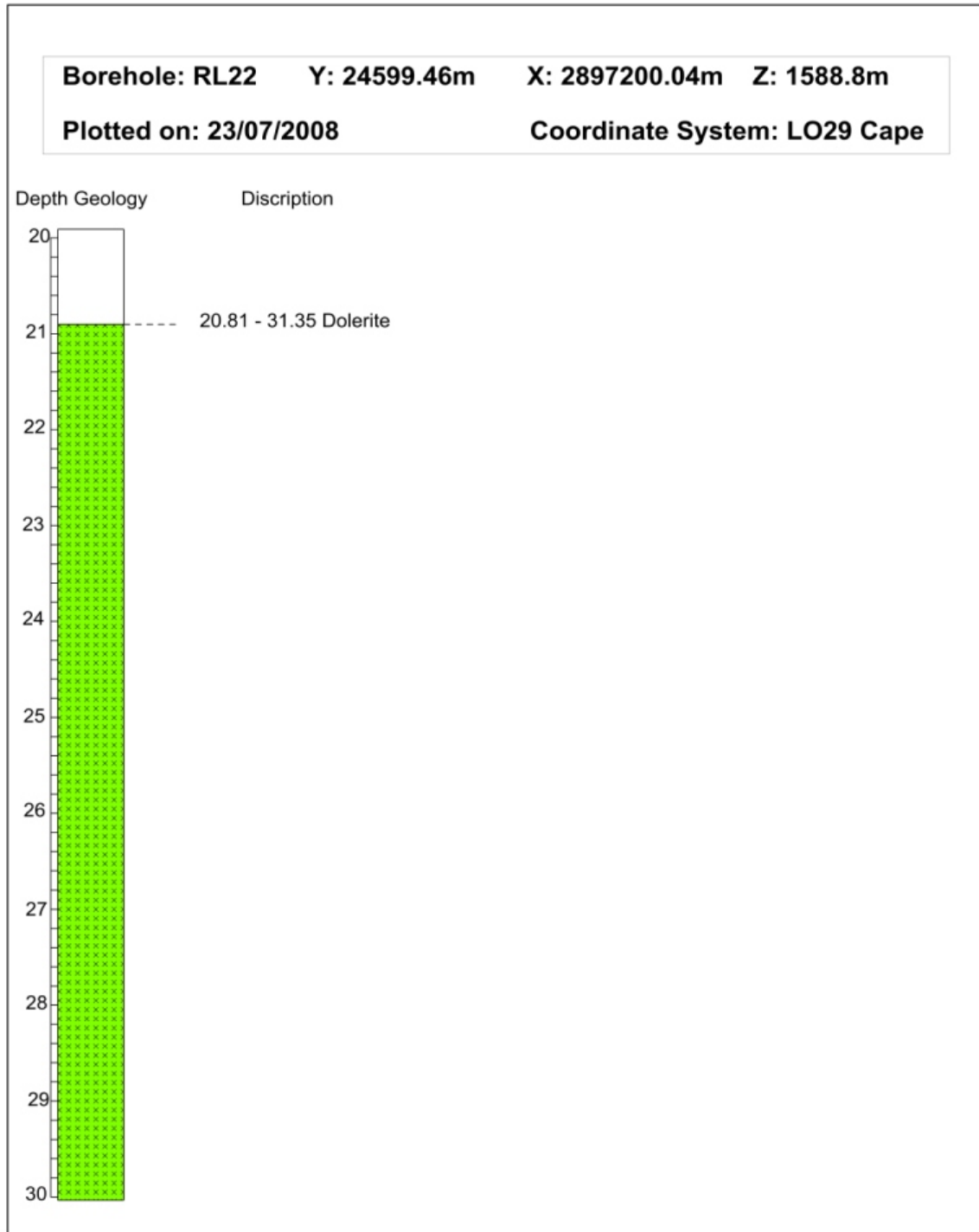


Figure 18b. The geological log for borehole R22 continued. The beginning of a thick dolerite, which extends up to eleven metres, is observed.

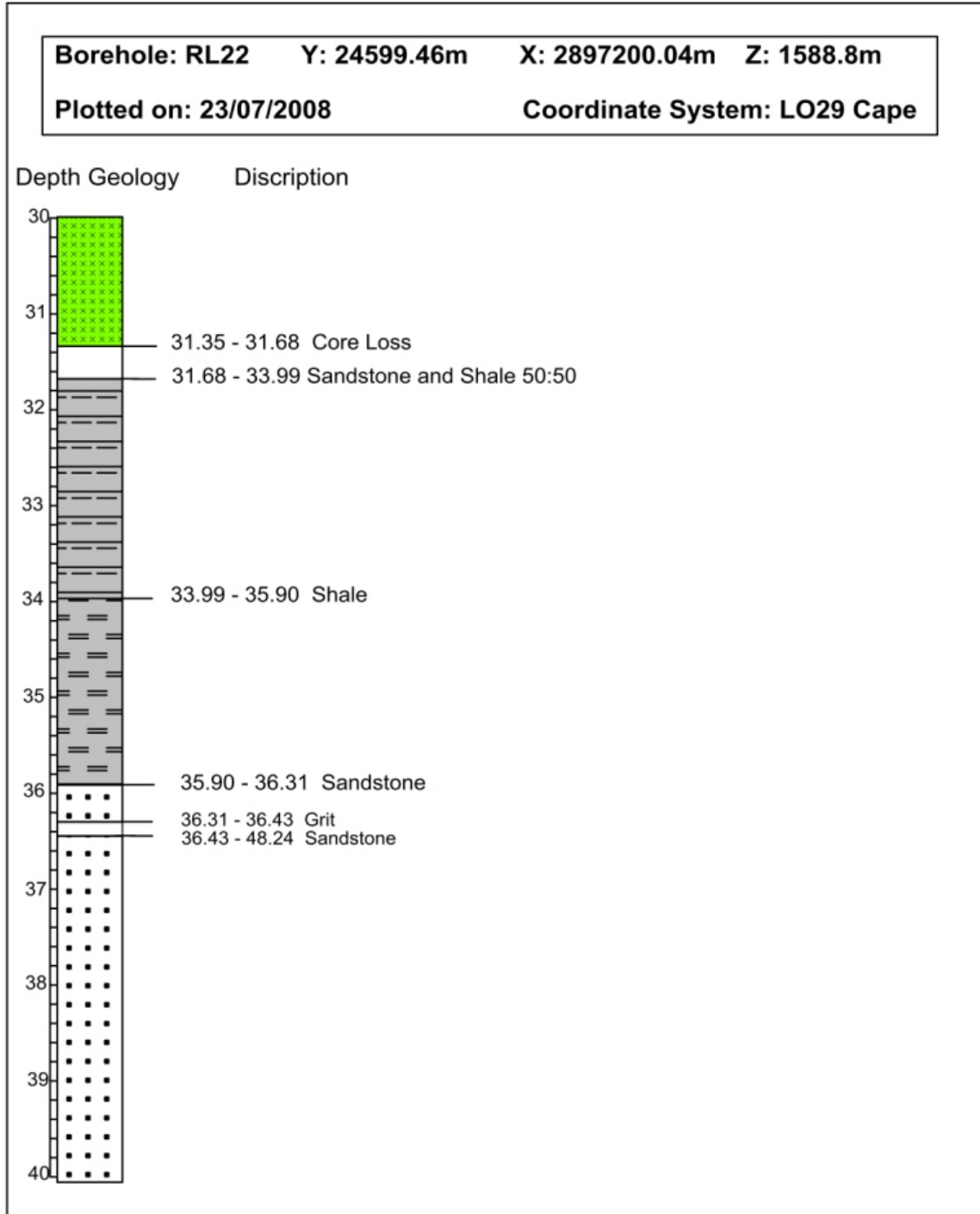


Figure 18c. End of the geological log for borehole R22.

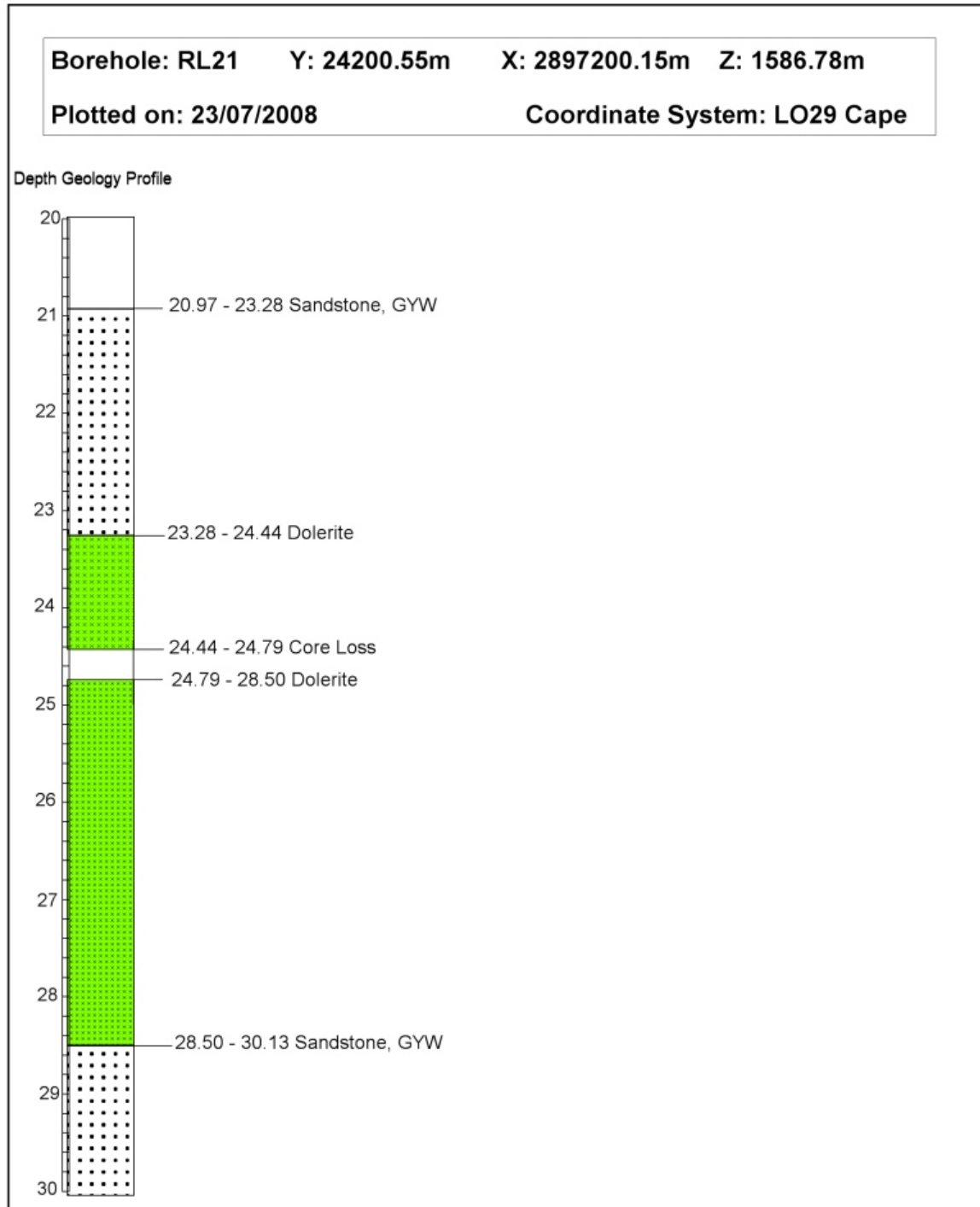


Figure 20. The geological log for borehole R21. A 5.22m thick dolerite is observed.

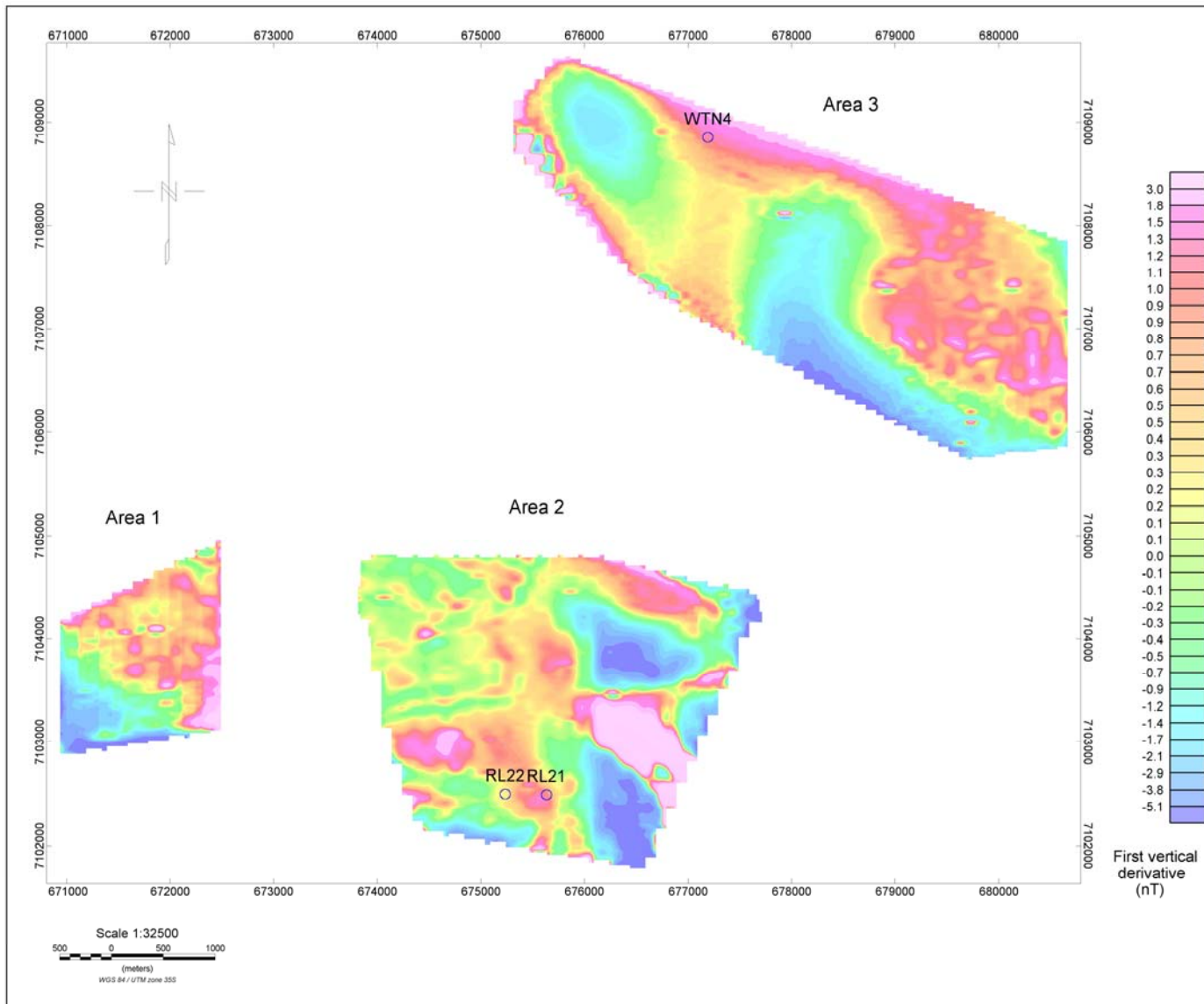


Figure 21. Positions of the boreholes used for interpretation superimposed on the first vertical derivative data.

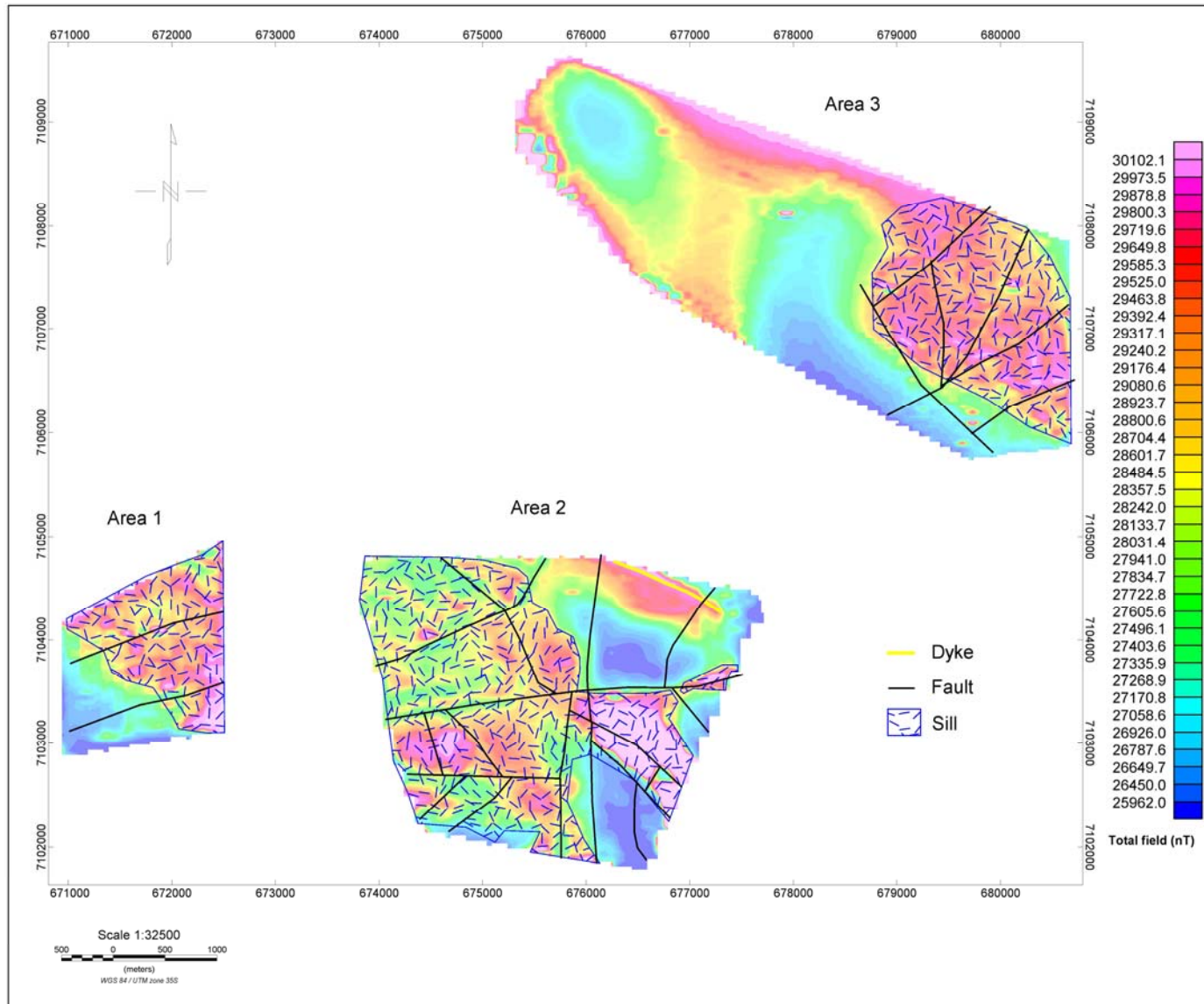


Figure 22. Interpreted structures for Delmas study areas superimposed on the first vertical derivative data.

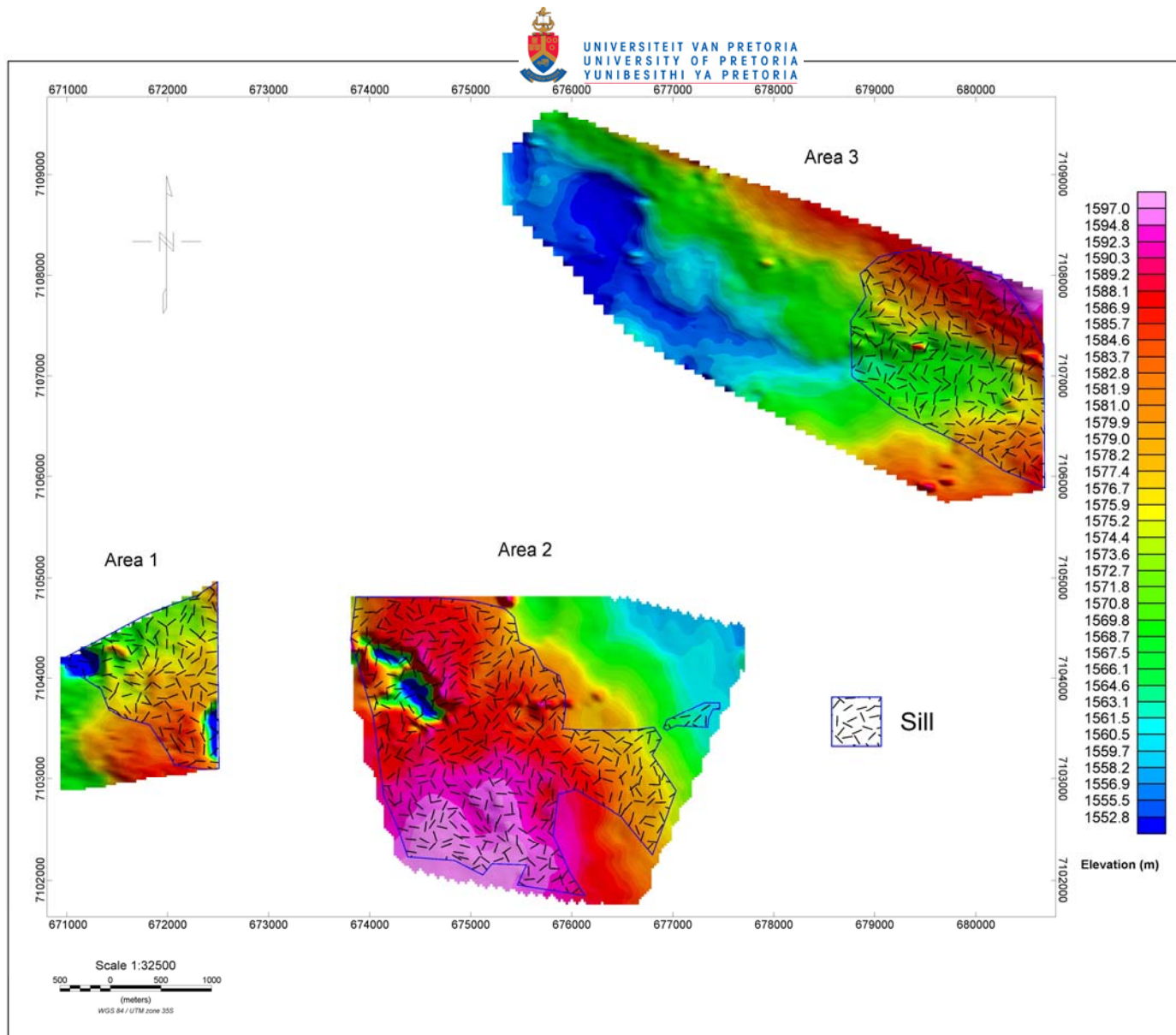


Figure 23. Interpreted sills for Delmas study areas superimposed on the DTM data.

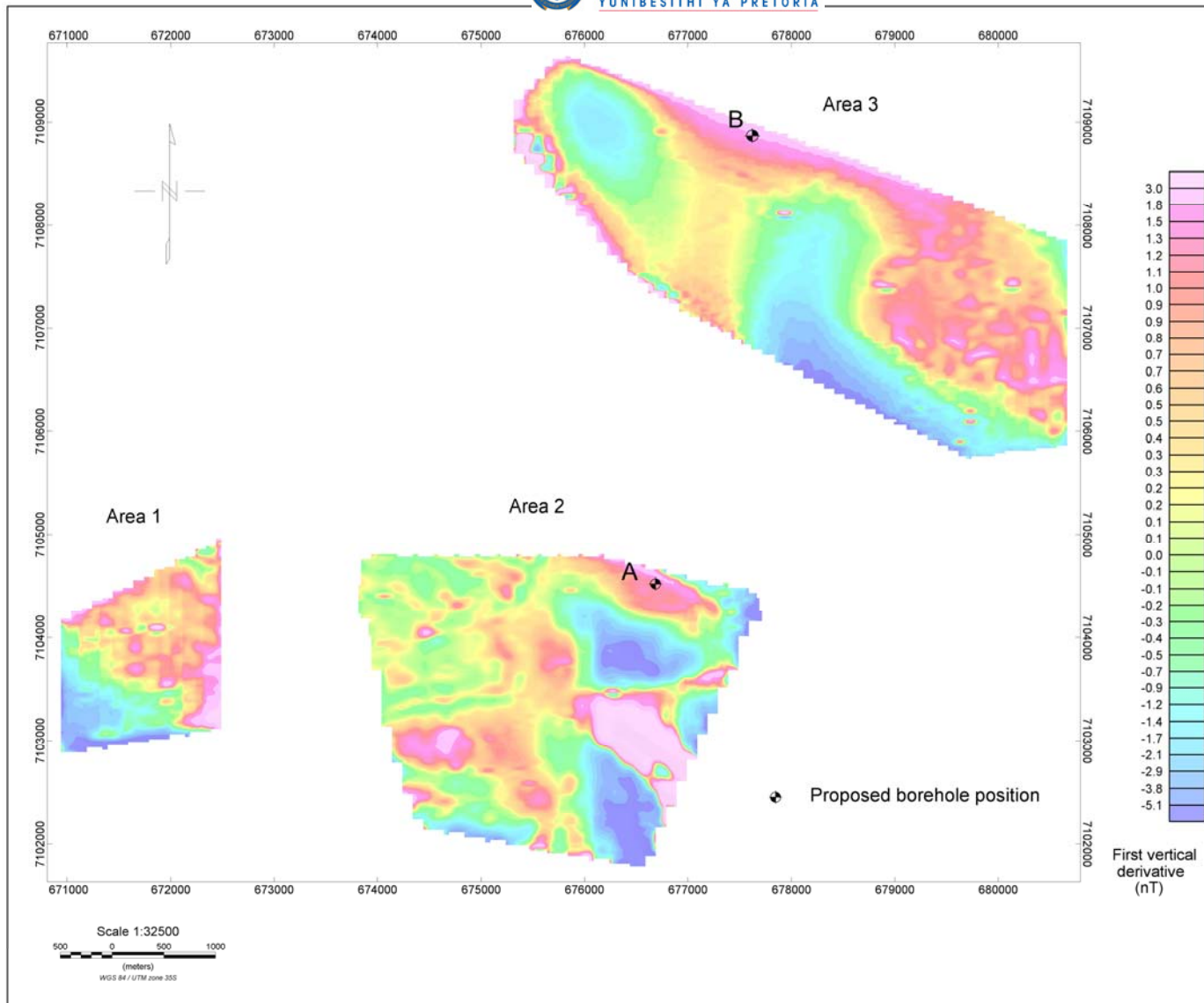


Figure 24. Positions of the proposed boreholes superimposed on the first vertical derivative data.

5.2. INTERPRETATION OF VANDYKSDRIF AREA 1 DATA.

Figures, 25, 26, 27 and 28 show the datasets used for interpretation: *total field magnetic data, analytic signal data, first vertical derivative data and comparison of ground magnetic, electromagnetic and airborne magnetic datasets* respectively. Figure 29 shows the interpretation, superimposed on the vertical derivative map.

A broad magnetic feature occurring in the middle of the survey area, oriented in a northwest-southeast direction, is the only magnetic feature observed. It is interpreted to be pre-Karoo basement (either the felsite or the diabase related to Bushveld Complex) as the borehole information does not show any presence of expected post-Karoo magnetic features (e.g., dolerite or diabase sills). Interpreted faulting in the area is mainly associated with this basement feature. The severity of faulting is observed around the centre of the feature continuing eastwards, where the feature was displaced. A major fault is also observed on the western area where it abruptly terminated the feature. There is no indication of the occurrence of the dykes and sills in this area.

For continuity in interpretation, the airborne magnetic data were compared with the available ground magnetic and electromagnetic data from the previous surveys. Figure 28 shows an area where the ground data are available. Figure 30 shows the faults, interpreted on airborne data, also displayed on ground data. For comparison, the ground magnetic data were upward continued to the height of the airborne magnetic data.

What is apparent from the comparison is the edge of the low magnetic feature at the northern parts of both datasets. This is the east-west feature observed in the central part of both the total field and first vertical derivative data on the airborne data. The datasets complements each other very well in terms of outlining interpreted faults 1 and 4. The interpreted fault 1 is better defined on the airborne data; while the interpreted fault 4 on the other hand is better defined on the ground data than on the airborne data. The definition of fault 1 on the airborne data correlates with the coal seam 2 floor contours as

seen overlain on the airborne data (Figure 31). The contours were brought in after interpretation, which was a good comparison.

The difference in defining the interpreted faults 1 and 2 could be due to that the airborne data involved the data outside the region of comparison for gridding, whereas the ground data grid was from the area of comparison only. To test the reason above, the airborne data were windowed such that the gridded data were from the same coverage boundary as the ground data. The results are shown in Figure 32 and it can be said that the data compares very well with very little differences. The EM34 data results show the lineaments which plot adjacent to the interpreted fault 1. The lineaments could be the fractures associated with the interpreted fault.

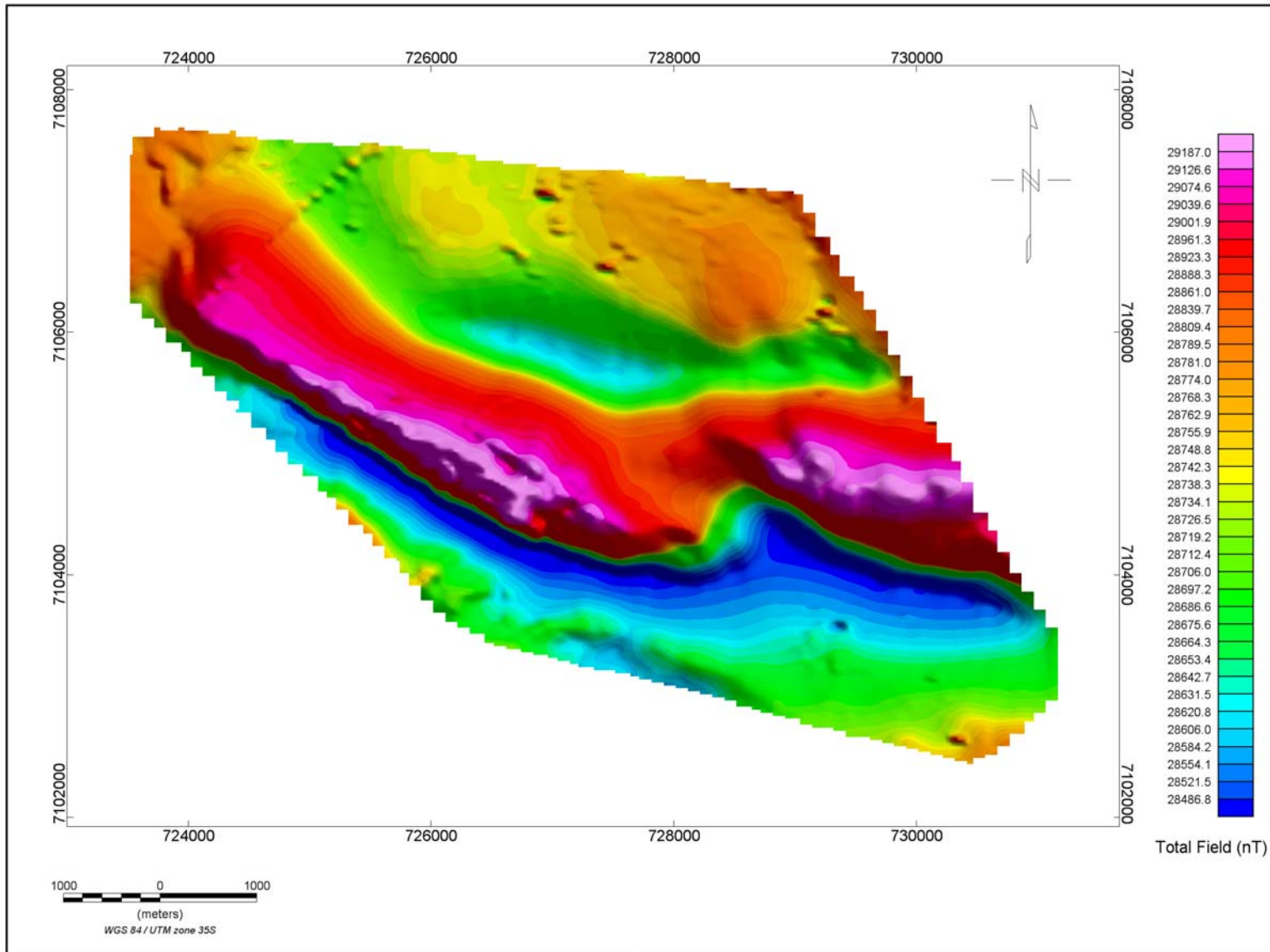


Figure 25. Total field magnetic map of Vandyksdrif study area 1 data.

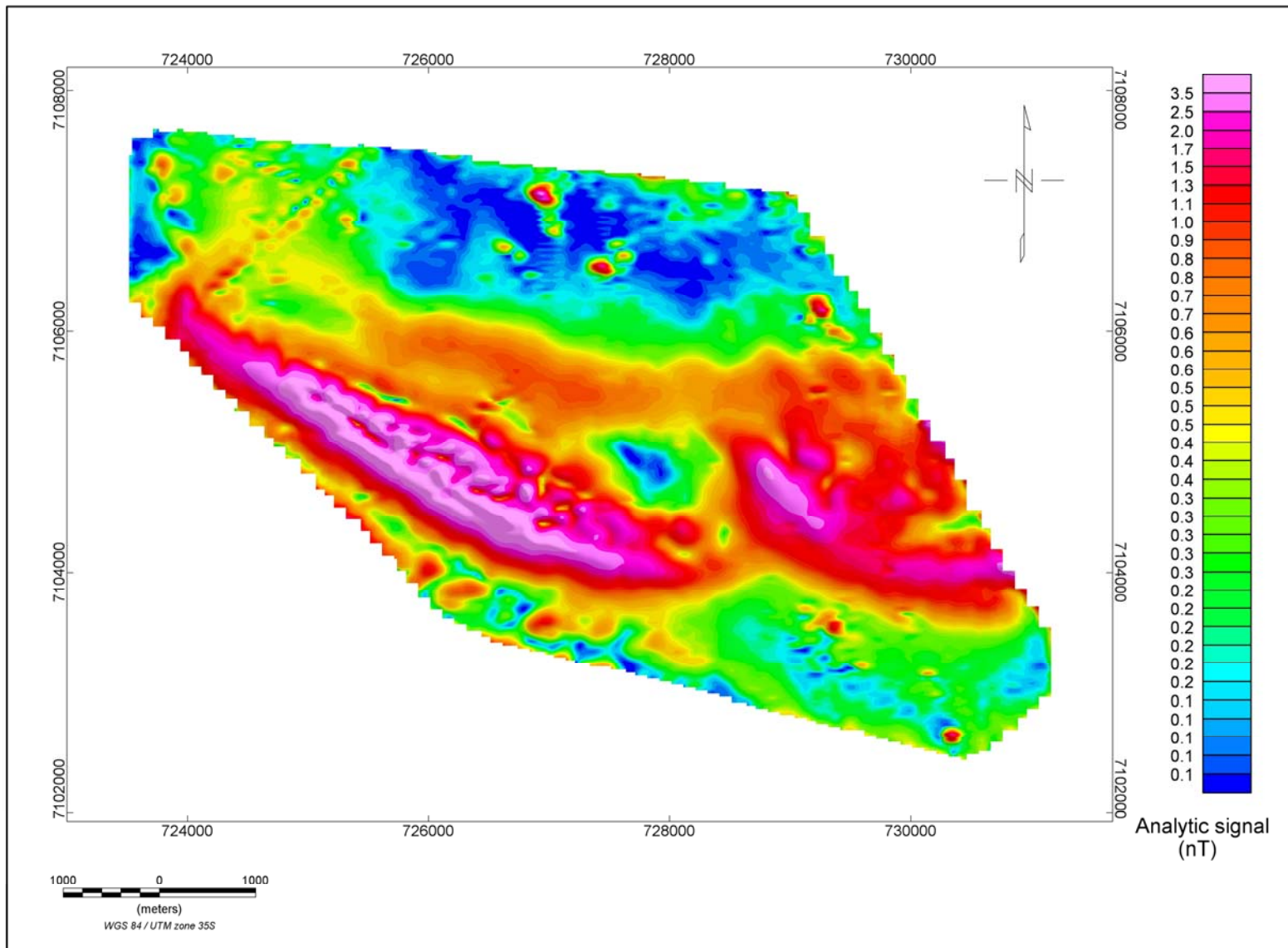


Figure 26. Analytic signal map of Vandyksdrif study area 1 data.

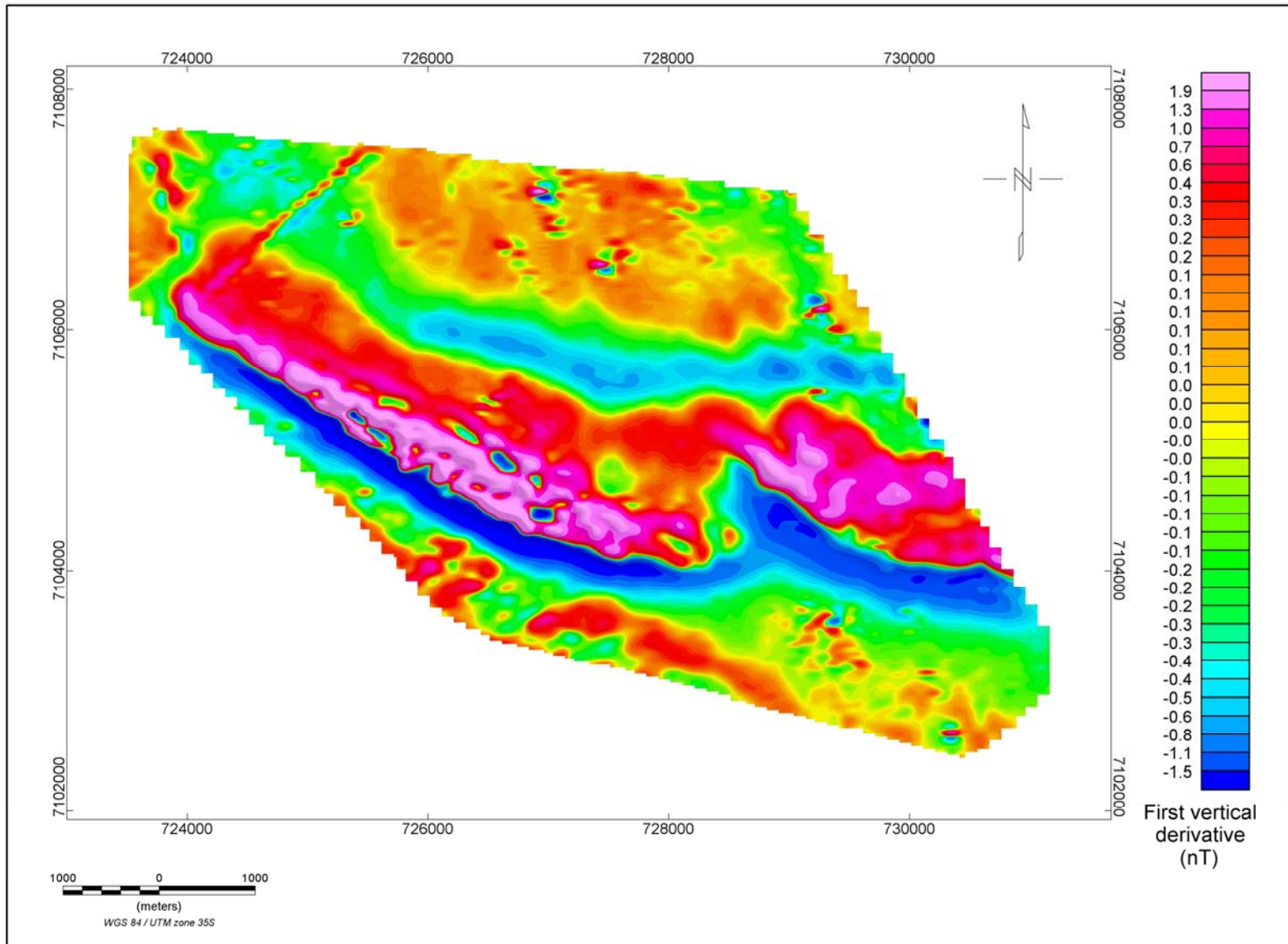


Figure 27. First vertical derivative map of Vandyksdrif study area 1 data.

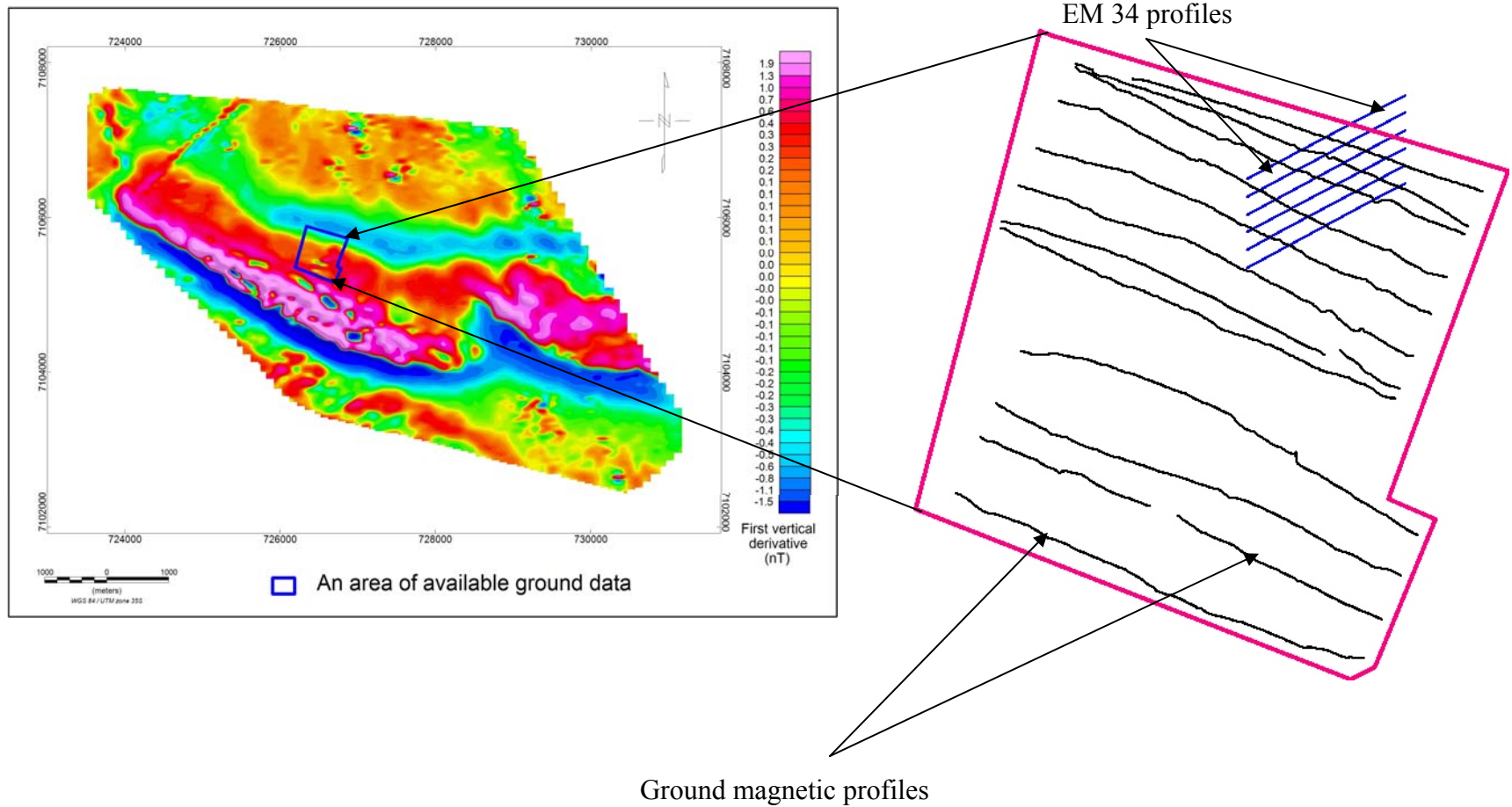


Figure 28. An area of both the ground and airborne data.

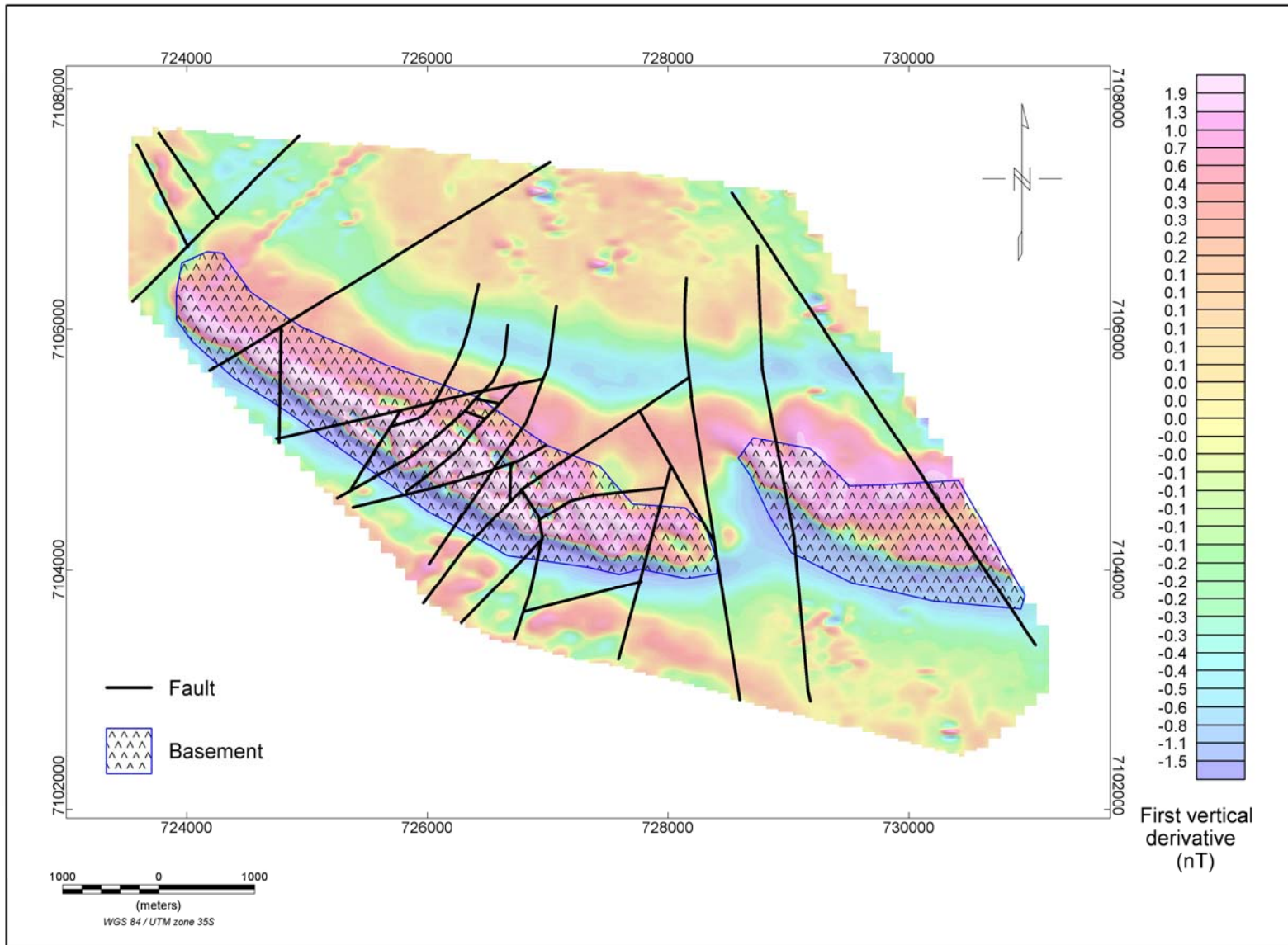


Figure 29. Interpreted structures for Vandyksdrif area 1 data superimposed on the first vertical derivative map.

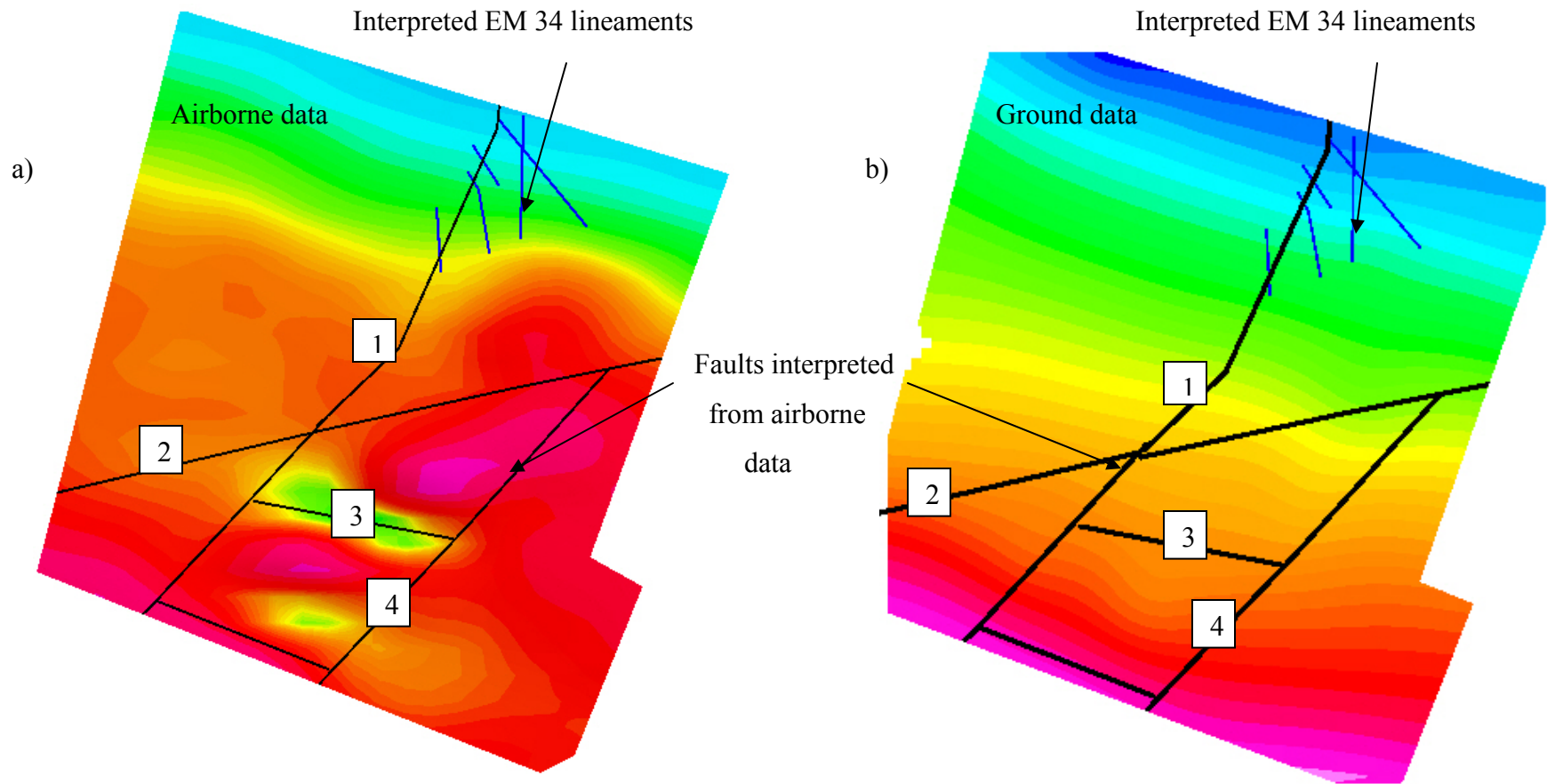


Figure 30. Comparison of ground and airborne datasets in the same area. a) is a clip from airborne data and, b) is the ground magnetic data. The lineaments from electromagnetic data are also displayed on both datasets.

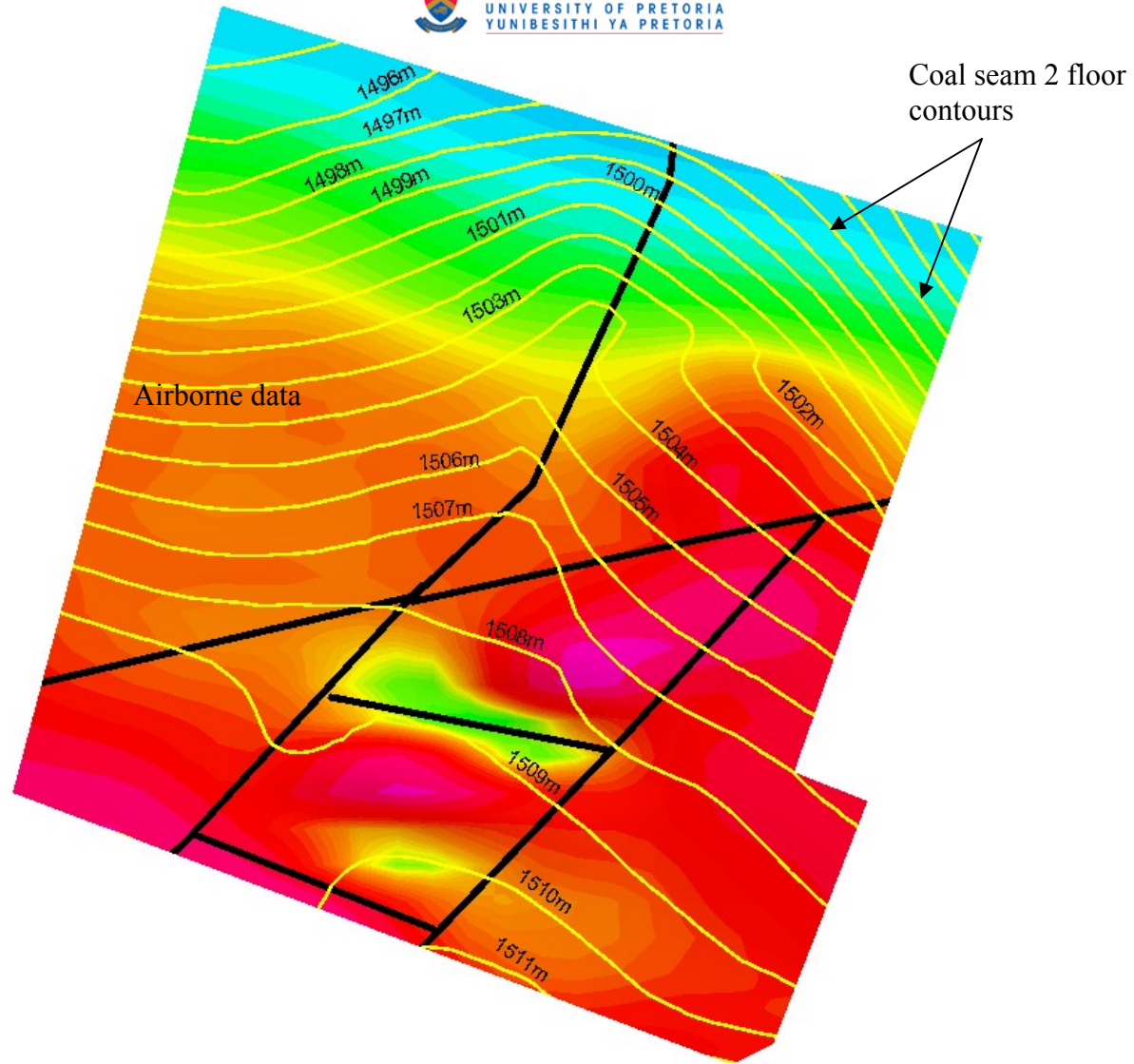


Figure 31. Coal seam 2 floor contours overlain on the first vertical derivative data of the airborne magnetic data. The contours are in metres above sea level.

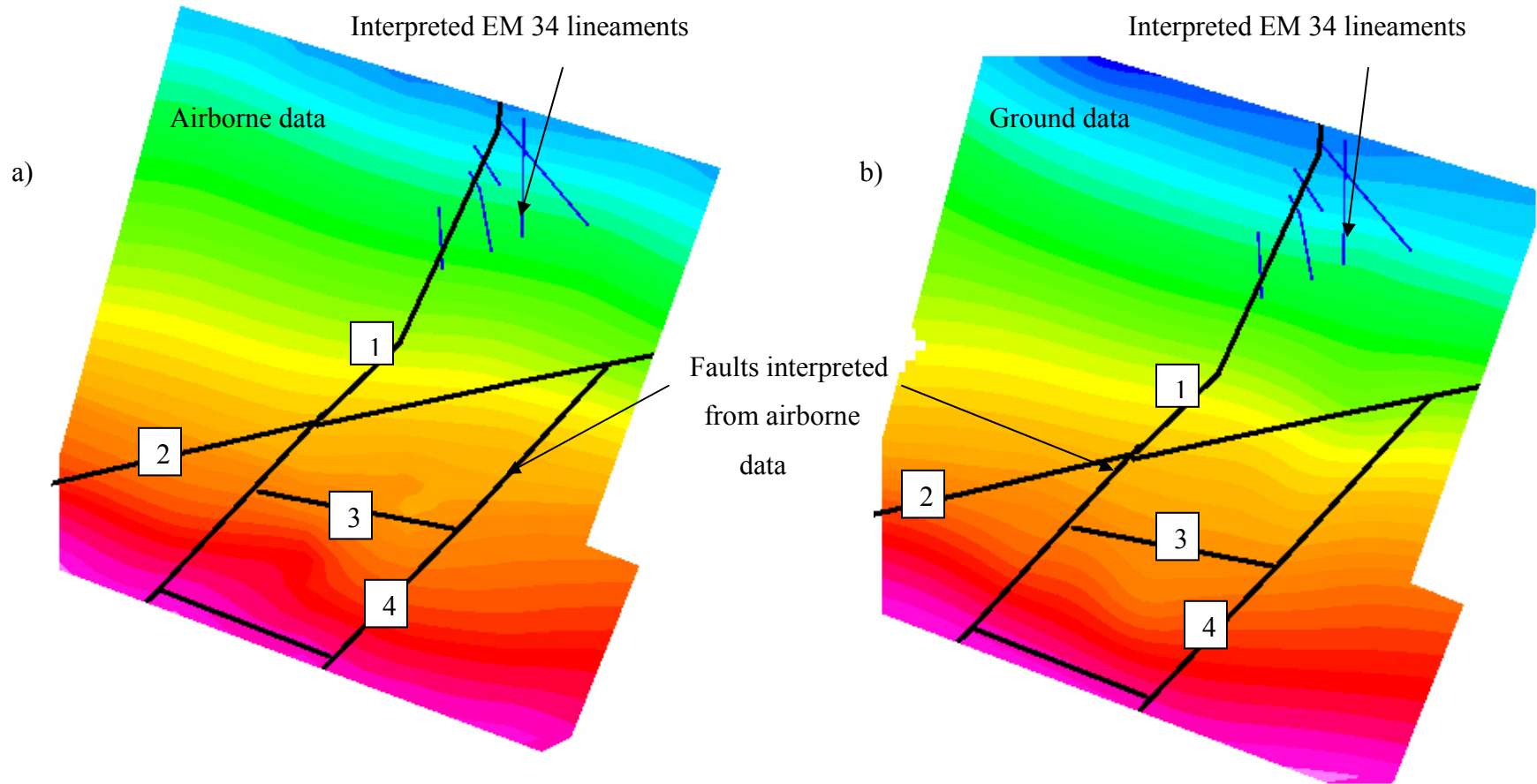


Figure 32. Comparison of ground and airborne datasets in the same area. a) is the windowed grid from the airborne data and, b) is a ground magnetic data.

5.3. INTERPRETATION OF VANDYKSDRIF AREA 2 DATA.

Figures 33, 34, 35, 36, 37, 38 and 39 show the datasets used for interpretation: *total field magnetic data, analytic signal data, first vertical derivative data, digital terrain model data and the three geological logs* respectively. Figure 40 shows the positions of the boreholes used to aid the interpretation. Figure 41 shows the interpretation, superimposed on the vertical derivative map.

Although it is mostly advisable to do interpretation on either first vertical derivative or analytic signal, total field magnetic map showed interpreted features much better than the other two. The analytic signal did not prove useful and thus its use in interpretation was omitted.

Faults, dolerite sills, basement feature and railway line were interpreted from the dataset. The interpreted dolerite sills occur on the northern half of the area, terminating towards the centre. The interpreted dolerite sills were confirmed from the borehole information (Figures 37, 38 and 39). These sills display the same weathering characteristics as those observed at Delmas region as shown on the first vertical derivative data. As is also the case in the Delmas region, the interpreted sills correspond to the high elevation area on digital terrain model data (Figure 42).

An interpreted feature believed to be the basement (felsites or the diabase) is observed south of the survey area. It is believed to be the basement because the sills encountered in the northern part are weathered in places, displaying the same characteristics as the sills found at Delmas, whereas the feature does not display the weathering characteristics.

A railway line cutting the study area almost in half is observed. It made interpretation of the aeromagnetic data difficult in this area. Railway lines are not always constant in signature due to the different factors such as: whether they're electrically charged during the survey or not, the train being on the railway line during the survey or not. The flight in one direction could have a train on it and the return flight be without it. Their magnetic

signatures will differ. Thus interpretation in the vicinity of the railway line was avoided to prevent being influenced by the railway line.

Four boreholes are recommended to verify some of the features especially in the vicinity of the railway line. The coordinates of the proposed boreholes are given in Table 2 and the positions are indicated on Figure 43.

Table 2. Positions of the recommended boreholes.

BH_ID	UTM_X	UTM_Y
1	735599.089	7111209.749
2	736273.187	7110859.884
3	735830.979	7110240.793
4	735169.651	7109660.503

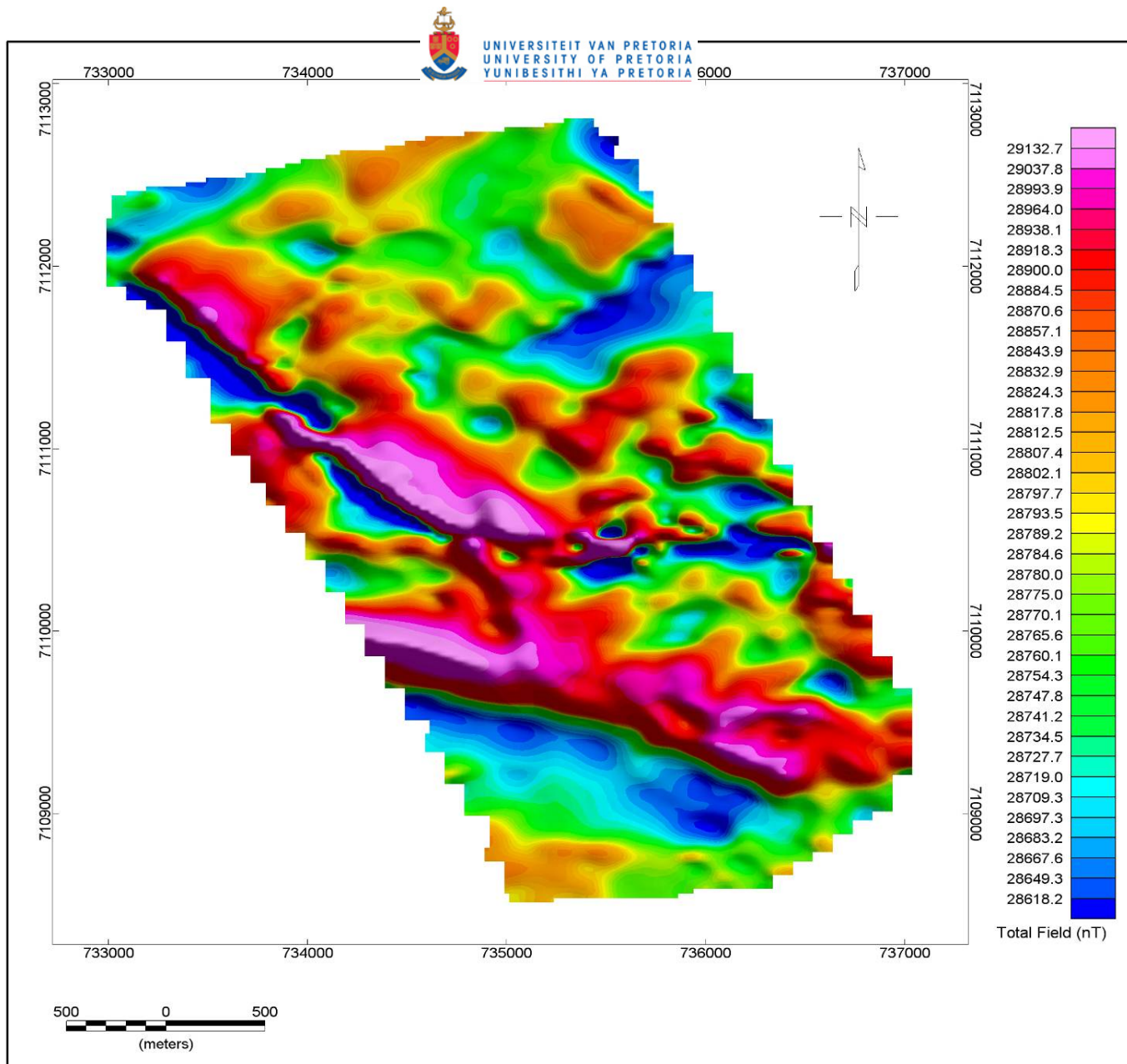


Figure 33. Total field magnetic map of Vandyksdrif study area 2 data.

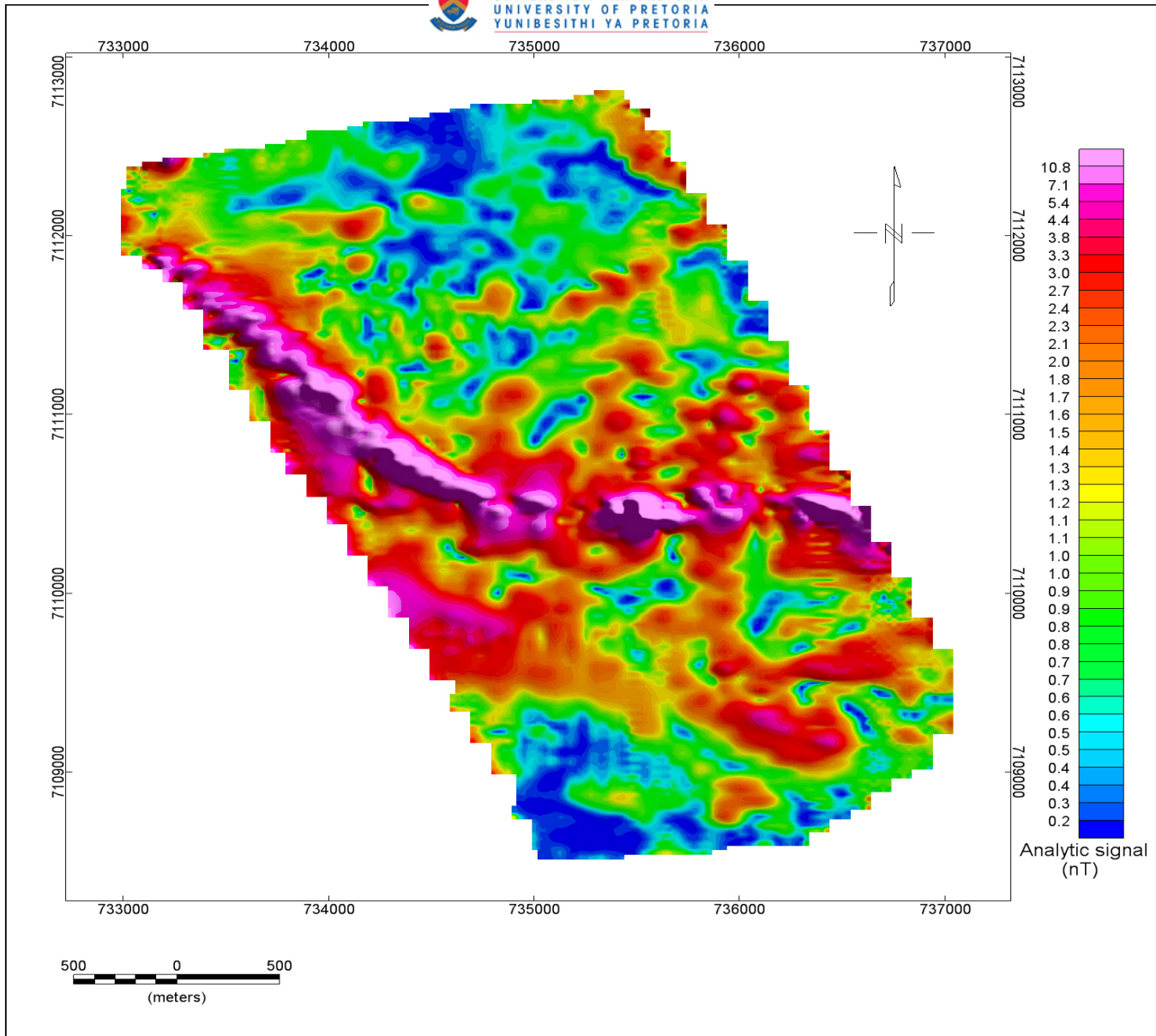


Figure 34. Analytic signal map of Vandyksdrif study area 2 data.

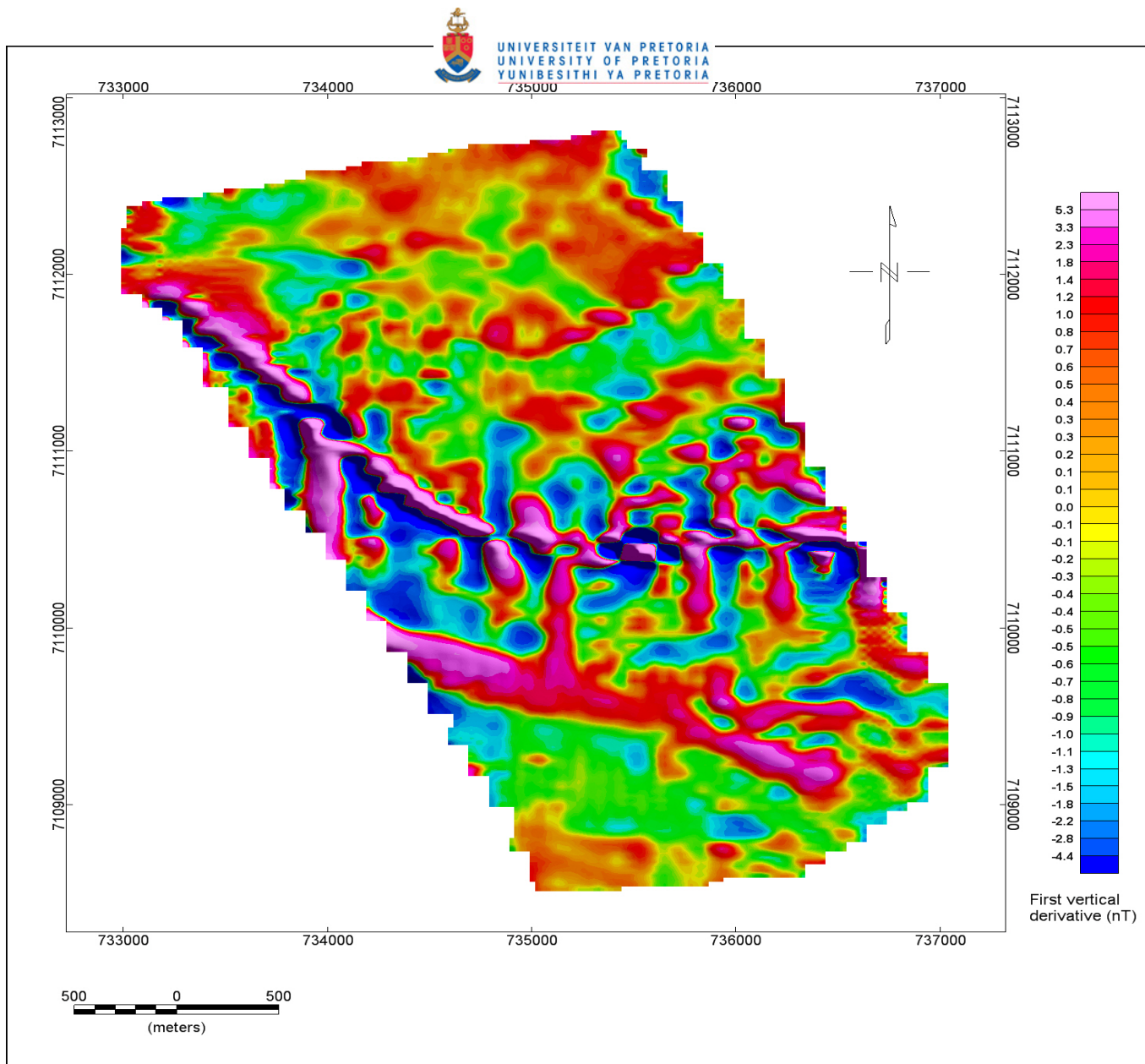


Figure 35. First vertical derivative map of Vandyksdrif study area 2 data.

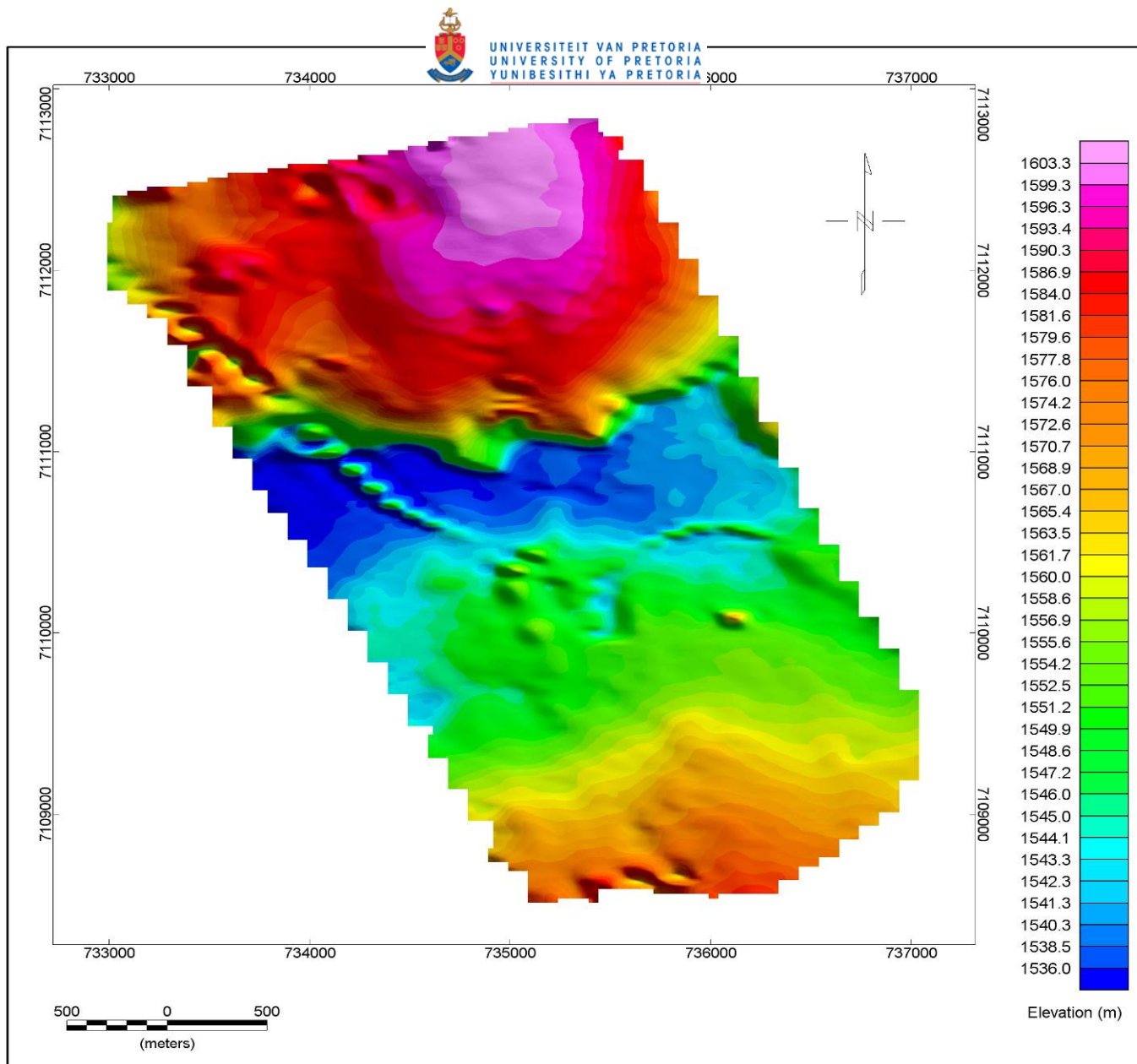


Figure 36. Digital terrain model map of Vandyksdrif area 2 data.

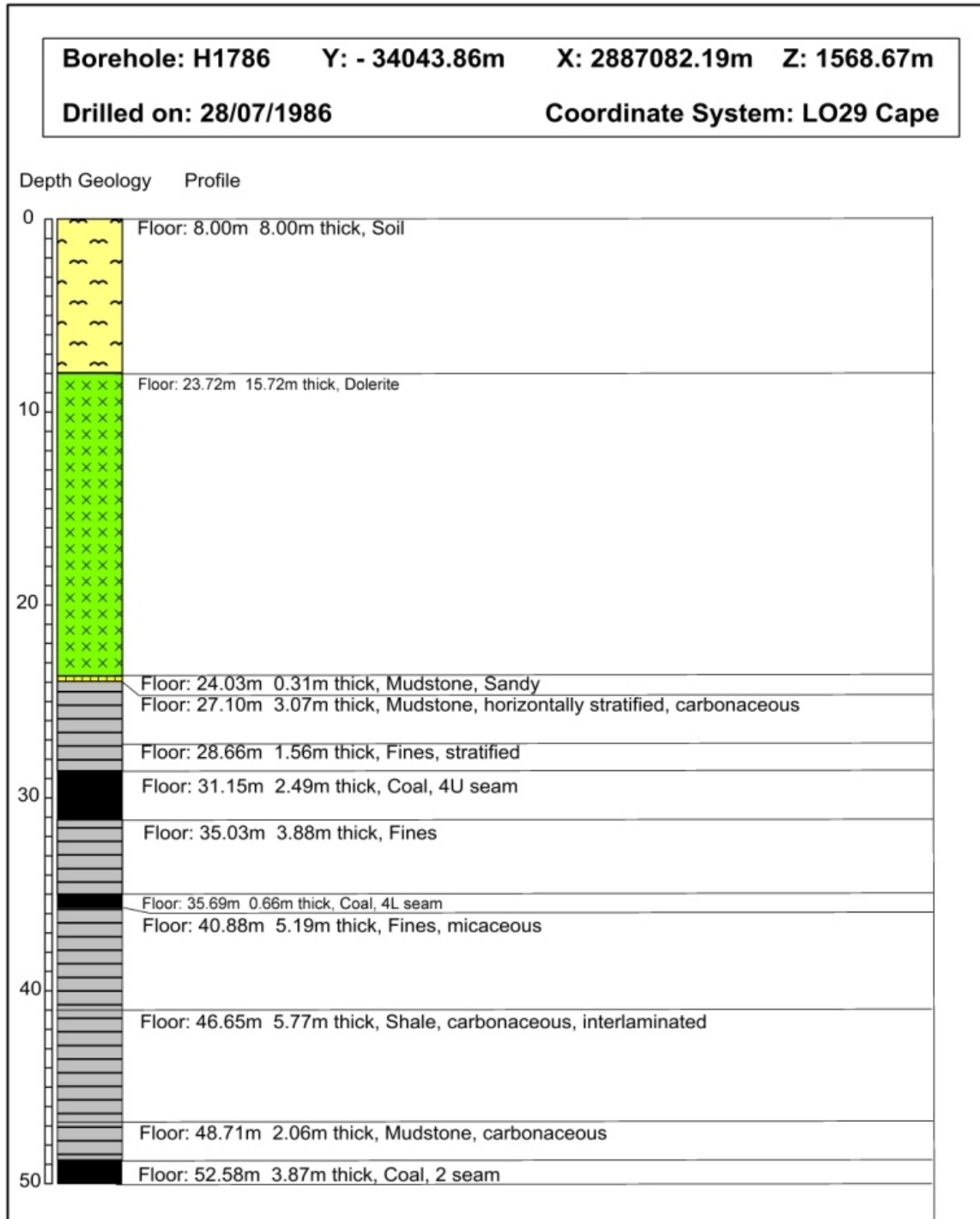


Figure 37. The geological log for borehole H1786 (from Parisi, 1986).

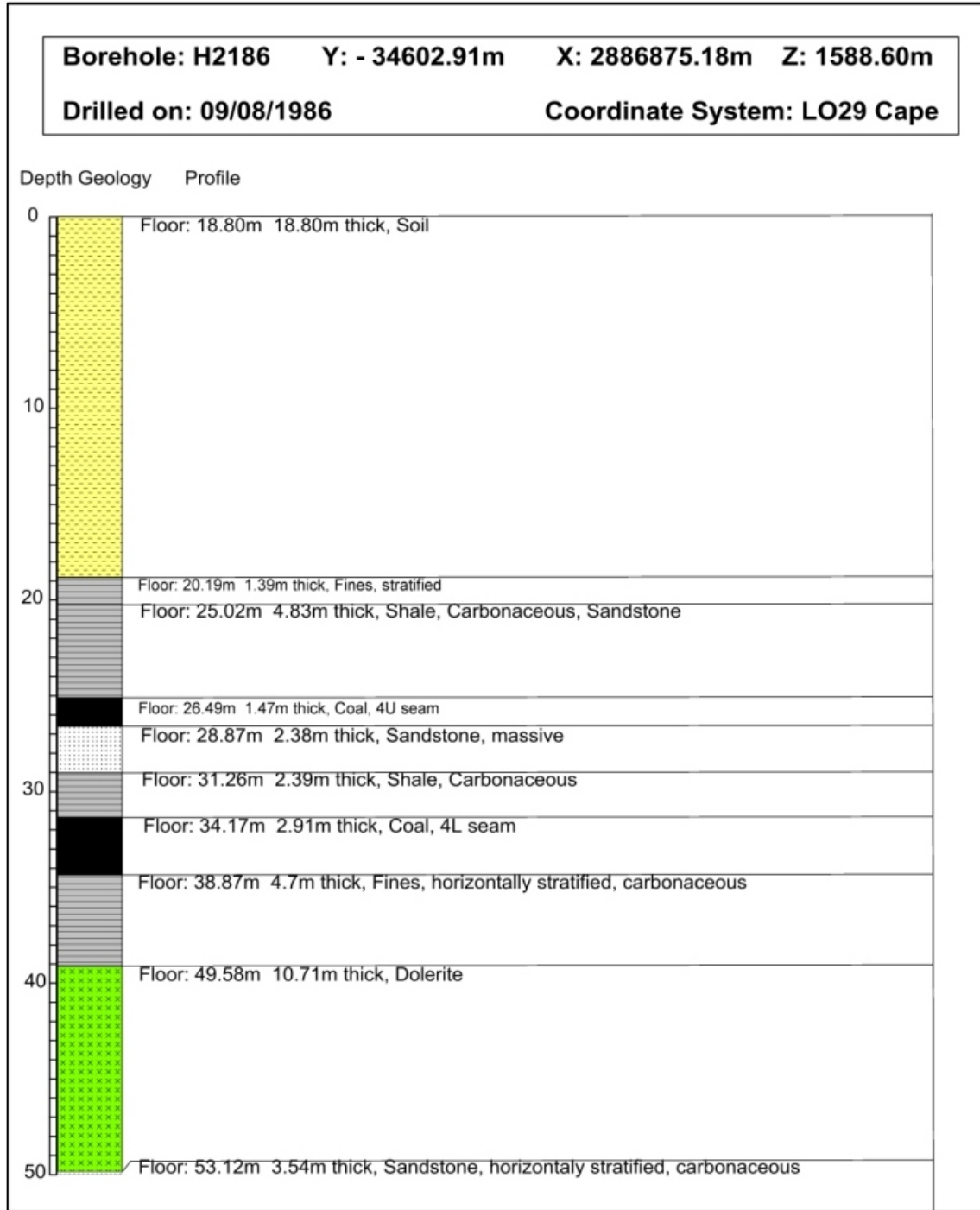


Figure 38. The geological log for borehole H2186 (from Parisi, 1986).

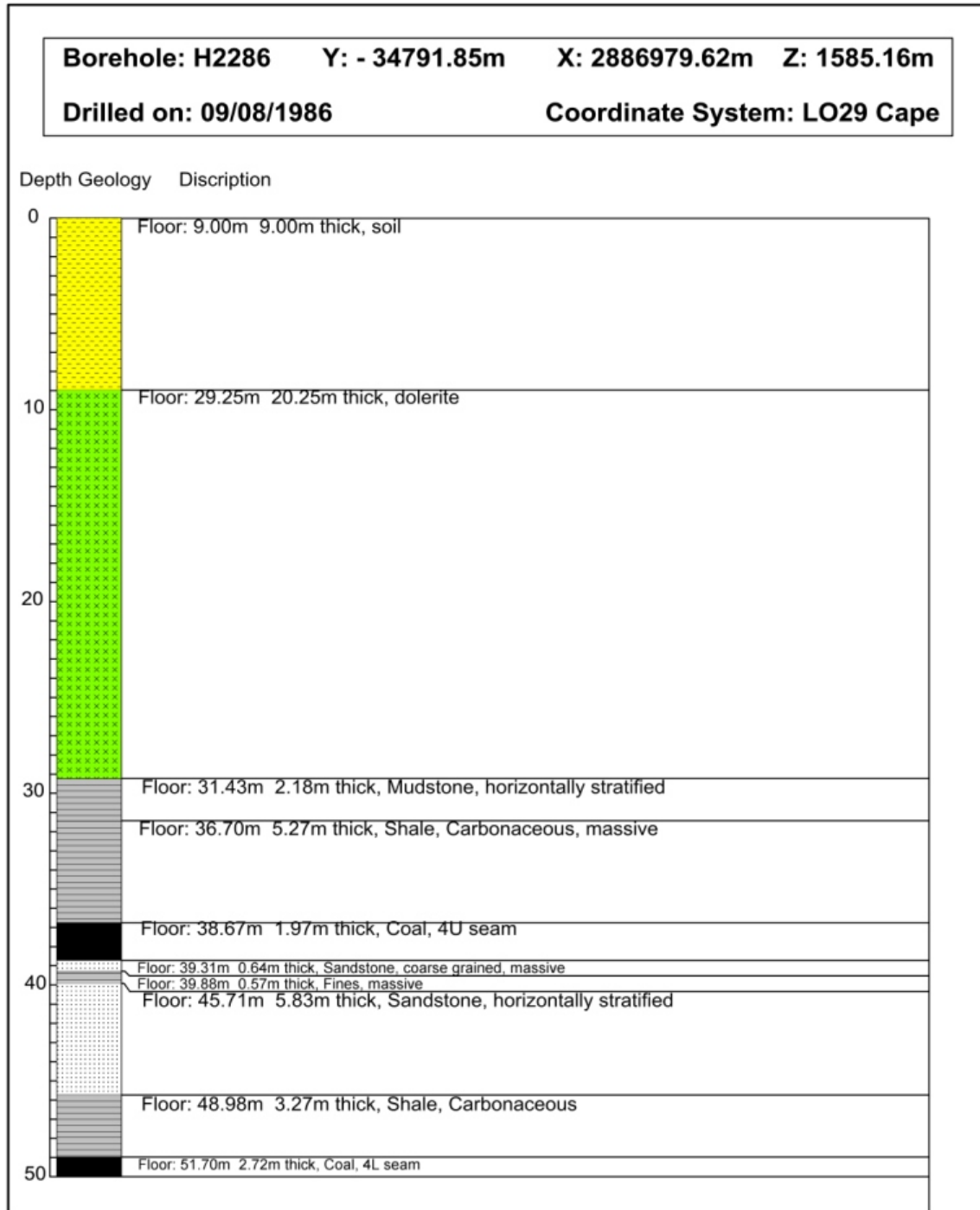


Figure 39. The geological log for borehole H2286 (from Parisi, 1986).

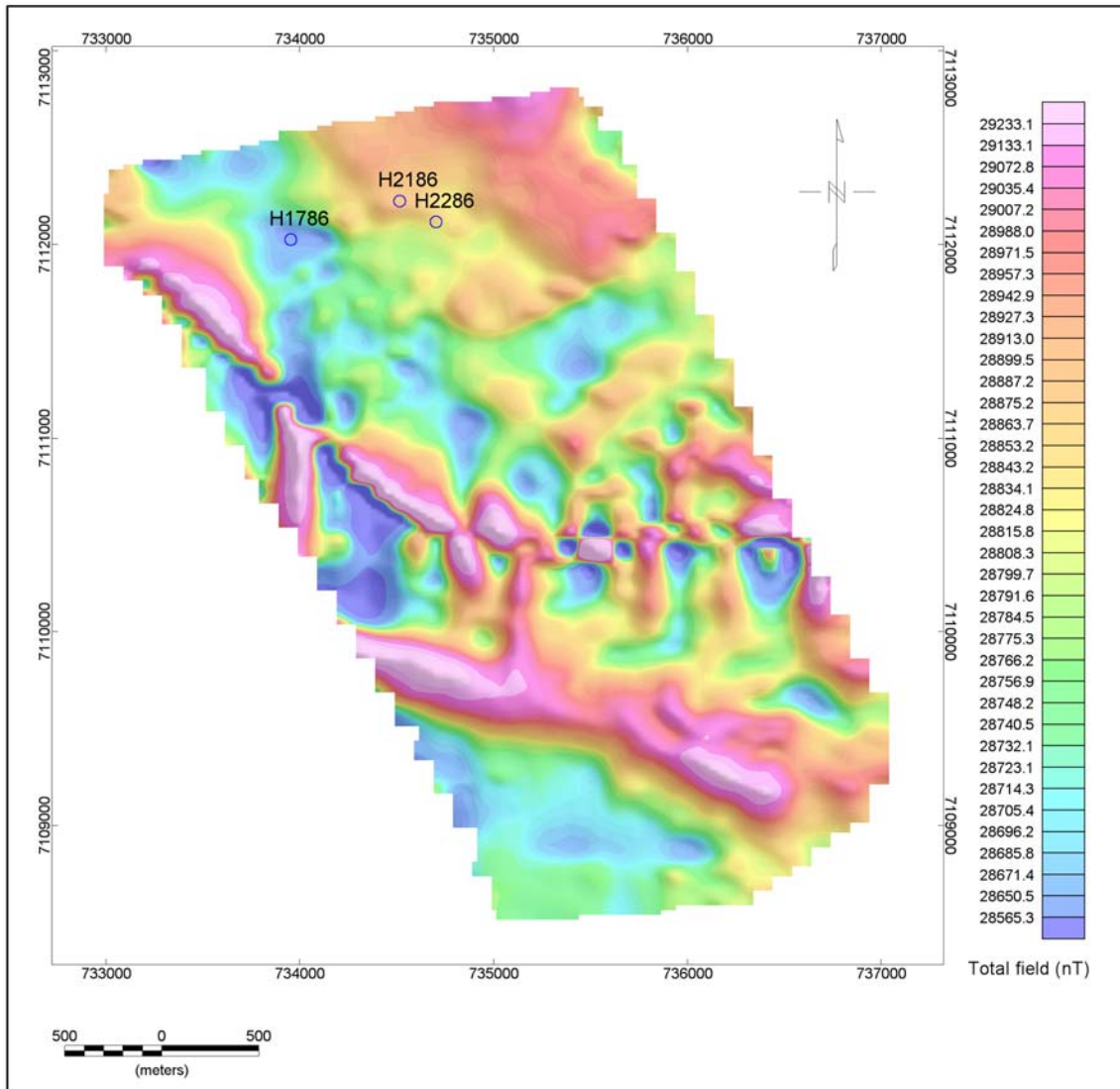


Figure 40. Positions of the boreholes used for interpretation.

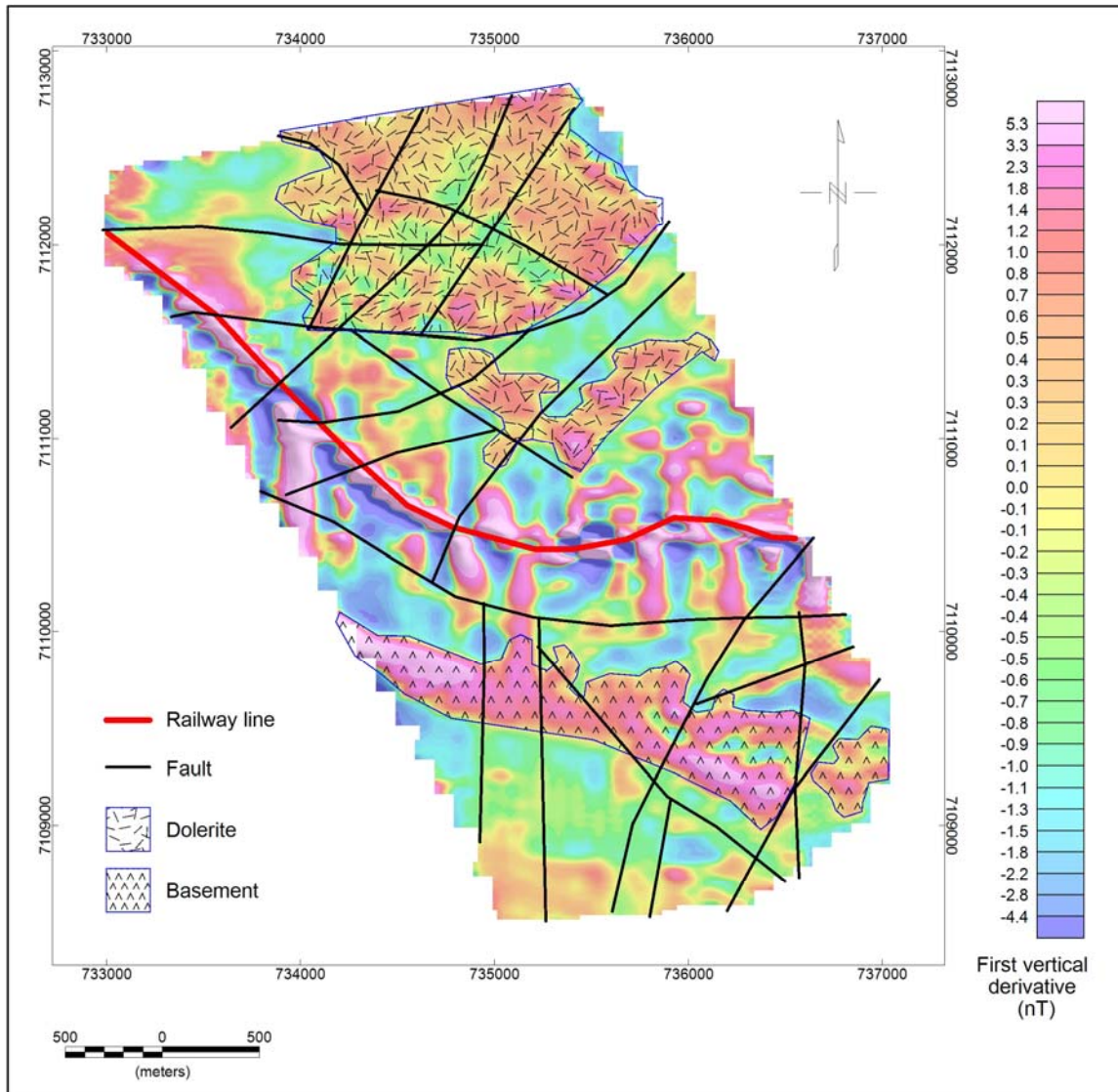


Figure 41. Interpreted structures for Vandyksdrif area 2 data superimposed on the first vertical derivative map.

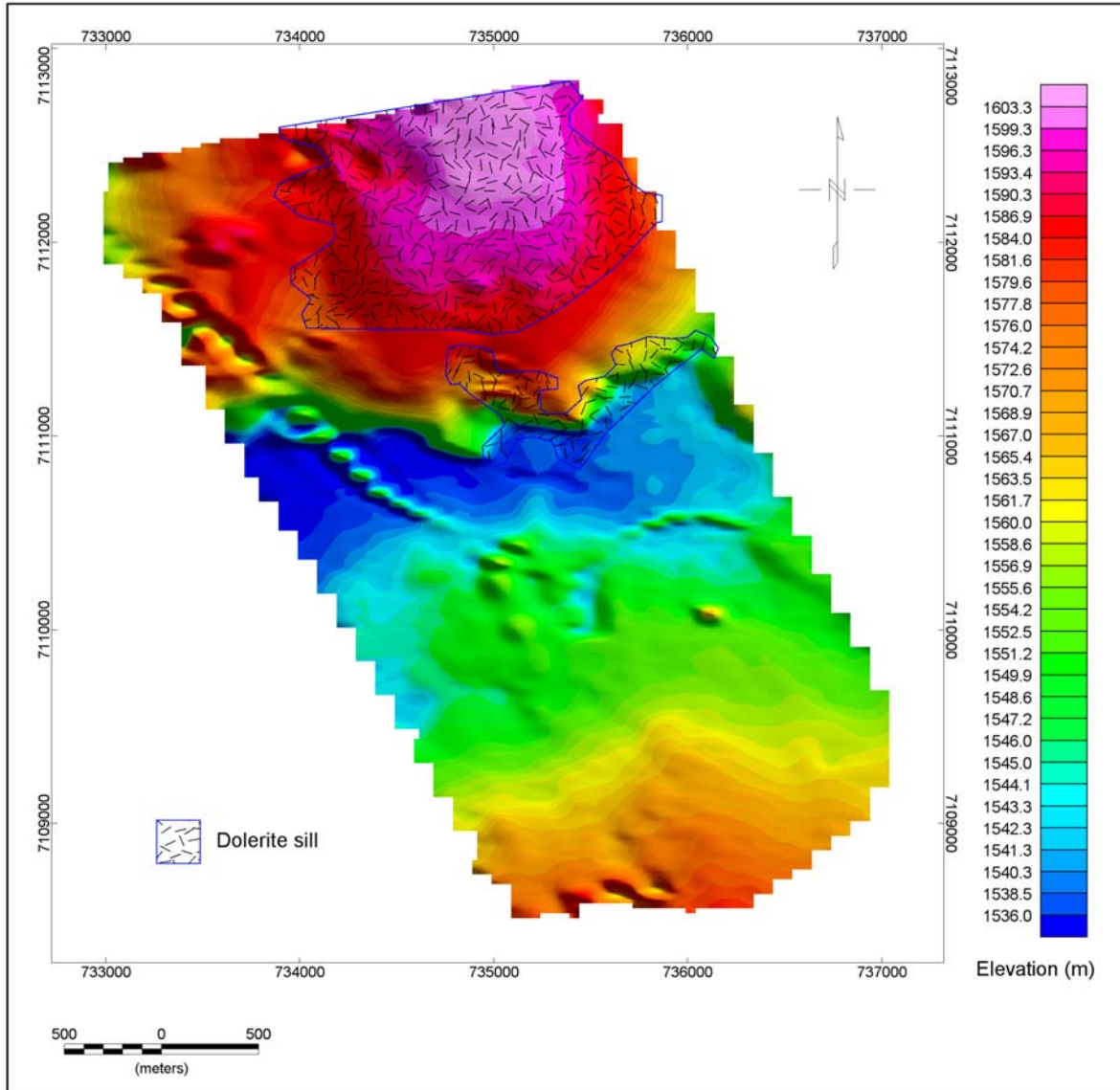


Figure 42. Interpreted sills superimposed on the digital terrain model data.

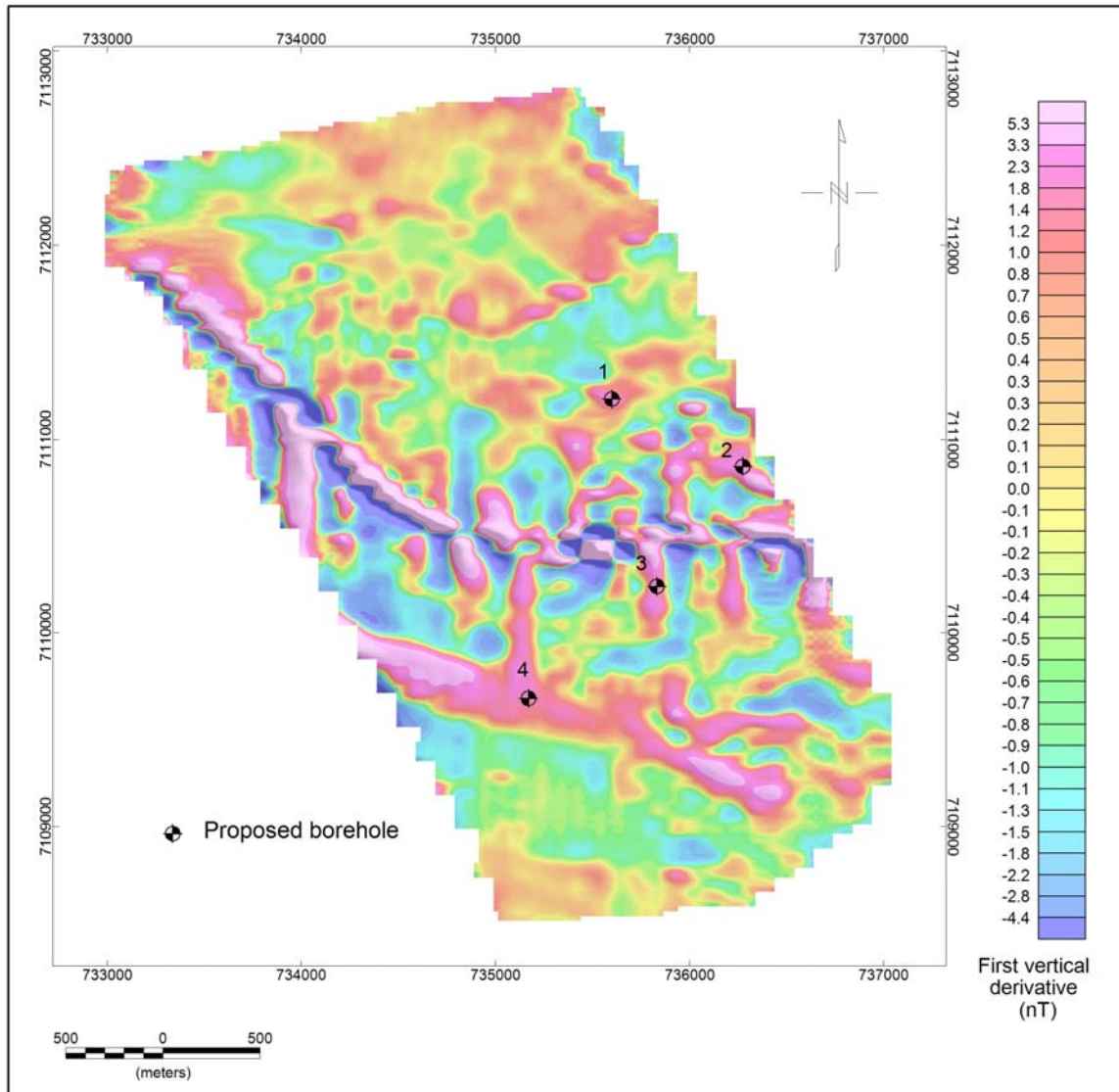


Figure 43. Positions of the proposed boreholes superimposed on the first vertical derivative data.

5.4. INTERPRETATION OF ARNOT DATA.

Figures 44, 45, 46 and 47 show the datasets used for interpretation: *total field magnetic data*, *analytic signal data*, *first vertical derivative data* and *the geological log* respectively. Figure 48 shows the interpretation, superimposed on the vertical derivative map.

First vertical derivative dataset does not differ much with the total field magnetic dataset, as such only the total field magnetic data and the analytic signal data are discussed. This could be because of a lot of shallow features dominating the data. The gap observed in the data is the Arnot power station where low level flying was not permitted. On the analytic signal dataset, only the highly magnetic features are outlined and the less magnetic ones as seen from the total field magnetic dataset disappear.

The most prominent features on the magnetic data are the lineaments interpreted as dykes; oriented in a northeast – southwest direction (almost north - south) through the middle of the surveyed area. These dykes seem to be an extension of the dykes that will be explained in the next section. They are more pronounced on the total field magnetic dataset than on the first vertical derivative and analytic signal datasets. The dykes are bounding a low magnetic body in the north believed to be the valley filled with Karoo sediments as seen on the analytic signal data.

The intrusions affected the entire area becoming less intense in the low magnetic areas bounded by the previously mentioned prominent dykes. The affected portions have the dykes and faults scattered everywhere as seen on the interpretation map (Figure 48). From northeast going south of the survey area, the dykes start as a unit and then branch as they reach the central area. The branches continue southwards until some of them terminate against an almost east west trending dyke. Further east, another dyke can be seen running from east going south westwards. It is terminated by the only dyke (that's visible in the area) running in a northwest - southeast direction.

From the north slightly towards northwest, another activity of dykes is observed. In this region, as observed on the total field magnetic data, the dykes are scattered from the north and terminate against what is believed to be a sill as we proceed southwest wards. The sill is one of the three sills interpreted on the western part of the survey area. Two parallel features, which connect the three interpreted sills, can be seen on the western corner of the area. It is not immediately clear if the features are sills or broad dykes and they are highly faulted. They are indentified as dyke/sill on the interpretation map.

Several other patches of sills are also outlined. Two main sill bodies were interpreted on the eastern half of the survey area, with three smaller ones to the west and one in the central area. The observed sills are believed to be the dolerites of the Karoo age as the borehole log shows (Figure 47).

Faults are occurring almost over the entire area, becoming more prominent around the sill areas. This means that the origin of the faults may be related to intrusions and the following scenarios could have happened: the faults could have been caused by the intrusions, or faulting could actually have taken place at the time of intrusions or the sill intrusions could have taken place along the faults which existed before. Long faults along the discussed prominent dykes are to be expected but in order not to cluster the interpretation with faults and dykes on top of each other, the dykes are the ones shown in these areas.

The survey area has a power station and as expected has the powerlines which affected the data. The powerlines together with a railway line are clearly enhanced on analytic signal dataset, Figure 49. The railway line signature disappears into the dykes at the northeastern part and as such it was very difficult to isolate. Its extent was therefore outlined using railway line database available from Arnot mine.

Three boreholes are proposed to verify some of the features. The positions of the proposed boreholes are indicated on Figure 50 and the coordinates are given in Table 3 below.

Table 3. Positions of the recommended boreholes.

BH_ID	UTM_X	UTM_Y
1	781069.879	7135430.247
2	781929.858	7134455.796
3	778454.424	7131608.346

Three profiles (Figures 51, 52 and 53 with the positions shown on Figure 50) were taken from the first vertical derivative data. This is because in high magnetic latitudes (i.e. the inclinations greater than 55° and in our case is 60°) the anomaly curves for the total field and the first vertical derivative look much the same (Roux, 1980). The idea was to have the profiles modelled but due to lack of borehole information, it would have been difficult to constrain the model. As the flight lines were cutting the profiles at an angle less than 90° , the profiles were digitized from the grid approximately perpendicular to the dykes and as such no compensation was necessary.

The zero line, the dyke centre, the depth to the top of the dyke and the dip were approximated by the method of cords (Werner, 1953) and the Horizontal Slope Distance method (Vacquier *et al*, 1951) from the profiles. A curve sheet is used to match anomalies and then reading off the dip value. The procedure is described in the South African Geophysical Association's manual for Technicians (The Magnetic Method by A.T. Roux, 1980). The tricky part is the curve matching as more than one standard curve (from the curve sheet) closely matches the anomaly curves. In that case a curve that looks the closest is chosen. Below is how the values were estimated:

Profile AC

1. The *zero line* and the *dyke centre* are depicted on the profile (Figure 51). *The depth to the top of the dyke* was estimated using the Horizontal Slope Distance method:

From the profile, H. S. D. = 56.14m

$$\begin{aligned} Z &= 1.3 \times 56.14\text{m} \\ &= 72.98\text{m} \end{aligned}$$

For the depth of the dyke below the surface, a terrain clearance of 35m was subtracted. That is 72.98m – 35m, which equals 37.98m

2. *Estimating the Dip*

The anomaly closely resembles the curve on line 90° at a dip of 105°. Drawing a line at 75° and where this line cuts the line of identical curve shape, the dip reads as follows:

Dip = 120° for ΔT anomaly

According to the curve sheet ΔZ Dip is the same as ΔT because 0° should be subtracted from ΔT Dip

\therefore Dip = 120° in the direction 75°

or Dip = 60° (180° - 120°) in the direction 105° (180° - 75°)

3. The *maximum* width of the dyke is *estimated* as a third of the value of the depth to the top of the dyke (i.e., $Z/3$). That is 72.98m divided by 3, which equals 24.33m

Profile AE

1. The *zero line* and the *dyke centre* are depicted on the profile (Figure 52). *The depth to the top of the dyke* was estimated using the Horizontal Slope Distance method:

From the profile, H. S. D. = 43.21m

$$Z = 1.3 \times 43.21\text{m}$$

$$= 56.17\text{m}$$

Subtracting terrain clearance of 35m, the depth of the dyke below the surface becomes 21.17m

2. *Estimating the Dip*

This anomaly also closely resembles the curve on line 300° at a dip of 120°. Following the same procedure as in profile AC and drawing a line at 320°, the dip read as follows:

Dip = 133° for ΔT anomaly

for ΔZ Dip 28° is subtracted from ΔT Dip

\therefore Dip = 106° in the direction 320°

or Dip = 74° (180° - 106°) in the direction 140° (320° - 180°)

3. The *maximum* width of the dyke is *estimated* as a third of the value of the depth to the top of the dyke (i.e., $Z/3$). In this case it is 56.17m divided by 3, which is equal to 18.72m.

Profile AF

1. The *zero line* and the *dyke centre* are depicted on the profile (Figure 53). The depth to the top of the dyke was estimated using the Horizontal Slope Distance method:

From the profile, H. S. D. = 27.07m

$$Z = 1.3 \times 27.07\text{m}$$

$$= 35.19\text{m}$$

Subtracting terrain clearance of 35m, the depth of the dyke below the surface becomes 0.19m.

2. *Estimating the Dip*

The anomaly closely resembles the curve on line 270° at a dip of 105°. The same procedure as on the previous profiles was followed by drawing a line at 285° this line

cuts the line of identical curve shape, the dip read as follows:

Dip = 120° for ΔT anomaly

for ΔZ Dip 16° is subtracted from ΔT Dip

\therefore Dip = 104° in the direction 285°

or Dip = 76° ($180^\circ - 104^\circ$) in the direction 105° ($285^\circ - 180^\circ$)

3. The *maximum* width of the dyke is *estimated* as 11.73m.

Looking at the dyke where the profile AF was taken (on the total field and analytic signal data), a change in the intensity of the magnetic field is observed. The change could be due to the interpreted fault nearby, whereby one part of the fault was down thrown; reducing the intensity of the magnetic field with depth. The less magnetic intensity part could also be part of the dyke being thrown up closer to the surface and exposed to weathering processes, again reducing the intensity of the magnetic field. This statement is supported by the shallower depth to the top of the dyke calculated for the profile.

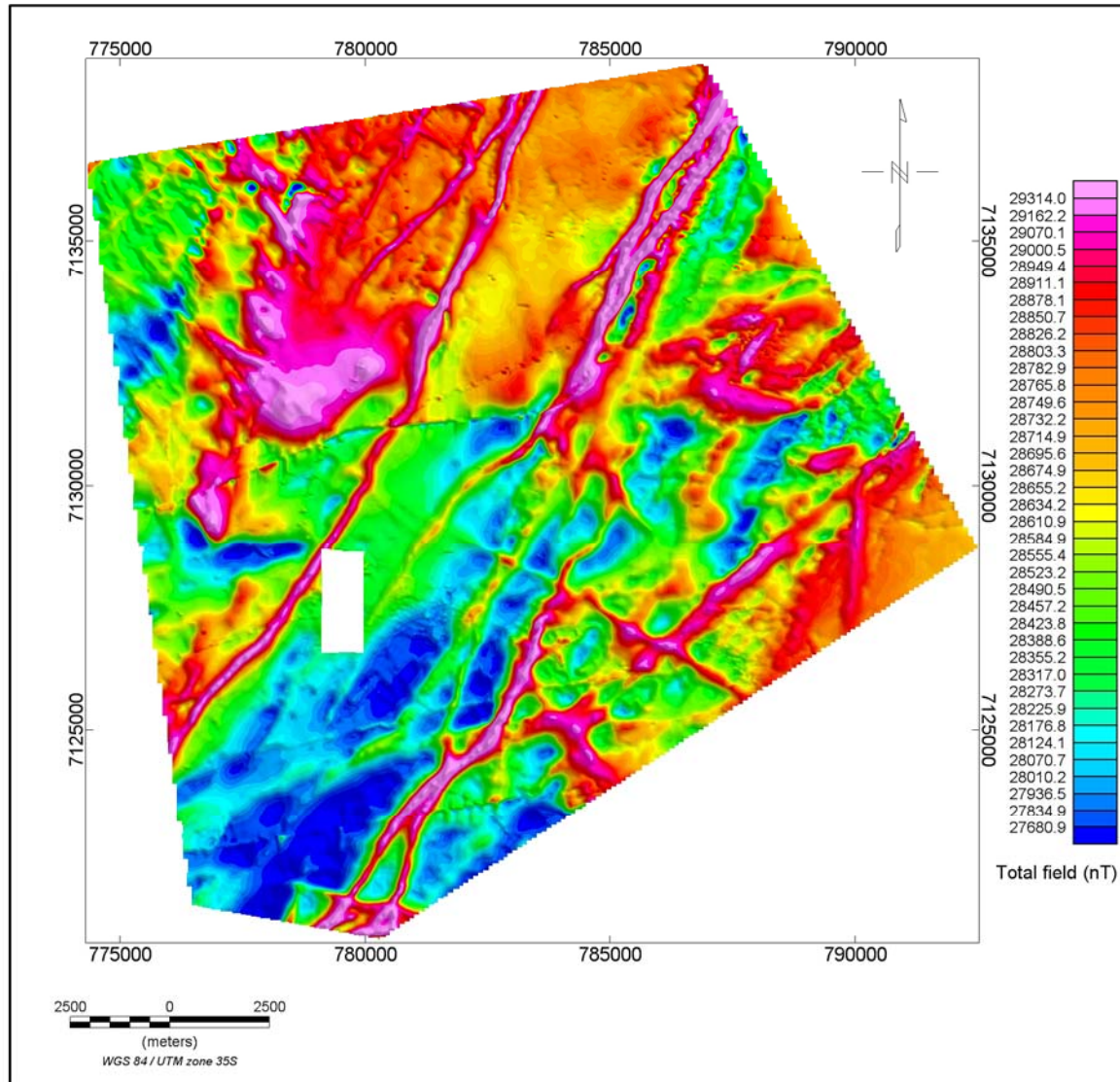


Figure 44. Total field magnetic intensity map of Arnot data.

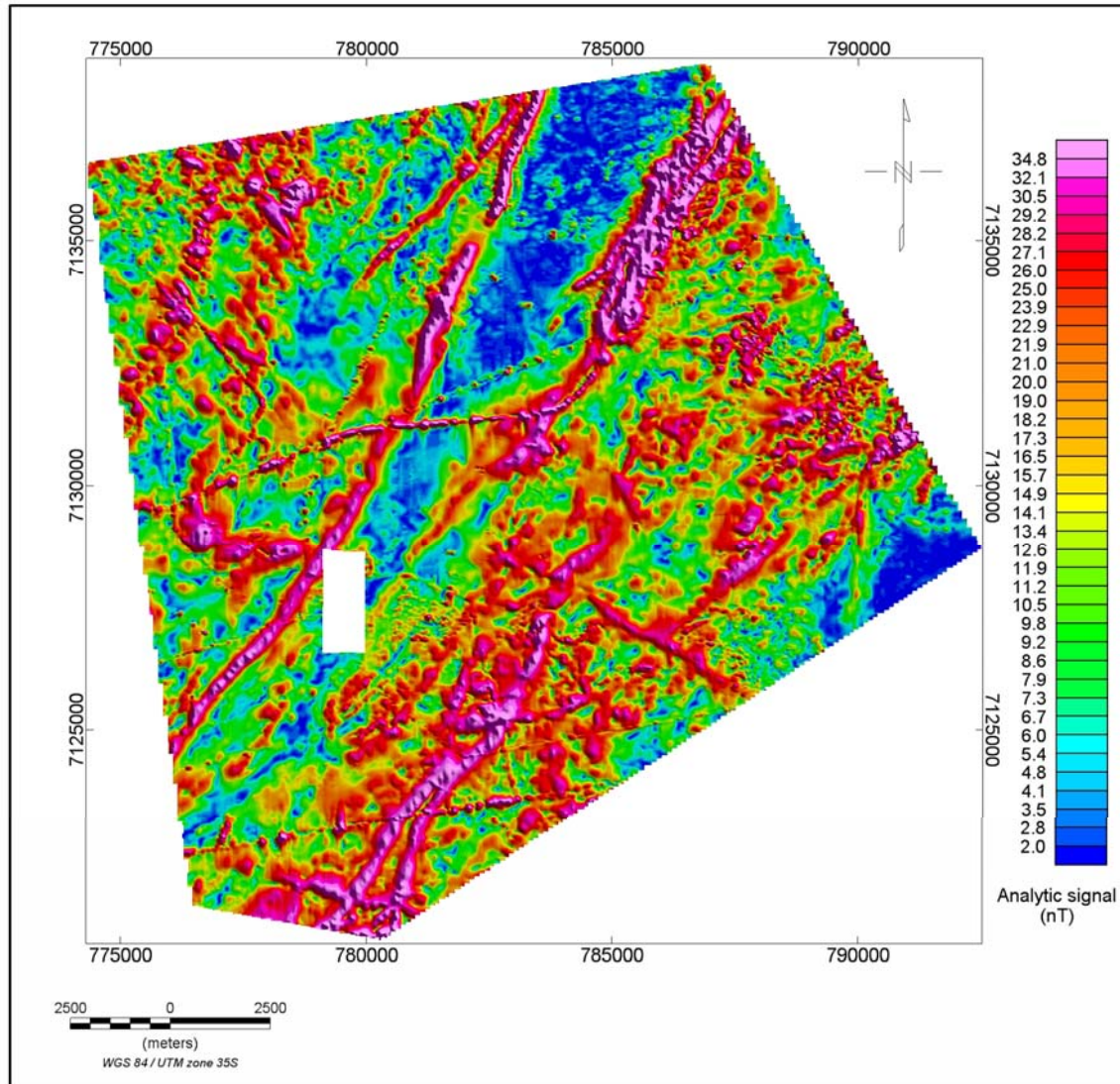


Figure 45. Analytic signal map of the Arnot data.

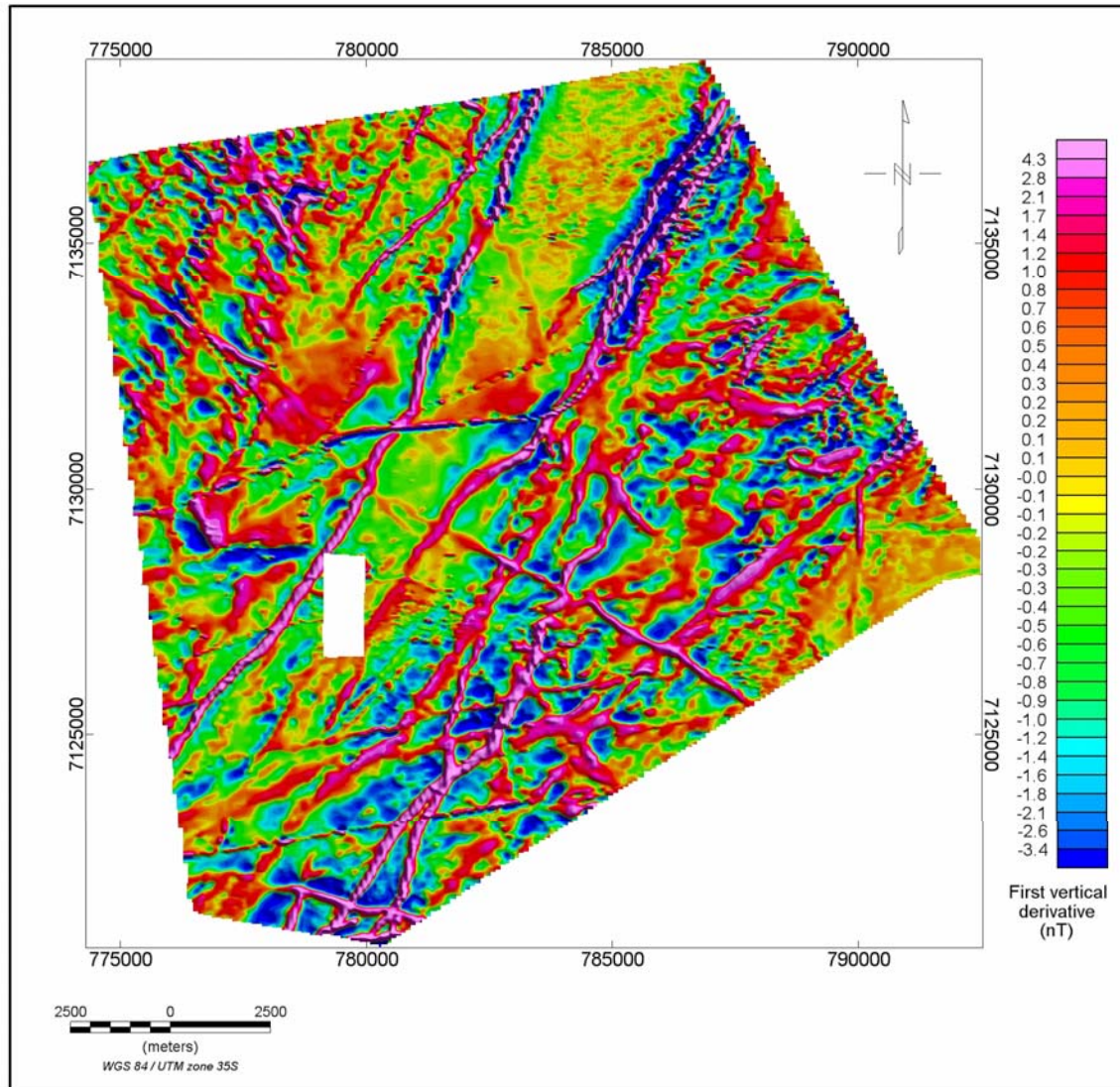


Figure 46. First vertical derivative map of Arnot data.

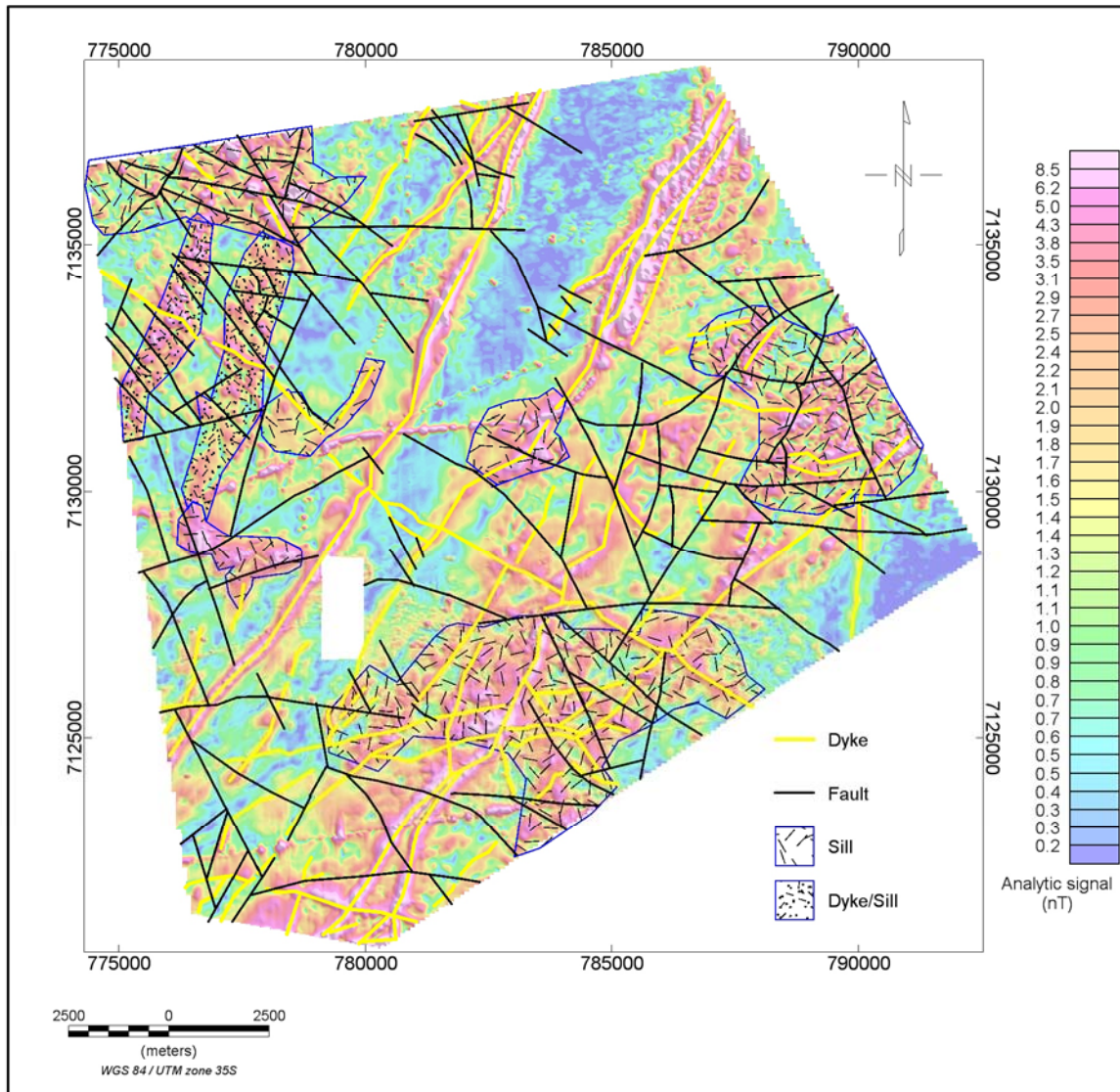


Figure 48. Interpreted structures for Arnot data superimposed on the analytic signal data.

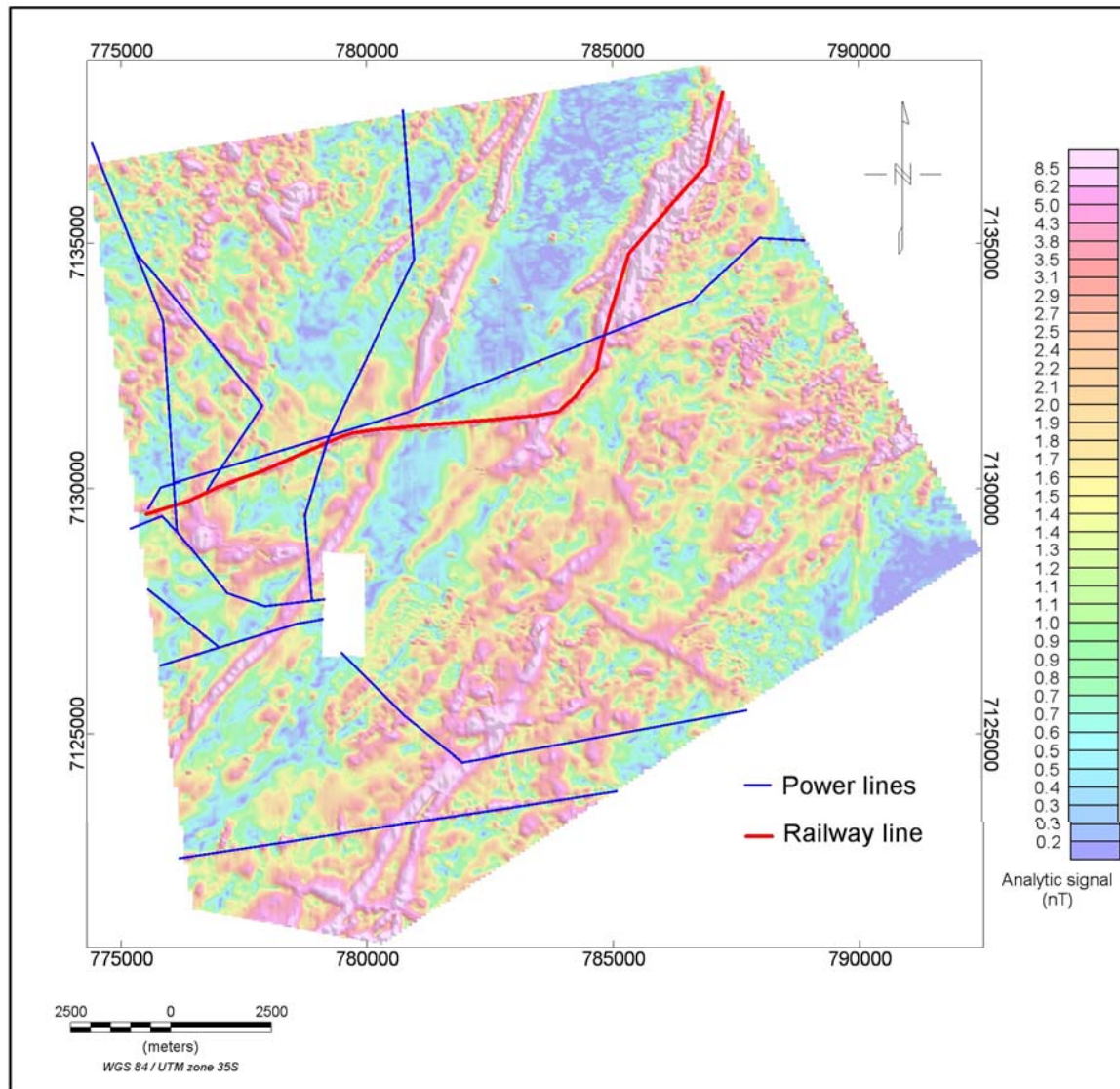


Figure 49. Cultural features observed on the Arnot data superimposed on the analytic signal data.

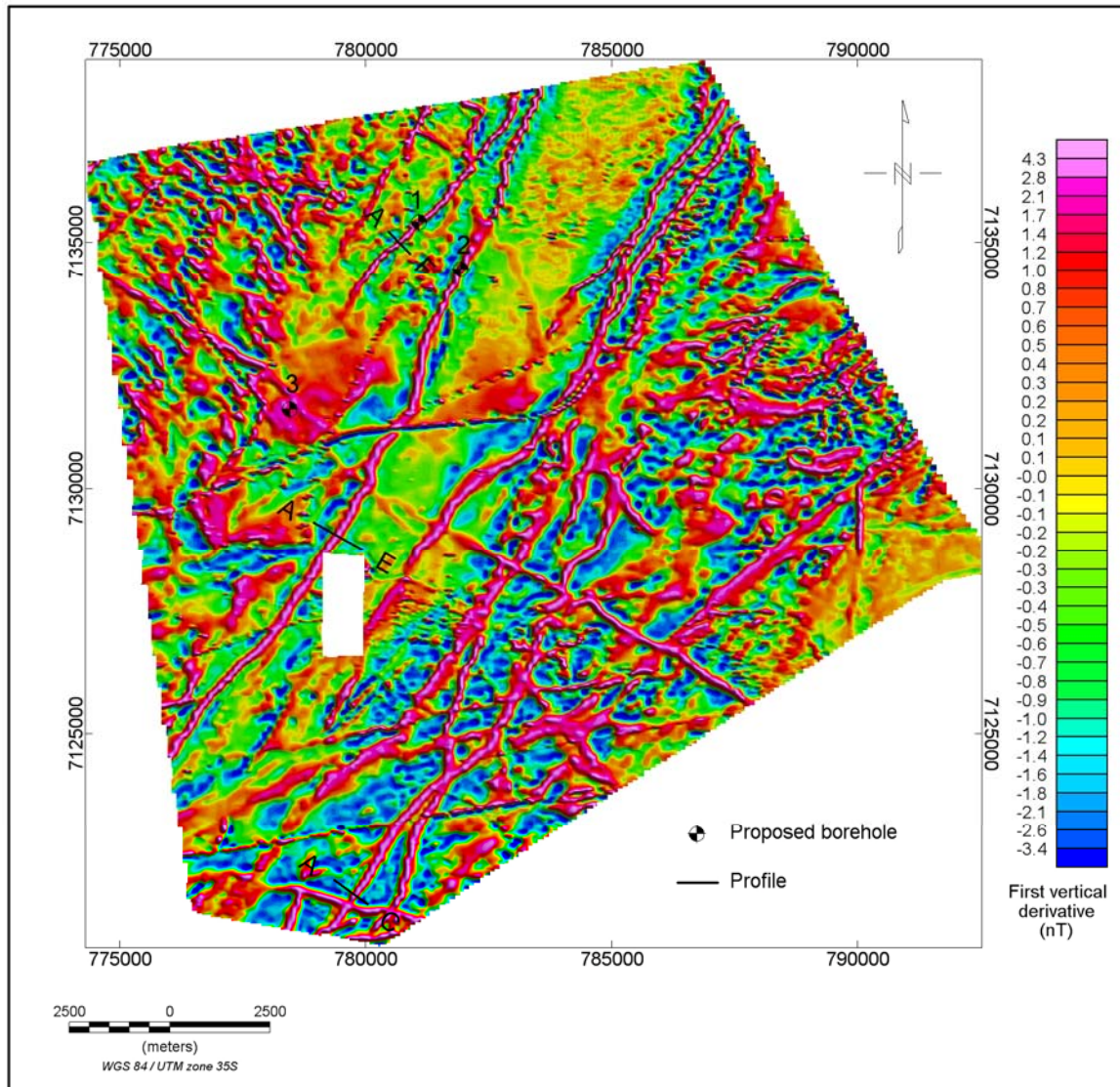


Figure 50. Positions of the proposed boreholes and the profiles superimposed on the first vertical derivative data.

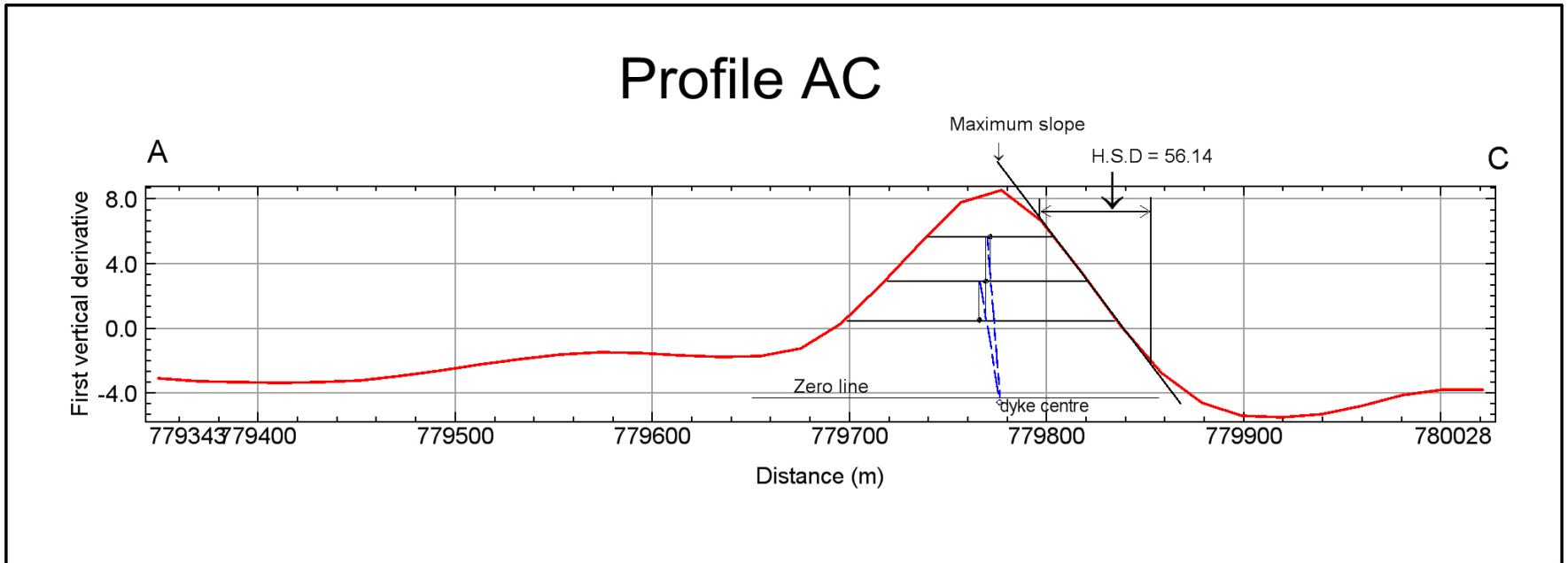


Figure 51. Profile AC.

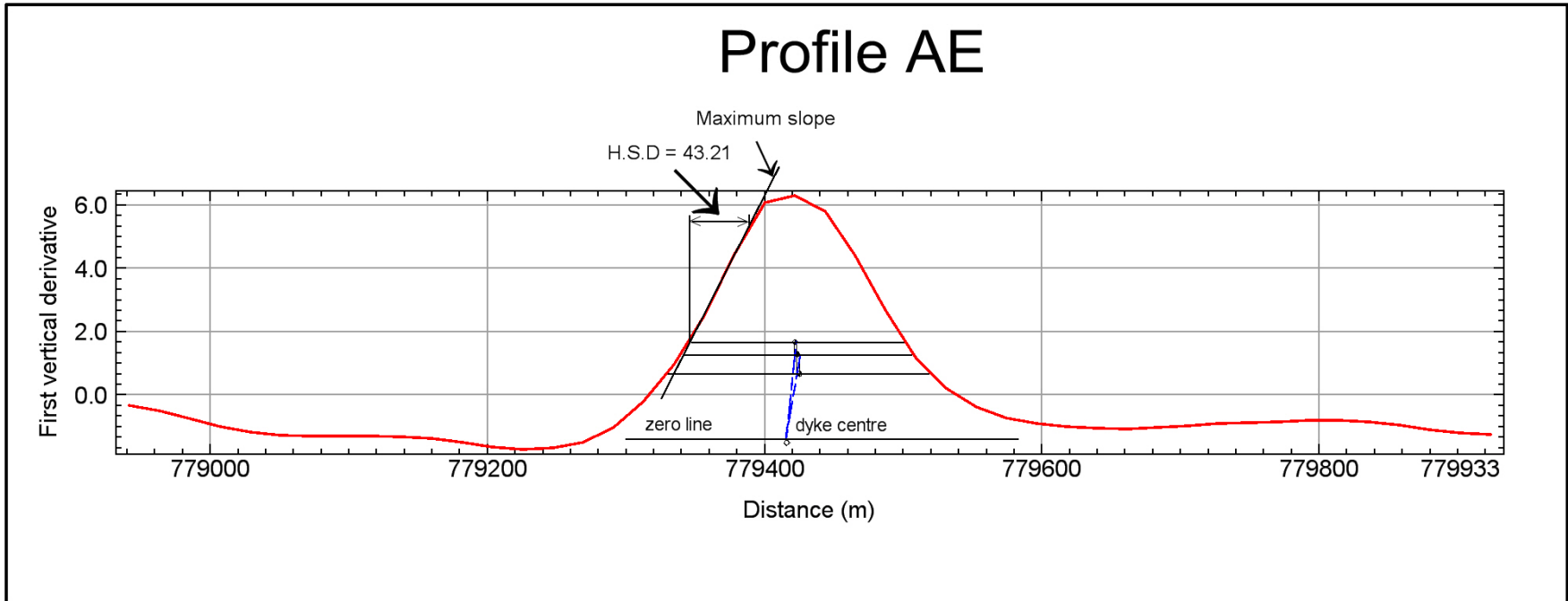


Figure 52. Profile AE.

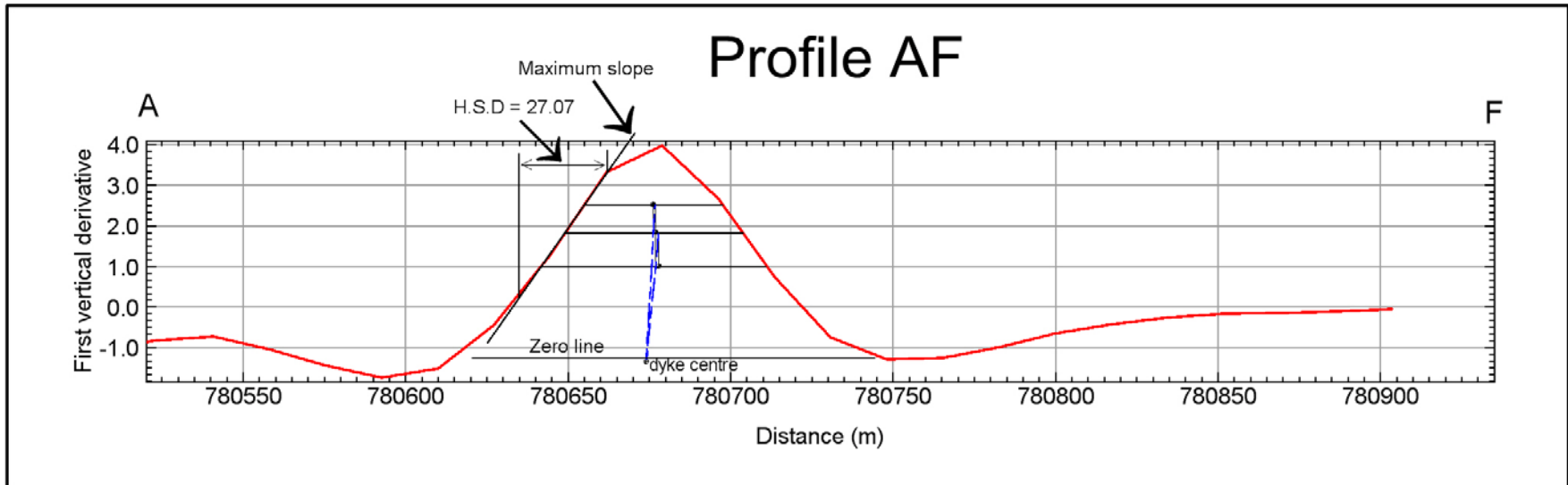


Figure 53. Profile AF

5.5. INTERPRETATION OF BELFAST DATA.

Figures 54, 55 and 56 show the datasets used for interpretation: *total field magnetic data*, *analytic signal data* and *first vertical derivative data*. Figure 57 shows the interpretation, superimposed on the vertical derivative map

Several dominant lineaments in a northeast – southwest direction, covering almost the entire survey area except the central area and a portion on the southeastern part, were identified. They are interpreted as dykes. They are clearly distinct on all forms of data presentation. Looking at the amplitudes of these dykes on the total field magnetic data, one notices two sets of dykes: the positively magnetic ones and the negatively magnetic others. The negative dykes are known as remanent dykes and they are usually older than the positive ones. Remanent dykes are negative because of an activity called magnetic reversal. The presence of remanent dykes and the ‘normal’ dykes in the same area signifies age difference of the dykes.

Some of the dykes could be part of the dyke swarm associated with the intrusion of the Bushveld Complex as seen on the regional magnetic map of the country (1: 1 000 000 magnetic map, Figure 58). They could also be associated with Olifants River Dyke Swarm (Jourdan *et al.*, 2006). Personal communication with the geophysicist (Maré, L.P., 2008) from the Council for Geoscience doing palaeomagnetic study of the dykes in the area confirms different ages for these dykes. They bound three low magnetic bodies, (represented by polygons A, B and C on Figure 59), believed to be the valleys filled with Karoo sediments. Two of the bodies are around the central part of the survey area and are separated by a dyke.

Two circular structures (numbered 1 and 2 on Figure 59) believed to be ring dykes on the western edge are interpreted. Ring-dykes are circular sheet intrusions that develop at a sub-volcanic level due to ascent of magma along a steep outward-dipping ring-fracture (O’Driscoll *et al.*, 2005). Magma ascent is triggered by central area subsidence, and when

fully formed, ring-dykes comprise a flat-lying roof as well as steeply outward-dipping walls on all sides.

Faults are observed throughout the entire study area with an east-west general trend except for the ones running along the prominent dykes. The prominent dykes observed probably follow faults.

Several patches of possible sills were also outlined. The main sill is situated on the southwestern edge of the survey area with the other ones occurring on the eastern part and around the central area. The interpreted sills and dykes were thought to be doleritic (part of the Olifants River Dyke Swarm) but the geological information suggests the diabase. The geological information received does not show any presence of dolerite or diabase leading to the suspicion that the observed features could be pre-Karoo or at depths below coal interest.

The sills in this area display the same characteristics as those observed in the Arnot region as seen on the analytic signal data. This suggests that the sills in these regions (Arnot and Belfast) could be of the same age. Regional magnetic data of the country (1: 1 000 000 magnetic map, Figure 58) shows that the dykes in the Arnot region to be possibly the extension of the dykes in the Belfast area.

Cultural features (powerlines lines and a railway line) are enhanced on the analytic signal data (Figure 60). The railway line influenced the signature of the dyke that divided the two central low magnetic bodies.

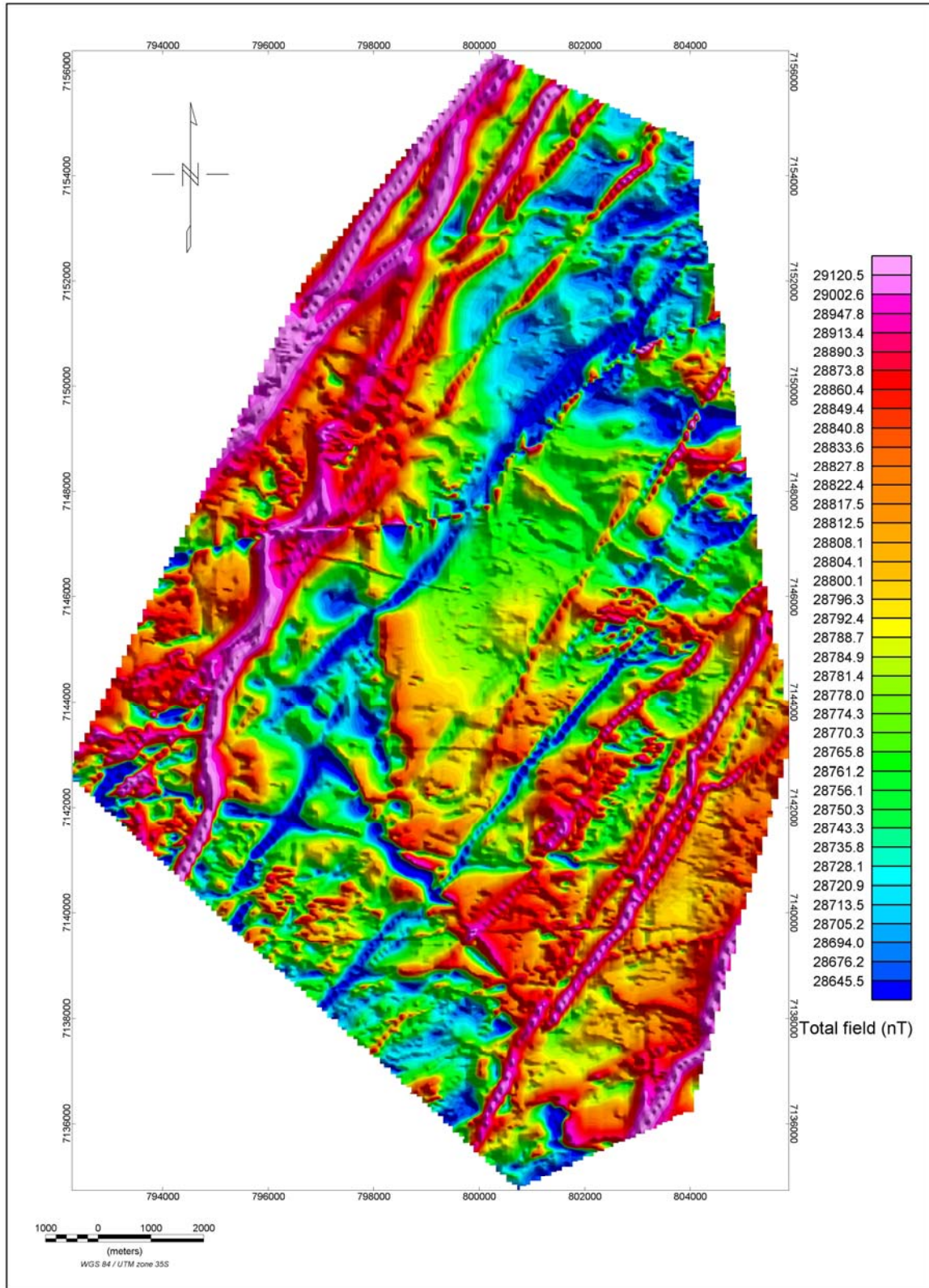


Figure 54. Total field magnetic intensity map of Belfast data.

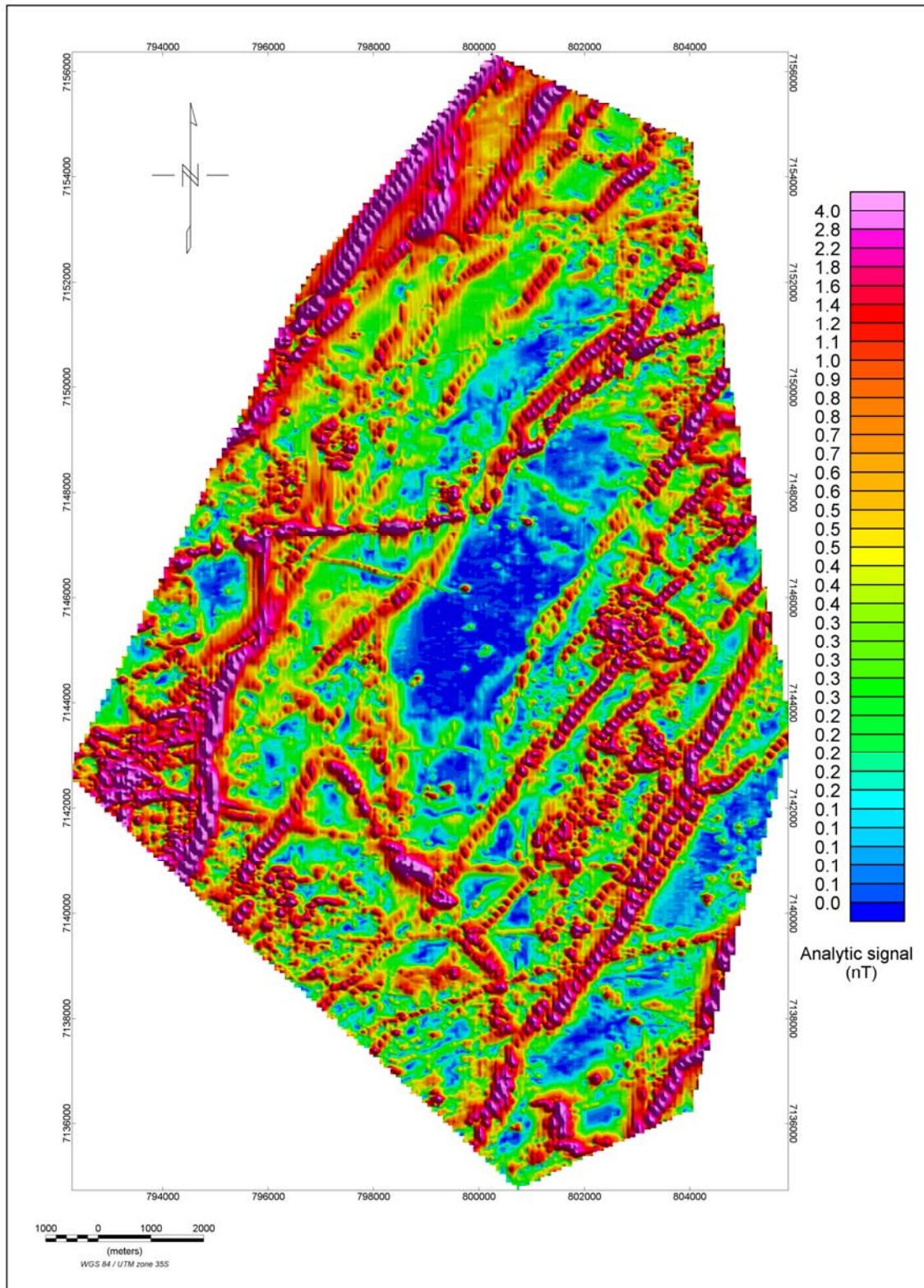


Figure 55. Analytic signal map of Belfast data.

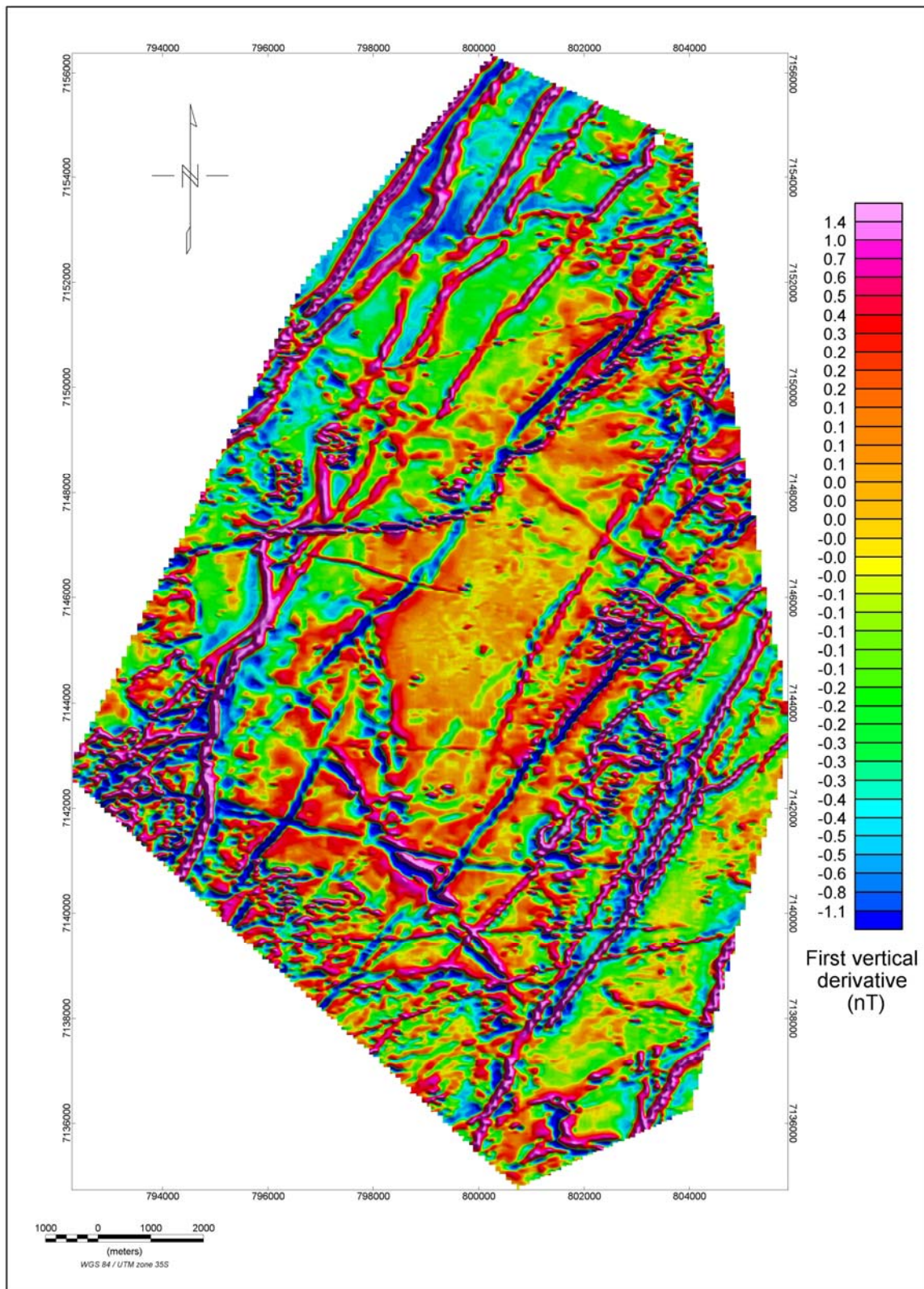


Figure 56. First vertical derivative map of Belfast data.

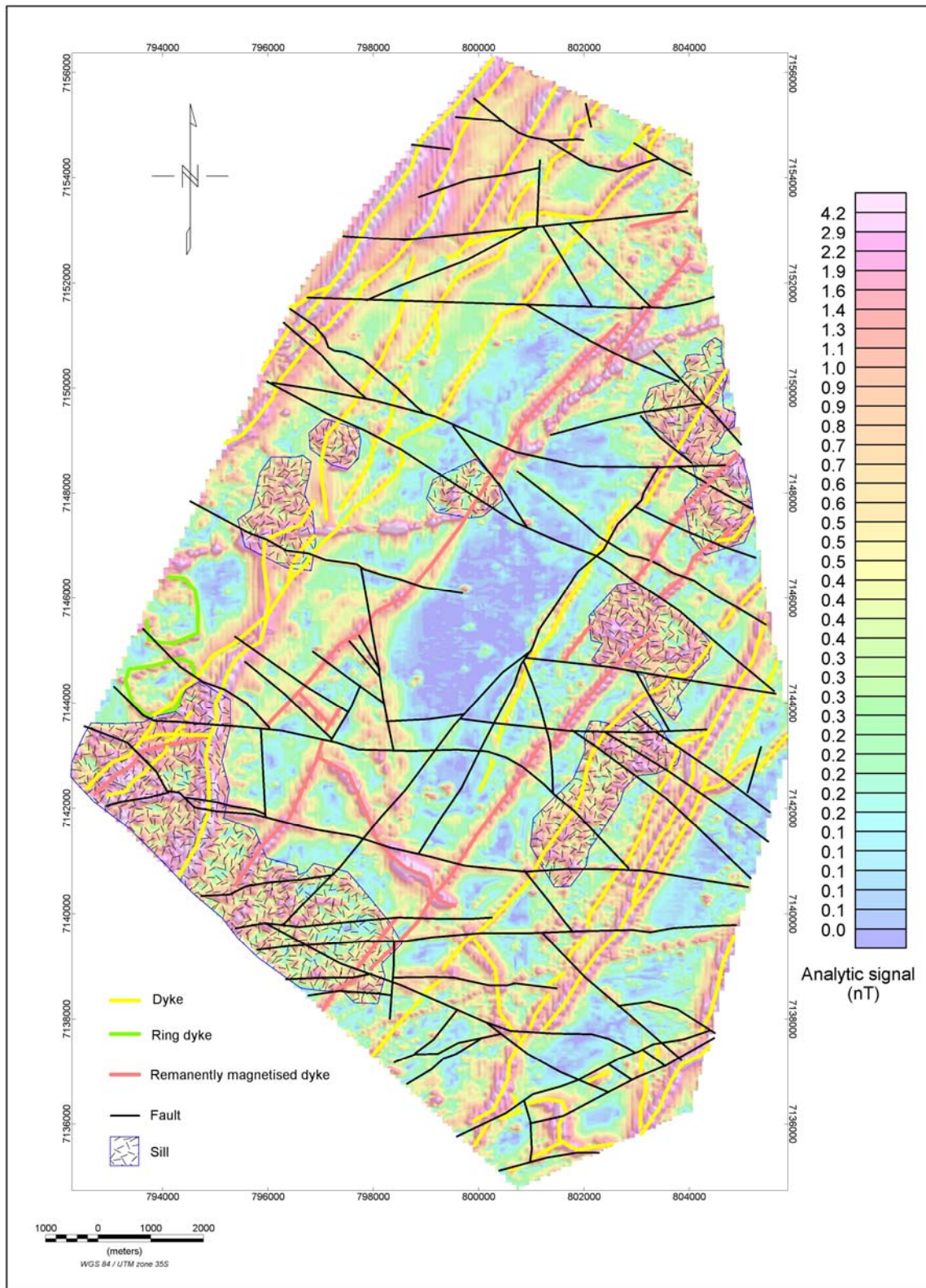


Figure 57. Interpreted structures for Belfast data superimposed on the analytic signal data.

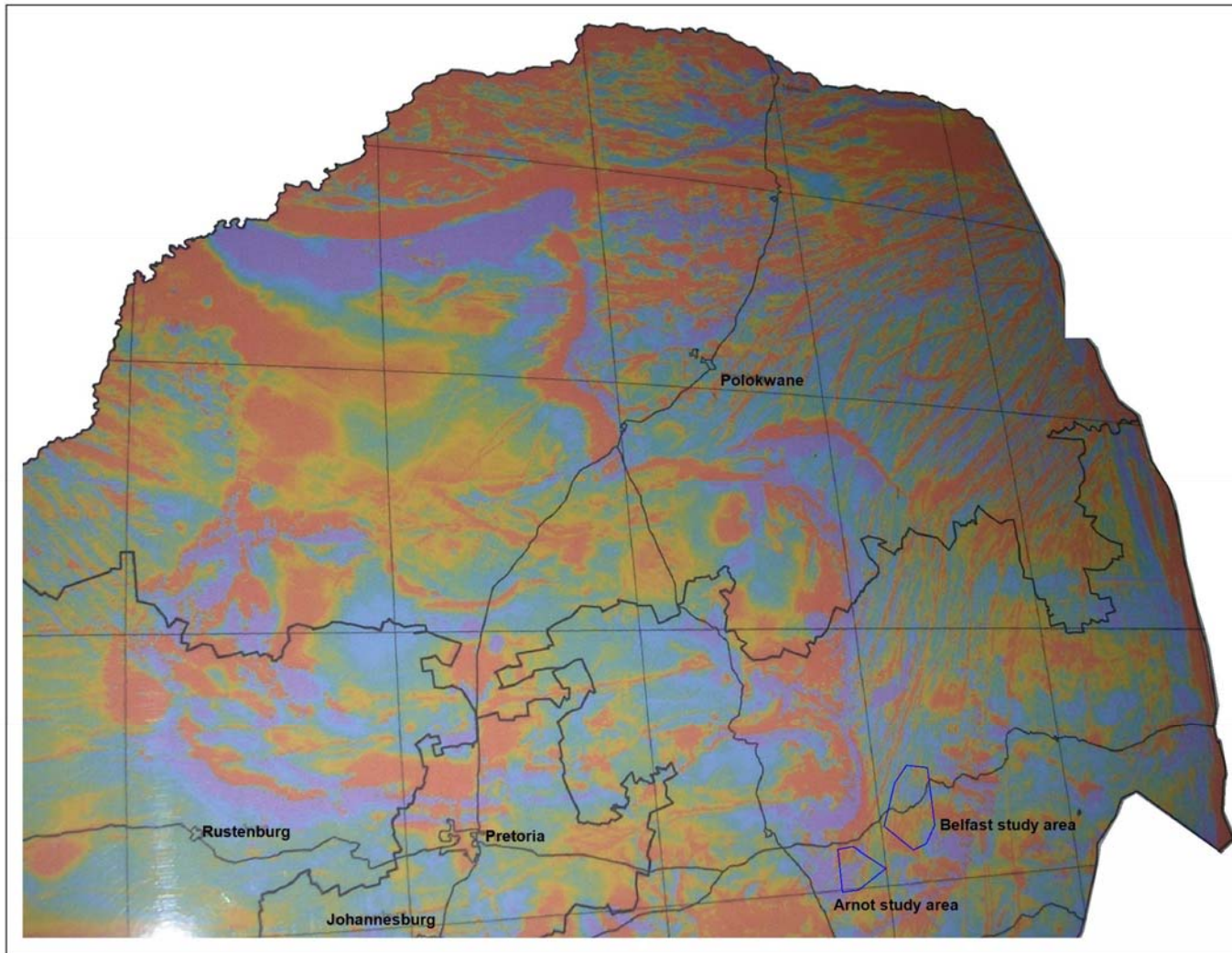


Figure 58. Regional magnetic map of South of Africa (modified from 1:1 000 000 magnetic map of South Africa).

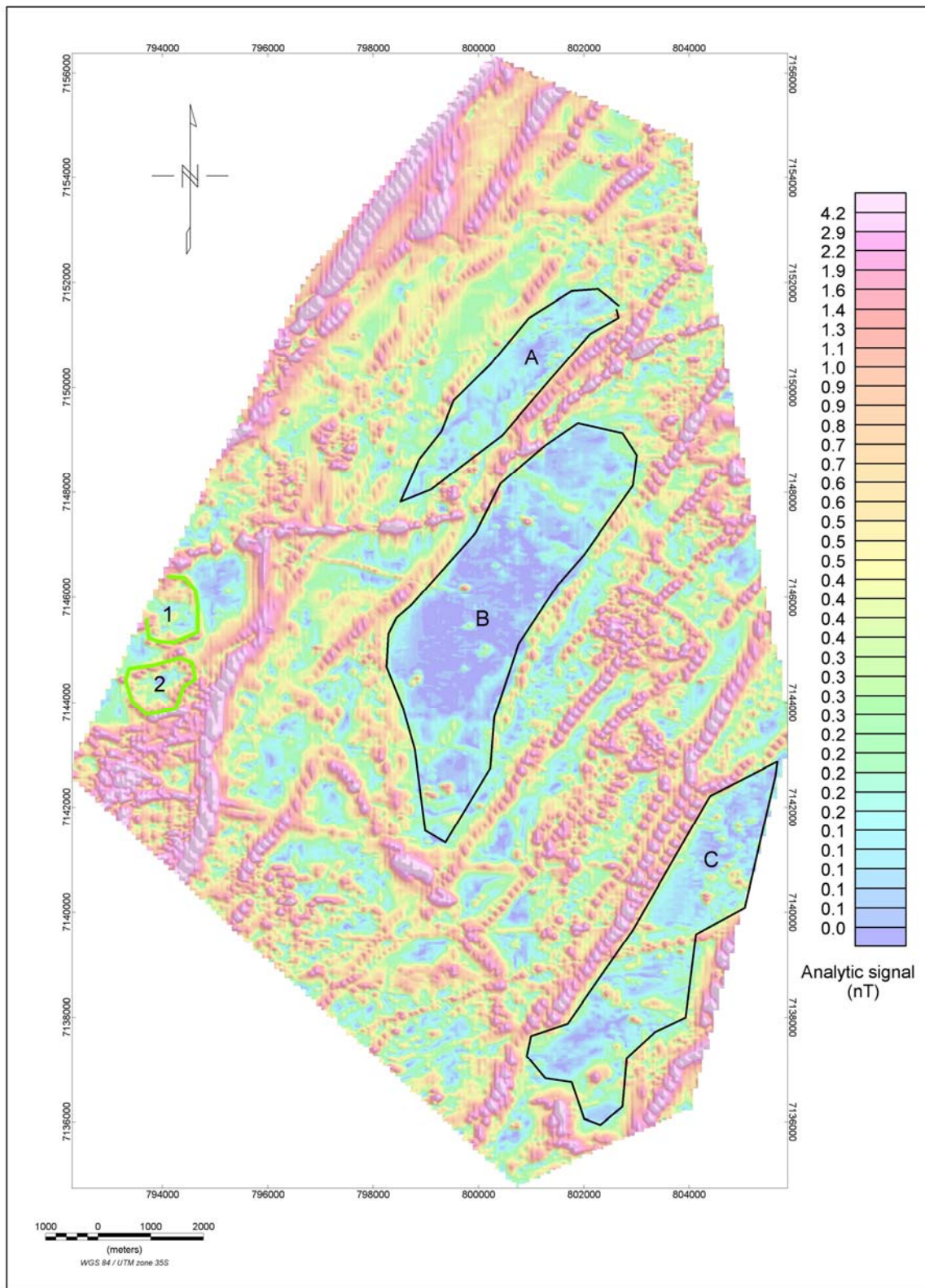


Figure 59. Low magnetic bodies (labelled A, B and C) and suspected ring dykes (labelled 1 and 2) observed on Belfast data superimposed on the analytic signal data.

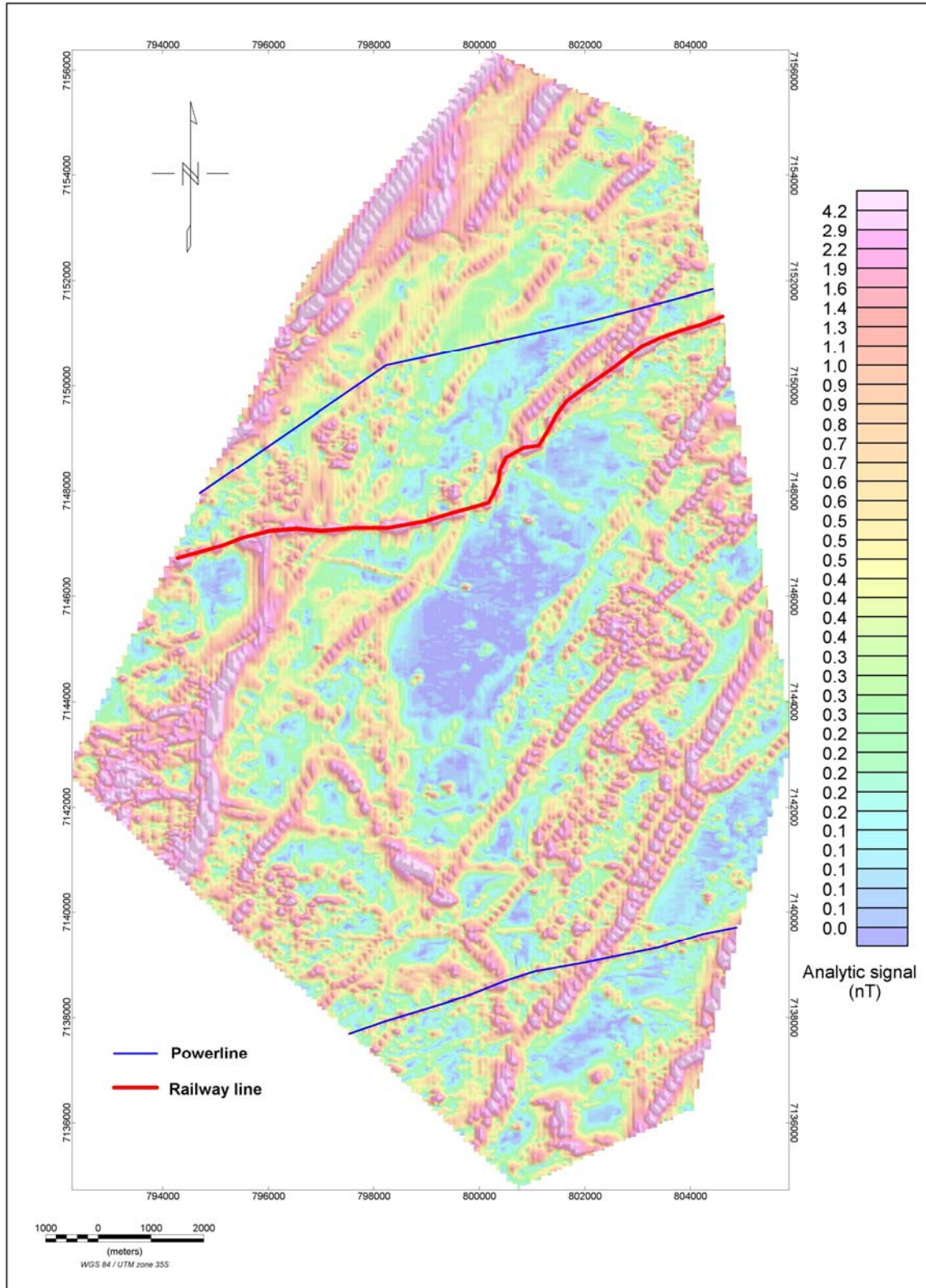


Figure 60. Cultural features observed on Belfast data superimposed on the analytic signal data.

5.6. CONCLUSIONS

The results show that the magnetic method can play a significant role in coal mining. The structures that normally affect mining activities (faults, dykes and sills) were identified. In some areas all the structures are present and in some, only the faults and sills are observed. Available borehole information confirmed some of the identified structures; however, not enough borehole information is available. It should, however, be stressed that a dyke anomaly position represents the top of the dyke and if the dyke has a dip less than 90° , the intersection of the dyke with the coal seam will show a displacement from the position on the interpreted map.

Even though it might not suffice to make a conclusive statement about the character of the Witbank coalfield as a whole from the data, looking at all the areas together one can say that the severe structural features are observed more towards the eastern side of the Witbank coalfield. This is where activities of various ages were also recorded: intrusion of Bushveld Complex, the Olifants River Dyke Swarm and the Karoo basalts. The Bushveld Complex and the ORDS dykes are pre-Karoo, thus, may not have much influence on coal mining. But faulting associated with them may have an influence on the Karoo rocks in the form of weak zones. Faulting in general appears to be pre-Karoo. Thus their influence on the coal will not be as severe as if it was post-Karoo even though weak zones will develop along the fault zones.

The areas on the central part of the coalfield reveal mainly the Karoo dolerite in the form of a sill and also a basement feature, believed to be Bushveld Complex related (felsites or the diabase).

The geologists at Arnot area were sceptical about the application of airborne magnetic method as they claimed that the dykes in the area are non-magnetic. However, the results confirmed one of the dykes, which was previously unknown and only encountered during mining. Other dykes, faults and sills were also identified. The borehole information used confirmed some of the dolerite sills outlined.



A recommendation is the drilling of boreholes to verify some of the identified structures (dykes and sills), which could pose challenges within the depth of interest and also to determine the displacement of the faults likely to affect mining. The displacement can be determined by drilling on both sides of the faults and observing the depths of same lithologies (or coal seams) on each borehole.

6. ACKNOWLEDGEMENTS

I would like to thank several people and institutions for the help intellectually and spiritually:

- ❖ *Dr. Magdel Combrinck, my mentor and thesis advisor. Your endless patience, kindness and knowledge will remain with me forever.*
- ❖ *Professor Willem Botha, my predecessor at Exxaro Resources Limited. Your knowledge and support has motivated and elevated me to goals I thought once impossible.*
- ❖ *Exxaro Resources Limited for providing airborne magnetic datasets used for the thesis.*
- ❖ *The students who participated during the discussions of various phases of individual theses: Obasanjo (Ountsche) and Carlo.*
- ❖ *Friends and family members for keeping me sane in times of hardship.*

Thank you.

7. REFERENCES

- Alva-Valdivia, L.M., Rivas-Sa´nchez, M.L., Goguitchaichvili, A. J., Urrutia-Fucugauchi, Gonzalez, A. and Vivallo W., 2003. Integrated magnetic studies of the El Romeral iron-ore deposit, Chile: implications for ore genesis and modeling of magnetic anomalies. *Journal of Applied Geophysics* **53**, p 137-151.
- Blakely, R.J., Langenheim, V.E., Ponce, D.A and Dixon, G.L., 2000. Aeromagnetic survey of the Amargosa desert, Nevada and California: a tool for understanding near-surface Geology and hydrology. U.S. Geological Survey Open-File Report 00-188, 39 pp.
- Blakely, R.J., 1995. *Potential Theory in Gravity and Magnetic Applications*: Cambridge University Press, Cambridge, UK, 441 pp.
- Brough, Dean & Louis, *Mine Surveying, 1928 Edition*
- Campbell, G., 1994. Geophysical contribution to mine-development planning. A risk reduction approach. *XV CMMI Congress, SAIMM 1994*.
- Cadle, A.B., Cairncross, B., Christie, A.D.M. and Roberts, D.L., 1993. The Karoo Basin of South Africa: type basin for the coal-bearing deposits of southern Africa. *International Journal of Coal Geology* **23**, p 117–157.
- Clark, D.A., 1997. Magnetic petrophysics and magnetic petrology: aids to geological interpretation of magnetic surveys. *AGSO Journal of Australian Geology and Geophysics*, Vol. **17(2)**, p 83-103.
- Criss, R.E. and Champion, D.E., 1984. Magnetic properties of granitic rocks from the southern half of the Idaho batholith-Influences of hydrothermal alteration and

implications for aeromagnetic interpretation: *Journal of Geophysical Research*, Vol. **89**, no. **B8**, p 7061-7076.

Dreyer, J.C., 1991. Waterberg coalfields: Geology resources, mining and products. Conf. on South Africa's Resources (Witbank, 6-9 Nov), p 39-41.

Dobrin, M.B. and Savit, C.H., 1988, *Introduction to Geophysical Prospecting*: McGraw-Hill Book Company, 867 pp.

Fitzgerald & Associates, 1996. INTREPID geophysical processing system and visualization tools. Desmond Fitzgerald and Associates, Unit 2, 1 Male Street, Brighton, Melbourne, Victoria 3186, Australia.

Fourie, P.G., 1998. Literature survey on the advance detection of dykes in underground coal mine workings. Project COL 503b, University of Pretoria, Pretoria, 59 pp.

Gemmel, G., 2001. Stratigraphy of Arnot colliery. Exxaro internal report.

Geosoft Inc., 1998. Topics in gridding. Geosoft ASEG workshop, Nov 1998, Hobart, Tasmania.

Grodner, M.W., 2002. A Regional, 3-D computer based sedimentological model of Witbank coalfield, South Africa. Unpublished M.Sc Thesis, Rand Afrikaans University, South Africa, 82 pp.

Gunn, P. J., Maidment, D. and Milligan, P.R., 1997. Interpreting aeromagnetic data in areas of limited outcrop. *AGSO Journal of Australian Geology and Geophysics*, Vol. **17(2)**, p 175-185.

Gunn, P.J., 1975. Linear Transformations of Gravity and Magnetic Fields. *Geophysical Prospecting*, Vol. **23 (2)**, p 300-312.

- Hanna, W.F., 1969. Negative aeromagnetic anomalies over mineralized areas of the Boulder batholith, Montana: U.S. Geological Survey Professional Paper **650-D**, p 159-167.
- Hatten, C.J. and Schweitzer, J.K., (1995). Evidence for synchronous extrusive and intrusive Bushveld magmatism. *J. Afr. E. Scie.*, **2114**, p 579-594.
- Holland, M. J., Cadle, A. B., Pinheiro, R. and Falcon, R. M. S., 1989. Depositional environments and coal petrography of the Permian Karoo Sequence: Witbank Coalfield, South Africa. *International Journal of Coal Geology* **11(2)**, p 143-169.
- Hunt, C.P., Moskowitz, B.M. and Banerjee, S.K., 1994. Magnetic properties of rocks and minerals, in: *Handbook of Physical Constants*, T.J. Ahrens, ed., Am. Geophys. Union, Washington, DC, p 189-204.
- Jourdan, F., Géraud, G. and Bertrand, H., 2006. Basement control on dyke distribution in Large Igneous Provinces: Case study of the Karoo triple junction. *Geological Society of South Africa Special Publication* **13**, p 1-26.
- Le Blanc Smith, G., 1980. Genetic Stratigraphy of the Witbank Coalfield. *Transactions Geological Society of South Africa* **83(3)**, p 313–326.
- Lurie, J., 1994. *South African geology for mining, metallurgical, hydrological and civil engineering*, Lupon Publishing CC, Pinegowrie, Republic of South Africa, p 124.
- Luyendyk, A.P.J., 1997. Processing of airborne magnetic data. *AGSO Journal of Australian Geology and Geophysics*, Vol. **17(2)**, p 31-38.
- Mahanyele, P.J. and Botha W.J., 2008. Detail geophysical interpretation of high resolution airborne magnetic data, Matla mine. Exxaro internal report. 18 pp.

- Milligan, P.R. and Gunn, P. J., 1997. Enhancement and presentation of airborne geophysical data. *AGSO Journal of Australian Geology and Geophysics*, Vol. **17(2)**, p 63-75.
- Nabighian, M. N., Grauch, V. J. S., Hansen, R. O., LaFehr, T. R., Li, Y., Peirce, J. W. Phillips, J. D. and Ruder., M. E., 2005. The historical development of the magnetic method in exploration. *Geophysics*, **70 (6)**, p 33-61.
- O'Driscoll, B., Troll, V.R., Reavy, R.J., and Turner, P. 2006. The Great Eucrite intrusion of Ardnamurchan, Scotland: re-evaluating the ring-dyke concept. *Geology*, **34 (3)**, p 189-192.
- Parisi, L., 1986. Anglo Coal exploration internal report.
- Pone, J. D.N., Hein, K.A.A., Stracher, G.B., Annegarn, H.J., Finkleman, R.B., Blake, D.R., McCormack, J.K. and Schroeder, P., 2007. The spontaneous combustion of coal and its by-products in the Witbank and Sasolburg coalfields of South Africa, *International Journal of Coal Geology* **72 (2007)**, p 124-140.
- Poole, G., Whetton, M.C. and Taylor, A., 1935. Magnetic observations on concealed dykes and other intrusions in the Northumberland Coalfield. *Transactions - Institution of Mining Engineers*, vol. **LXXXIX**, p 1934-1935.
- Robson, D.A., 1964. The Acklington Dyke - A proton magnetometer survey. *Proceeding of the Yorkshire Geological Society*, vol. **34**, March 1964.
- Roest, W. R., Verhoef, J. and M. Pilkington., 1992. Magnetic interpretation using the 3D analytic signal. *Geophysics*, **57**, p 116-125.

- Roux, A.T., 1908. Geophysical Field Manual For Technicians. No.1. The Magnetic Method: South African Geophysical Association, South Africa. 71 pp.
- Saul, S.J. and Pearson, M.J., 1998. Levelling of aeromagnetic data. Canadian Journal of Exploration Geophysics, Vol. **34**. (1 & 2), p 9-15.
- Schouten, J. A., 1971. A fundamental analysis of magnetic anomalies over ocean ridges. Geophysical Research, **I**, p 111-144.
- Snyman, C.P., 1998. Coal. In: Wilson, M.G.C. and Anhaeusser, C.R., Eds. The Mineral Resources of South Africa, Sixth Edition, Handbook **16**. Council for Geoscience, Pretoria, p 136-205.
- SACS: South African Committee for Stratigraphy, 1980. Stratigraphy of South Africa. Part 1: Lithostratigraphy of the Republic of South Africa, South West Africa/Namibia and the Republics of Bophuthatswana, Transkei and Venda (Compiled by Kent, L.E.). Handbook **8**, 690p. Geological Survey of South Africa.
- Spector, A., 1968. Spectral analysis of aeromagnetic data. Unpublished Ph.D. Thesis. Department of Physics, University of Toronto, Canada.
- Stanimirovic, J., 2002. Geological controls on No.4 Seam roof conditions at the New Denmark Colliery, Highveld coalfield, Karoo Basin, South Africa. Unpublished M.Sc Thesis, Rand Afrikaans University, South Africa, 154 pp.
- Steenkamp, B., 2007. Aeromagnetic survey report. Exxaro internal report.
- Telford, W.M., Geldart, L.P., Sheriff, R.E. and Keys, D.A., 1976. Applied Geophysics. 1st Edition. Cambridge University Press, 860 pp.
- Telford, W.M., Geldart, L.P. and Sheriff, R.E., 1990. Applied Geophysics. 2nd Edition

Cambridge University Press, Cambridge, 770 pp.

Tudor, P., 2006. An independent competent person's report on mining assets of Exxaro Resources limited. www.exxaro.com/pdf/icpr/a/geology/coal.htm

Uludağ, S., PhMips, H.R. and Eroğlu, H.N., 2001. Assessing Spontaneous Combustion Risk in South African Coal Mines Using a GIS Tool. *17* International Mining Congress and Exhibition of Turkey- IMCET 2001*, ©2001, ISBN 975-395-417-4

Urquhart, W.E.S. 2003. Airborne Geophysical Survey Workshop, Sept. 18, 2003.
<http://www.geoexplo.com/index.html>

Vacquier, V., Steenland, N. C. Henderson, R. G. and Zietz, I., 1951. Interpretation of aeromagnetic maps. *Geol. Soc. Am. Memoir* 47:151 pp.

Van Ryneveld, C., 2008. Moabsvelden exploration results. Exxaro internal report

Werner, S., 1953. Interpretation of magnetic anomalies at sheet like bodies. *Sveriges Geol. Undersok, Arsbok* **43**, no. 06.

Winter, M.F., Cairncross, B. and Cadle, A.B., 1987. A genetic stratigraphy for the Vryheid Formation in the northern Highveld Coalfield, South Africa. *South African Journal of Geology* **90** (4), p 333–343.

Geophysical Exploration for Engineering and Environmental Investigations, Engineering Design Manual (EM 1110-1-1802), 1995. Available by the US Army Corps of Engineers. Washington, DC: Department of the Army Corps of Engineers.
(www.usace.army.mil/usace-docs/eng-manuals/em1110-1-1802/toc.htm).

Geology map of 2528 Pretoria, scale 1: 250 000, 1986. Compiled by L.E. Coetzee, Geological Survey, Pretoria.

Geology map of 2530 Barberton, scale 1: 250 000, 1986. Compiled by F. Walraven and F. J. Hartzler, Geological Survey, Pretoria.

Geology map of 2628 East Rand, scale 1: 250 000, 1986. Compiled by N. Keyser, G.A. Botha and G.H. Groenewald, Geological Survey, Pretoria.

The regional magnetic map of South Africa, scale 1: 1000 000, 1997. Compiled by the geophysics division, Council for Geoscience, Pretoria.